Combined measurements of Higgs boson couplings in proton–proton collisions at $$\sqrt{s}=13\,\text {Te}\text {V} $$ s = 13 Te

Citation: The European Physical Journal C. 2019 May 20;79(5):421

As Published: https://doi.org/10.1140/epjc/s10052-019-6909-y

Publisher: Springer Berlin Heidelberg

Persistent URL: https://hdl.handle.net/1721.1/131622

Version: Final published version: final published article, as it appeared in a journal, conference proceedings, or other formally published context

Eur. Phys. J. C (2019) 79:421
https://doi.org/10.1140/epjc/s10052-019-6909-y

THE EUROPEAN PHYSICAL JOURNAL C

Regular Article - Experimental Physics

Combined measurements of Higgs boson couplings in proton–proton collisions at $\sqrt{s} = 13\,\text{TeV}$

CMS Collaboration*

CERN, 1211 Geneva 23, Switzerland

Received: 27 September 2018 / Accepted: 2 May 2019 / Published online: 20 May 2019

Abstract Combined measurements of the production and decay rates of the Higgs boson, as well as its couplings to vector bosons and fermions, are presented. The analysis uses the LHC proton–proton collision data set recorded with the CMS detector in 2016 at $\sqrt{s} = 13\,\text{TeV}$, corresponding to an integrated luminosity of $35.9\,\text{fb}^{-1}$. The combination is based on analyses targeting the five main Higgs boson production mechanisms (gluon fusion, vector boson fusion, and associated production with a W or Z boson, or a top quark-antiquark pair) and the following decay modes: $\text{H} \to \gamma\gamma$, ZZ, WW, $\tau\tau$, bb, and $\mu\mu$. Searches for invisible Higgs boson decays are also considered. The best-fit ratio of the signal yield to the standard model expectation is measured to be $\mu = 1.17 \pm 0.10$, assuming a Higgs boson mass of 125.09 GeV. Additional results are given for various assumptions on the scaling behavior of the production and decay modes, including generic parametrizations based on ratios of cross sections and branching fractions or couplings. The results are compatible with the standard model predictions in all parametrizations considered. In addition, constraints are placed on various two Higgs doublet models.

1 Introduction

Understanding the mechanism behind electroweak symmetry breaking (EWSB) remains one of the main objectives of the physics program at the CERN LHC. In the standard model (SM) of particle physics [1–4], EWSB is realized through the addition of a complex scalar doublet field. A salient feature of this is the prediction of one physical, neutral, scalar particle, the Higgs boson (H) [5–10]. The Higgs scalar field can also account for the fermion masses through Yukawa interactions [2,11]. The Higgs boson was discovered by the ATLAS and CMS Collaborations [12–14], and is the subject of much study. The Yukawa coupling strengths are free parameters in the SM and do not explain the observed pattern of fermion masses. Furthermore, it is not understood why the Higgs boson mass is near the electroweak scale, since it is not protected in the SM from large quantum corrections [15–19]. This has led to the development of many beyond the SM (BSM) theories that can alter the properties of the Higgs boson [20–24]. Precision measurements of the properties of the Higgs boson are therefore an important test of the SM.

This paper describes combined measurements of the Higgs boson production rates, decay rates, and couplings using analyses of $\sqrt{s} = 13\,\text{TeV}$ proton–proton collision data recorded with the CMS detector in 2016. The data set corresponds to an integrated luminosity of $35.9\,\text{fb}^{-1}$. The following decay channels are included in the combination: $\text{H} \to \gamma\gamma$, $\text{H} \to \text{ZZ}$, $\text{H} \to \text{WW}$, $\text{H} \to \tau\tau$, $\text{H} \to \text{bb}$, and $\text{H} \to \mu\mu$, as shown in Fig. 1. Here and in what follows, we do not distinguish between particles and antiparticles in our notations of production and decay processes. Searches for invisible decays of the Higgs boson, which are predicted to be considerably enhanced by several BSM theories [25–28], are also considered for selected measurements. The data samples considered for each decay channel are ensured to have negligible overlap to avoid introducing nontrivial correlations.

The analyses included in this combination target production via gluon fusion (ggH), vector boson fusion (VBF), associated production with a vector boson (VH, V= W or Z), and associated production with a pair of top quarks (ttH). The prediction for ggH production has advanced to next-to-next-to-next-to-leading order (N^3LO) in perturbative quantum chromodynamics (QCD) [29,30] and next-to-leading order (NLO) for electroweak (EW) corrections, reducing its uncertainty from $^{+7.6\%}_{-8.1\%}$ (next-to-NLO) to $^{+4.6\%}_{-6.7\%}$. The calculations of the VBF and VH cross sections are performed at next-to-NLO QCD and NLO EW accuracy, while the calculation of the ttH cross section is performed at NLO QCD and NLO EW accuracy. The updated theoretical predictions used for the various production and decay modes in this paper can be found in Refs. [29–52] and are summarized in Ref. [53]. Examples of leading-order (LO) Feynman diagrams for these production processes can be seen in Figs. 2 and 3. In addition

* e-mail: cms-publication-committee-chair@cern.ch

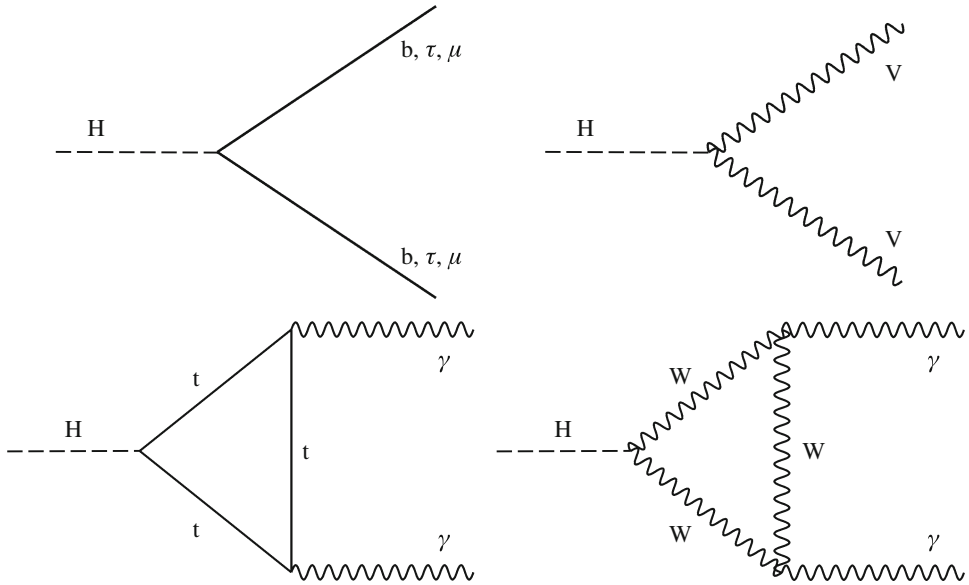

Fig. 1 Examples of leading-order Feynman diagrams for Higgs boson decays in the H → bb, H → ττ, and H → μμ (upper left); H → ZZ and H → WW (upper right); and H → γγ (lower) channels

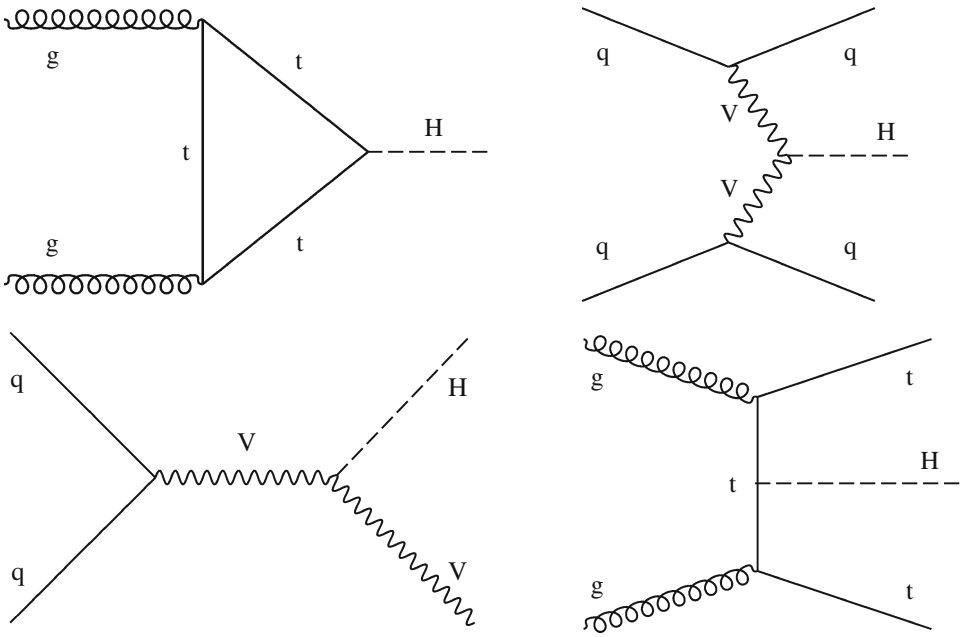

Fig. 2 Examples of leading-order Feynman diagrams for the ggH (upper left), VBF (upper right), VH (lower left), and ttH (lower right) production modes

to the five main production processes, the contributions due to Higgs boson production in association with a single top quark (tH) and either a W boson (tHW) or a quark (tHq), as shown in Fig. 4, are included in the analyses that have some sensitivity to them.

For certain measurements in this paper, such as ggH production and H → γγ decay, the interference between the diagrams that contribute to the process is considered. In addition, the tH cross section is small in the SM, being approximately 14% of the ttH cross section, due to the destructive interference between the diagrams shown in Fig. 4, which involve the coupling of the Higgs boson to W bosons (tHW process) and top quarks (tHq process). This interference becomes constructive, however, when the relative sign between these couplings is negative, and so the tH process is sensitive to the relative sign of the HWW and ttH couplings.

The ATLAS and CMS Collaborations have published combined measurements of Higgs boson production rates, decay rates, and couplings with the $\sqrt{s} = 7$ and 8 TeV LHC Run 1 data [54,55]. A combination of the Run 1 ATLAS and CMS analyses has also been performed [56]. All results were found to be in agreement, within their uncertainties, with the predictions of the SM. In this paper, due to the larger integrated luminosity and increased signal cross section at $\sqrt{s} = 13$ TeV, the measured precision for several parameters of interest has significantly increased with respect to

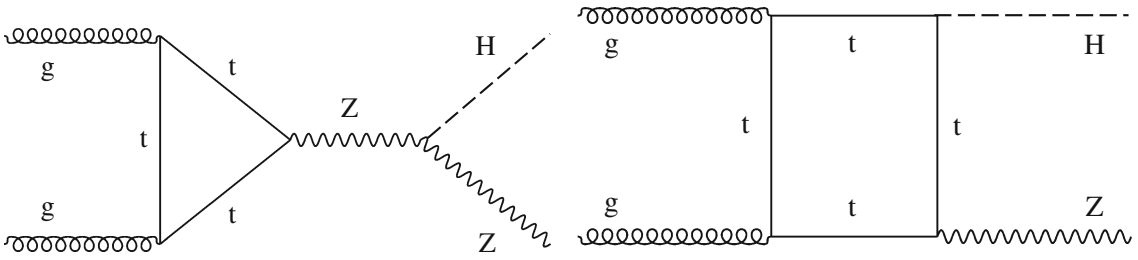

Fig. 3 Examples of leading-order Feynman diagrams for the gg → ZH production mode

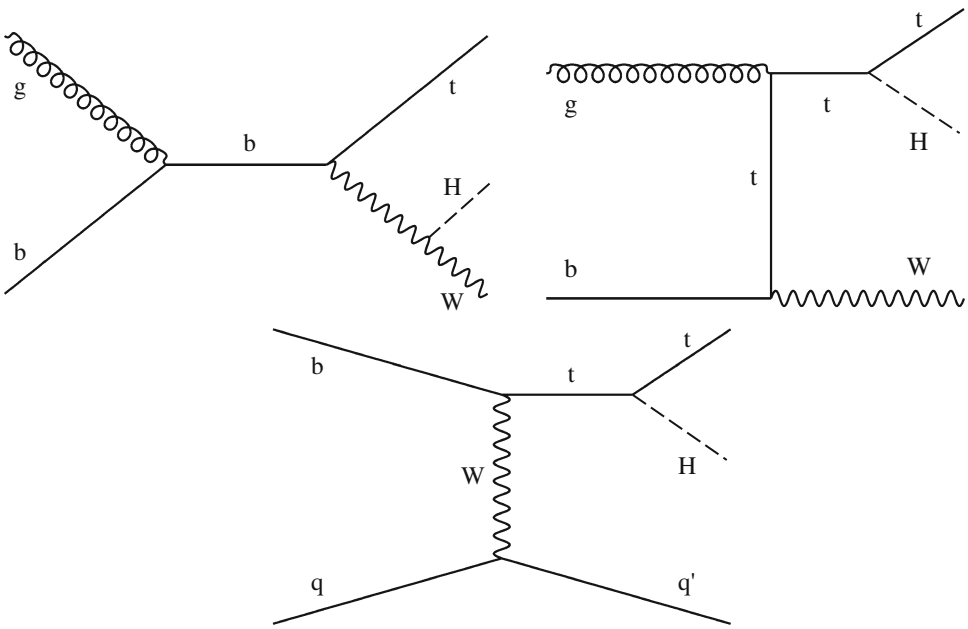

Fig. 4 Examples of leading-order Feynman diagrams for tH production via the tHW (upper left and right) and tHq (lower) modes

Ref. [56]. In particular, the predicted cross sections for the dominant ggH production mode and the ttH production mode increase by factors of approximately 2.3 and 3.8, respectively, between $\sqrt{s} = 8$ and 13 TeV. In addition, some of the theoretical predictions have improved, as mentioned earlier.

This paper is organized as follows: A brief description of the CMS detector is given in Sects. 2, 3 provides a summary of the various analyses included in the combination, and Sect. 4 describes the modifications made to these analyses to ensure a common signal and uncertainty model. Section 5 outlines the statistical procedure used to derive the results, and Sect. 6 outlines the treatment of the systematic uncertainties. Section 7 reports the results of the signal parametrizations in terms of signal strength modifiers and fiducial cross sections, while Sect. 8 describes the results obtained from an alternative set of signal parametrizations in terms of Higgs boson couplings. Section 9 details interpretations in terms of various two Higgs doublet models. The paper is summarized in Sect. 10.

2 The CMS detector

The central feature of the CMS apparatus is a superconducting solenoid of 6 m internal diameter, providing a magnetic field of 3.8 T. Within the solenoid volume are a silicon pixel and strip tracker, a lead tungstate crystal electromagnetic calorimeter, and a brass and scintillator hadron calorimeter, each composed of a barrel and two endcap sections. Forward calorimeters extend the pseudorapidity coverage provided by the barrel and endcap detectors. Muons are detected in gas-ionization chambers embedded in the steel flux-return yoke outside the solenoid. A more detailed description of the CMS detector, together with a definition of the coordinate system used and the relevant kinematic variables, can be found in Ref. [57].

3 Analyses included in the combination

In this section, the individual analyses included in the combination are briefly described. More detailed information on

each analysis can be found in the corresponding references. Many of the analyses split their primary data sample in multiple event categories with specific signatures that enhance the discrimination power between different Higgs boson production processes. This is achieved through selections that require the presence of additional leptons or jets, as expected in the decay of a W or Z boson in the WH and ZH modes, or in top quark decays in the ttH mode, and that exploit the distinctive kinematic properties of the final state objects, such as the presence of two jets with a large separation in pseudorapidity $\Delta\eta_{\mathrm{jj}}$, and a large invariant mass m_{jj}, in the VBF topology. In some categories, the kinematic features of an event as a whole are used to select particular production processes. For example, requiring a large missing transverse momentum $p_{\mathrm{T}}^{\mathrm{miss}}$, defined as the magnitude of the negative vector sum over the transverse momenta p_{T} of all particles reconstructed in an event, targets ZH production in which the Z boson decays to neutrinos. The event categories within and amongst the individual analyses are constructed to ensure a negligible level of overlap (i.e. the same event entering more than one category). In many cases, this is accomplished by synchronizing the object (e.g. electron, muon, tau, or jet) identification definitions and imposing strict requirements on the number of reconstructed objects. In other cases, the orthogonality is ensured by imposing opposing requirements on higher level observables formed using multiple objects. For rare cases where potential overlap is not explicitly removed, the lists of selected data events were checked and found to contain a negligible number of duplications. In total, up to 265 event categories are considered, and there are over 5500 nuisance parameters corresponding to various sources of experimental and theoretical systematic uncertainty. A summary of the production and decay modes, which are described in more detail in the following sections, is shown in Table 1.

3.1 $\mathrm{H} \to \gamma\gamma$

The $\mathrm{H} \to \gamma\gamma$ analysis [58] provides good sensitivity to nearly all Higgs boson production processes. Since the $\mathrm{H} \to \gamma\gamma$ decay proceeds mainly through W- and top-loop processes, interference effects make its branching fraction sensitive to the relative sign of the fermion and vector boson couplings. The analysis measures a narrow signal peak in the diphoton invariant mass ($m_{\gamma\gamma}$) spectrum over a smoothly falling continuum background, originating mainly from prompt, nonresonant diphoton production, or from events where at least one jet is misidentified as an isolated photon.

Exclusive event categories are defined using dedicated selections based on additional reconstructed objects to separate the different Higgs boson production mechanisms. The presence of additional leptons, $p_{\mathrm{T}}^{\mathrm{miss}}$, or jets is used to classify events into one of the following categories: ttH leptonic, ttH hadronic, ZH leptonic, WH leptonic, loose VH leptonic with low $p_{\mathrm{T}}^{\mathrm{miss}}$ requirement, VBF, VH $p_{\mathrm{T}}^{\mathrm{miss}}$, and VH hadronic. The VBF category is divided into three subcategories of increasing purity against ggH production. Finally, the remaining events are divided into four untagged categories with increasing signal purity.

In each event class, the background in the signal region (SR) is estimated from a fit to the observed $m_{\gamma\gamma}$ distribution in data. The dominant experimental uncertainties in the measurement of the rate of Higgs boson production in the $\mathrm{H} \to \gamma\gamma$ decay channel are related to the modeling of the electromagnetic shower shape observables used in the photon identification and the background shape parametrization.

3.2 $\mathrm{H} \to \mathrm{ZZ}$

Despite the $\mathrm{H} \to \mathrm{ZZ}^{(*)} \to 4\ell$ ($\ell = \mathrm{e}$ or μ) decay having the lowest branching fraction of the decay channels considered, it also has the lowest background contamination, resulting in very good sensitivity to production processes with large cross sections, such as ggH. It is also the most important decay channel in constraining the HZZ coupling. The $\mathrm{H} \to \mathrm{ZZ}^{(*)} \to 4\ell$ [59] analysis measures a narrow four-lepton invariant mass peak over a small continuum background. The dominant irreducible background in this analysis is due to nonresonant ZZ production with both Z bosons decaying to a pair of charged leptons, and is estimated from simulation. The 4e, 4μ, and $2\mathrm{e}2\mu/2\mu2\mathrm{e}$ decay channels are treated separately to better model the different mass resolutions and background rates arising from jets misidentified as leptons.

To separate the different Higgs boson production mechanisms, the following categories are defined on the basis of the presence of jets, b-tagged jets, leptons, $p_{\mathrm{T}}^{\mathrm{miss}}$, and various matrix element discriminants that make use of the information about the additional objects: VBF (1- and 2-jet), VH hadronic, VH leptonic, ttH, VH $p_{\mathrm{T}}^{\mathrm{miss}}$, and untagged categories.

In the $\mathrm{H} \to \mathrm{ZZ}^{(*)} \to 4\ell$ analysis, the dominant experimental uncertainties are related to the lepton efficiencies and the determination of the Z+jets background from data.

3.3 $\mathrm{H} \to \mathrm{WW}$

The $\mathrm{H} \to \mathrm{WW}^{(*)} \to \ell\nu\ell\nu$ analysis [60] profits from the fact that the $\mathrm{H} \to \mathrm{WW}$ decay mode has one of the largest branching fractions and has a relatively low-background final state. As a result, this decay channel has very good sensitivity to most production processes, in particular ggH and VBF. Imposing tight lepton identification criteria and requiring the absence of b-tagged jets helps to reduce the misidentified lepton and top quark backgrounds, respectively. Several event categories with varying signal-to-background ratios are defined to improve the sensitivity to the signal.

Table 1 Summary of the event categories in the analyses included in this combination. The first column indicates the decay channel and the second column indicates the production mechanism targeted by an analysis. The third column provides the total number of categories per production tag, excluding control regions. Notes on the expected fractions of different Higgs signal production and decay modes with respect to the total signal yield in the given category are given in the fourth column. Where the numbers do not sum to 100%, the remaining contributions are from other signal production and decay processes. Finally, where relevant, the fifth column specifies the approximate expected relative mass resolution for the SM Higgs boson

Decay tags	Production tags	Number of categories	Expected signal fractions	Mass resolution
$H \to \gamma\gamma$, Sect. 3.1				
$\gamma\gamma$	Untagged	4	74–91% ggH	≈1–2%
	VBF	3	51–80% VBF	
	VH hadronic	1	25% WH, 15% ZH	
	WH leptonic	2	64–83% WH	
	ZH leptonic	1	98% ZH	
	VH $p_{\mathrm{T}}^{\mathrm{miss}}$	1	59% VH	
	ttH	2	80–89% ttH, ≈8% tH	
$H \to ZZ^{(*)} \to 4\ell$, Sect. 3.2				
4μ, $2e2\mu/2\mu2e$, 4e	Untagged	3	≈95% ggH	≈1–2%
	VBF 1, 2-jet	6	≈11–47% VBF	
	VH hadronic	3	≈13% WH, ≈10% ZH	
	VH leptonic	3	≈46% WH	
	VH $p_{\mathrm{T}}^{\mathrm{miss}}$	3	≈56% ZH	
	ttH	3	≈71% ttH	
$H \to WW^{(*)} \to \ell\nu\ell\nu$, Sect. 3.3				
$e\mu/\mu e$	ggH 0, 1, 2-jet	17	≈55–92% ggH, up to ≈15% $H \to \tau\tau$	≈20%
	VBF 2-jet	2	≈47% VBF, up to ≈25% $H \to \tau\tau$	
$ee+\mu\mu$	ggH 0, 1-jet	6	≈84–94% ggH	
$e\mu$+jj	VH 2-jet	1	22% VH, 21% $H \to \tau\tau$	
3ℓ	WH leptonic	2	≈80% WH, up to 19% $H \to \tau\tau$	
4ℓ	ZH leptonic	2	85–90% ZH, up to 14% $H \to \tau\tau$	
$H \to \tau\tau$, Sect. 3.4				
$e\mu$, $e\tau_h$, $\mu\tau_h$, $\tau_h\tau_h$	0-jet	4	≈70–98% ggH, 29% $H \to WW$ in $e\mu$	≈10–20%
	VBF	4	≈35–60% VBF, 42% $H \to WW$ in $e\mu$	
	Boosted	4	≈48–83% ggH, 43% $H \to WW$ in $e\mu$	
VH production with $H \to bb$, Sect. 3.5				
$Z(\nu\nu)H(bb)$	ZH leptonic	1	≈100% VH, 85% ZH	≈10%
$W(\ell\nu)H(bb)$	WH leptonic	2	≈100% VH, ≈97% WH	
$Z(\ell\ell)H(bb)$	Low-$p_{\mathrm{T}}(V)$ ZH leptonic	2	≈100% ZH, of which ≈20% ggZH	
	High-$p_{\mathrm{T}}(V)$ ZH leptonic	2	≈100% ZH, of which ≈36% ggZH	
Boosted H Production with $H \to bb$, Sect. 3.6				
bb	$p_{\mathrm{T}}(H)$ bins	6	≈72–79% ggH	≈10%
ttH production with $H \to$ leptons, Sect. 3.7.1				
2ℓss	ttH	10	$WW/\tau\tau \approx 4.5$, ≈5% tH	
3ℓ		4	$WW : \tau\tau : ZZ \approx 15 : 4 : 1$, ≈5% tH	
4ℓ		1	$WW : \tau\tau : ZZ \approx 6 : 1 : 1$, ≈3% tH	
$1\ell+2\tau_h$		1	96% ttH with $H \to \tau\tau$, ≈6% tH	
2ℓss$+1\tau_h$		2	$\tau\tau : WW \approx 5 : 4$, ≈5% tH	
$3\ell+1\tau_h$		1	$\tau\tau : WW : ZZ \approx 11 : 7 : 1$, ≈3% tH	
ttH production with $H \to bb$, Sect. 3.7.2				
bb	$t\bar{t} \to$ jets	6	≈83–97% ttH with $H \to bb$	

Table 1 continued

Decay tags	Production tags	Number of categories	Expected signal fractions	Mass resolution
	$t\bar{t} \to 1\ell$+jets	18	≈65–95% ttH with H → bb, up to 20% H → WW	
	$t\bar{t} \to 2\ell$+jets	3	≈84–96% ttH with H → bb	
Search for H → $\mu\mu$, Sect. 3.8				
$\mu\mu$	S/B bins	15	56–96% ggH, 1–42% VBF	≈1–2%
Search for invisible H decays, Sect. 3.9				
Invisible	VBF	1	52% VBF, 48% ggH	
	ggH + ≥ 1 jet	1	80% ggH, 9% VBF	
	VH hadronic	1	54% VH, 39% ggH	
	ZH leptonic	1	≈100% ZH, of which 21% ggZH	

Events are selected that contain two leptons, denoted 2ℓ, which may be of different or same flavor. The different-flavor eμ decay channel dominates the sensitivity since it has the largest branching fraction and is the least contaminated by backgrounds. The same-flavor ee and $\mu\mu$ final states are also considered, although their sensitivity is limited by the contamination from Drell–Yan (DY) background events with misreconstructed $p_{\mathrm{T}}^{\mathrm{miss}}$. Given the large background contribution from tt production in both the different-flavor and same-flavor final states, events are further categorized into categories with 0, 1, and 2 associated jets, with the 0-jet category dominating the overall sensitivity. In addition, events are further categorized on the basis of the p_{T} of the subleading lepton, since the background from misidentified leptons is larger in the low-p_{T} region. In the different-flavor final state, dedicated 2-jet categories are included to enhance the sensitivity to VBF and VH production mechanisms.

The analysis also includes categories that are sensitive to the associated production of the Higgs boson with a vector boson that decays leptonically. Two 3ℓ categories that are sensitive to WH production are defined by requiring the presence of a total of three leptons (electrons or muons). The two are distinguished by whether or not they contain a pair of leptons with the same flavor and opposite sign. Events with four charged leptons, in which one pair is consistent with a Z boson decay, are separated into two categories depending on whether the remaining pair consists of same-flavor leptons or not. These 4ℓ categories are sensitive to the ZH production mode. The signal extraction method depends on the event category.

When measuring the rate of Higgs boson production in the H → WW decay channel, the dominant experimental uncertainties arise from the determination of the top quark pair, WW and DY backgrounds from data, and the uncertainties related to the p_{T} and η dependent lepton reconstruction and identification efficiencies.

3.4 H → $\tau\tau$

The H → $\tau\tau$ analysis [61] benefits from a relatively large branching fraction and a reasonable mass resolution of ≈10–20%, providing competitive sensitivity to both the ggH and VBF production processes. It also provides the best sensitivity for the direct measurement of a fermionic Higgs boson coupling. The analysis utilizes the four most sensitive $\tau\tau$ final states: eμ, eτ_{h}, $\mu\tau_{\mathrm{h}}$, and $\tau_{\mathrm{h}}\tau_{\mathrm{h}}$, where τ_{h} denotes a hadronically decaying τ lepton. In the analysis of each $\tau\tau$ decay channel, events are divided into three categories labeled 0-jet, boosted, and VBF.

The VBF category requires the presence of two additional jets with large m_{jj} and $\Delta\eta_{\mathrm{jj}}$, designed to increase the purity of VBF events. The 0-jet category does not have much sensitivity to the signal, but is useful to constrain systematic uncertainties in the background model. The boosted category contains all remaining events, and is binned as a function of p_{T} of the $\tau\tau$ system to increase the sensitivity to ggH production. There is a nonnegligible contribution from the H → WW process in some categories, and this is treated consistently as an H → WW signal in this combined measurement.

The $p_{\mathrm{T}}^{\mathrm{miss}}$ and τ_{h} energy scale uncertainties are the dominant experimental uncertainties in the measurement of the Higgs boson production rate in the H → $\tau\tau$ decay channel, followed by the uncertainties in the determination of the Z($\tau\tau$)+jets background from data.

3.5 VH production with H → bb

The H → bb decay has the largest expected branching fraction in the SM (58.1% for $m_{\mathrm{H}} = 125.09$ GeV) and a reasonable mass resolution of 15%. By requiring VH production it is possible to increase the signal purity with respect to the inclusive case for which the background from QCD multijet production is dominant. The analysis of the H → bb decay targeting VH production (VH(bb)) [62] pro-

vides the best sensitivity to the WH and ZH processes as well as to the bbH coupling. Selected events are categorized based on the presence of two b-tagged jets, and two ($Z(\ell\ell)H(bb)$), one ($W(\ell\nu)H(bb)$) or no ($Z(\nu\nu)H(bb)$) electrons or muons in the final state. The $Z(\ell\ell)H(bb)$ categories are subdivided into low-boost ($50 < p_T(Z) < 150\,GeV$) and high boost ($p_T(Z) > 150\,GeV$) regions. Events selected in the $Z(\nu\nu)H(bb)$ category are further required to have $p_T^{miss} > 170\,GeV$.

The main backgrounds come from Z or W boson production in association with light- and heavy-flavor (LF and HF) jets, as well as from top quark pair and diboson production. The dominant experimental uncertainties in in this analysis are related to the determination of these backgrounds, and uncertainties in the b tagging discriminator shapes and efficiencies.

3.6 Boosted H production with H → bb

The H → bb decay is also measured in an analysis that targets inclusive production of the Higgs boson [63], exploiting the higher signal to background ratio at high $p_T(H)$ (the transverse momentum of the Higgs boson). The decay products of a high-p_T H → bb system are reconstructed using the anti-k_T algorithm [64,65] with a distance parameter of 0.8 (AK8 jet), and the soft-drop algorithm [66,67] is used to reconstruct the jet mass m_{SD}, which peaks at the Higgs boson mass for signal events. Events containing substantial p_T^{miss}, or identified and isolated electrons, muons or τ leptons are vetoed to reduce the background contributions from vector boson production and top quark processes.

The main background component, QCD multijet production, is estimated from a signal-depleted Control Region (CR). The selected events are divided according to the jet p_T into six bins of increasing width from 450 GeV to 1 TeV.

The dominant experimental uncertainties in this analysis are the uncertainties related to the extrapolation of the QCD multijet and top quark pair backgrounds from the CRs.

3.7 ttH production

Measurements of the rate of the ttH production process provide a direct test of the Higgs boson's coupling to top quarks. A recent measurement by CMS combining the $\sqrt{s} = 7$, 8 and 13 TeV datasets was able to establish the first 5σ observation of the ttH production process [68]. Dedicated analyses targeting the H → leptons [69] and H → bb [70,71] decay channels using $\sqrt{s} = 13\,TeV$ data are described in this section.

3.7.1 ttH *production with* H → *leptons*

The analysis of ttH production with H → leptons [69] is mainly sensitive to the Higgs boson decaying to $\tau\tau$, WW or ZZ with electrons, muons and/or τ_h in the final state. This analysis provides the best sensitivity to the ttH production process. The main irreducible backgrounds come from ttV and diboson production. Reducible backgrounds containing misidentified leptons or leptons with misidentified charge are estimated from CRs in data. Events are categorized according to their lepton content. The light-lepton (e/μ) categories are defined as:

- 2ℓss: Events with two leptons having the same sign and at least four additional jets. A veto on the presence of hadronic tau decays is applied. Further categories based on lepton charge, flavor and the number of b-tagged jets are defined within this class.
- 3ℓ: Events containing three leptons, with the sum of lepton charges equal to ± 1, and at least two additional jets of which one or two are b tagged.
- 4ℓ: Events with four leptons, with an explicit veto on H → $ZZ^{(*)}$ → 4ℓ events as these are selected by the analysis described in Sect. 3.2.

The τ_h categories, which require the presence of hadronically decaying τ leptons, are defined as:

- $1\ell{+}2\tau_h$: Events with two oppositely charged τ_h candidates and an additional e/μ, at least three additional jets, and at least one b-tagged jet.
- 2ℓss$+1\tau_h$: Events containing three leptons, with sum of lepton charges equal to ± 1, and at least two additional jets of which one or two are b tagged. These events are further sorted into two subcategories based on whether or not all of the jets expected in the ttH process are reconstructed.
- $3\ell{+}1\tau_h$: Events with three light leptons, one τ_h and at least two additional jets and one b-tagged jet.

In the e/μ and τ_h categories, the dominant experimental uncertainties on the measurement of the rate of Higgs boson production in the ttH mode are related to the lepton reconstruction efficiencies, and the estimation of the reducible background contributions from data.

3.7.2 ttH *production with* H → bb

There are two analyses that target the associated production of the Higgs boson with a pair of top quarks in the H → bb decay mode [70,71]. The leptonic analysis requires at least one lepton to be present in the final state, from the tt decay system, while the hadronic analysis selects events in the all-hadronic final state. These analyses provide good sensitivity

to the ttH production process and improve the precision in the measurement of the bbH coupling.

In the leptonic analysis, events are sorted into the 1ℓ or 2ℓ classes, depending on the presence of one or two well-identified leptons. Events are further categorized based on the number of reconstructed jets (Nj) and the number of jets that are tagged as b jets (Nb) in each event. The largest background is due to top quark pair production with additional jets that contain heavy flavor hadrons. In the 1ℓ class, three categories are used: 4j $\geq$3b, 5j $\geq$3b, and 6j $\geq$3b. In each category a multi-classification deep neural network (DNN) [72] is used to define six classes on the basis of the most probable event hypothesis for each event, yielding a total of 18 categories. In the 2ℓ class, there are two jet categories: $\geq$4j 3b and $\geq$4j $\geq$4b. The $\geq$4j $\geq$4b category is further divided into two subcategories.

The all-hadronic final-state analysis selects events that contain at least seven jets, at least three of which are tagged as b jets. These events are divided into seven categories: 7j 3b, 7j $\geq$4b, 8j 3b, 8j $\geq$4b, $\geq$9j 3b, and $\geq$9j $\geq$4b. Events containing electrons or muons are vetoed to maintain an orthogonal selection to the leptonic final state analysis. The dominant background is QCD multijet production, with other important backgrounds coming from tt+jets processes.

The dominant experimental uncertainties in the measurement of the rate of ttH production with H $\to$ bb decay in the leptonic and all-hadronic final states are due to uncertainties in the determination of the ttbb backgrounds and b tagging efficiencies. In the all-hadronic final state, the uncertainty in the determination of the QCD multijet background also has a significant contribution to the overall systematic uncertainty.

3.8 Search for H $\to \mu\mu$

The H $\to \mu\mu$ search [73] is the only analysis included here that is sensitive to the coupling of the Higgs boson to second-generation fermions. The analysis searches for a narrow peak in the dimuon invariant mass ($m_{\mu\mu}$) spectrum above a large continuum background from DY production of muon pairs. Events are categorized using variables that are uncorrelated with $m_{\mu\mu}$, in order to avoid introducing an irregular shape in the background spectrum. Variables that distinguish between the ggH and VBF signals, and the DY and tt backgrounds, are used to define event categories with varying signal-to-background ratios. The categories are further divided based on the momentum of the muon with the largest $|\eta|$ in the dimuon pair, to exploit the differences in the $m_{\mu\mu}$ resolution. Since there are more variables associated with VBF production that can be used to separate signal and background, the events with the highest BDT output value are most compatible with that process.

In each event category, the background is estimated from a fit to the observed $m_{\mu\mu}$ distribution. As in the H $\to \gamma\gamma$ analysis, the parameters of the functions used to describe the background contribute to the statistical uncertainty in the measurements. This is the dominant source of uncertainty in constraining the rate of Higgs boson decay in the H $\to \mu\mu$ decay channel. The observed upper limit on the cross section times branching fraction of H $\to \mu\mu$ obtained in Ref. [73] is 2.93 times the SM value.

3.9 Search for H $\to$ invisible

The direct search for the Higgs boson decaying into particles that cannot be detected provides a constraint on the invisible Higgs boson branching fraction ($\mathcal{B}_{\text{inv}}$), which is predicted to be enhanced in BSM scenarios [25–28,74]. The search is performed using events with large $p_{\text{T}}^{\text{miss}}$, and containing additional particles consistent with Higgs boson production via the VBF [75], ZH with Z $\to \ell\ell$ [76], VH with the W or Z boson decaying hadronically, or ggH modes [77].

Events selected in the VBF category are required to contain two jets, with a large m_{jj} and a large $\Delta\eta_{\text{jj}}$. The VH hadronic and ggH categories comprise events containing either a high-p_{T} AK8 jet, consistent with a boosted, hadronically decaying vector boson, or a jet from initial-state radiation, reconstructed in the fiducial volume of the tracker. The dominant backgrounds in these categories are due to the Z($\nu\nu$)+jets and W($\ell\nu$)+jets processes. These are estimated from dedicated lepton and photon CRs in data. In all three categories, the dominant uncertainties are related to the extrapolation of the lepton and photon CRs to determine the Z($\nu\nu$)+jets and W($\ell\nu$)+jets backgrounds in the SR.

The ZH leptonic category is defined by selecting events that contain a pair of oppositely charged electrons or muons consistent with the decay of a Z boson. The dominant backgrounds arise from Z($\ell\ell$)Z($\nu\nu$) and W($\ell\nu$)Z($\nu\nu$) diboson production and are estimated using a combination of CRs in data containing additional leptons, and simulated events. The dominant uncertainty in this category is related to theoretical uncertainties in the higher-order corrections used in the simulation of these backgrounds.

The observed upper limit on the branching fraction of H $\to$ invisible assuming SM Higgs production rates is 26% [75]. As described later in Sect. 8, the H $\to$ invisible analyses are included only in models for which a nonzero invisible branching fraction of the Higgs boson is considered.

4 Modifications to the input analyses

This section describes the changes in each analysis, as implemented for this combination, compared to their respective publications.

4.1 Gluon fusion modeling

In order to consistently combine the various analyses, it is necessary to use the same theoretical predictions for the signal. The most significant difference between the input analyses is the modeling of the dominant ggH production mode in the $H \to ZZ$, $H \to \tau\tau$, $H \to \gamma\gamma$, and $H \to WW$ decay channels. The published results in these analyses used different generators with next-to-leading order matrix elements merged with parton showering (NLO+PS). In order to synchronize these analyses and take advantage of the most accurate simulation of ggH available, a reweighting is applied. Gluon fusion events are generated using the POWHEG 2.0 [78–81], MADGRAPH5_aMC@NLO version 2.2.2 [82,83], and NNLOPS [84,85] generators. The NNLOPS simulation, which is the highest order parton shower matched ggH simulation available, includes the effects of finite quark masses. Events are separated into 0, 1, 2, and $\geq$3 jet bins, where the jets used for counting are clustered from all stable particles, excluding the decay products of the Higgs boson or associated vector bosons, and have $p_T > 30$ GeV. The sums of weights in each sample are first normalized to the inclusive N^{3}LO cross section. The ratio of the $p_T(H)$ distribution from the NNLOPS generator to that from the POWHEG or MADGRAPH5_aMC@NLO generators in each jet bin is applied to the ggH signal samples. The reweighting procedure has been checked against fully simulated NNLOPS samples in the $H \to \gamma\gamma$ and $H \to \tau\tau$ decay channels and was found to give results compatible within the statistical uncertainty of the simulated samples. The $H \to \mu\mu$ and boosted $H \to bb$ analyses, which are much less sensitive to ggH production than other decay channels, use the NLO + PS simulation.

4.2 Theoretical uncertainties in gluon fusion

The ggH cross section uncertainty scheme for the $H \to ZZ$ and $H \to \tau\tau$ decay channels has been updated to the one proposed in Ref. [53], as already used in the $H \to \gamma\gamma$ and $H \to WW$ analyses. This uncertainty scheme includes 9 nuisance parameters accounting for uncertainties in the cross section prediction for exclusive jet bins (including the migration between the 0- and 1-jet, as well as between the 1- and $\geq$2-jet bins), the 2-jet and $\geq$3-jet VBF phase spaces, different $p_T(H)$ regions, and the uncertainty in the $p_T(H)$ distribution due to missing higher-order finite top quark mass corrections. The boosted $H \to bb$ search, which is only sensitive to ggH in the high $p_T(H)$ tail, uses a dedicated prediction in this region, and hence the theoretical uncertainties assigned are assumed to be uncorrelated with the other analyses.

4.3 Statistical uncertainties in simulation

In the combination, many of the nuisance parameters originate from the use of a limited number of Monte Carlo events to determine SM signal and background expectations. Some of the input analyses have been modified to use the "Barlow-Beeston lite" approach, which assigns a single nuisance parameter per bin that scales the total bin yield [86,87]. This differs from the previous implementation, which utilized separate nuisance parameters for each process per bin. With the Barlow-Beeston approach, the maximum likelihood estimator for each of these nuisance parameters is independent from the others, and can be solved for analytically. This has been found to provide a significant reduction in the minimization time, while reproducing the results obtained with the full treatment to within 1%.

5 Combination procedure

The overall statistical methodology used in this combination is the same as the one developed by the ATLAS and CMS Collaborations, and described in Ref. [56]. The procedures used in this paper are described in more detail in Refs. [14,88,89] and are based on the standard LHC data modeling and handling toolkits ROOFIT [90] and ROOSTATS [91].

The parameters of interest (POI) $\vec{\alpha}$ for a particular model are estimated with their corresponding confidence intervals using a profile likelihood ratio test statistic $q(\vec{\alpha})$ [92], in which experimental or theoretical uncertainties are incorporated via nuisance parameters (NP) $\vec{\theta}$:

$$q(\vec{\alpha}) = -2\ln\left(\frac{L(\vec{\alpha}, \hat{\hat{\theta}}_{\vec{\alpha}})}{L(\hat{\hat{\alpha}}, \hat{\hat{\theta}})}\right). \quad (1)$$

The likelihood functions in the numerator and denominator of Eq. (1) are constructed using products of probability density functions of signal and background for the various discriminating variables used in the input analyses, as well as constraint terms for certain NPs. The probability density functions are derived from simulation for the signal and from both data and simulation for the background. The quantities $\hat{\hat{\alpha}}$ and $\hat{\hat{\theta}}$ denote the unconditional maximum likelihood estimates of the parameter values, while $\hat{\hat{\theta}}_{\vec{\alpha}}$ denotes the conditional maximum likelihood estimate for fixed values of the parameters of interest $\vec{\alpha}$. The choice of the POIs, e.g., signal strengths (μ), couplings modifiers, production cross sections, branching fractions or related ratios of the above quantities, depends on the specific model under consideration, while the remaining parameters are treated as NPs. An individual NP represents a single source of systematic uncertainty, and its effect is therefore considered fully correlated between all of the input analyses included in the fit.

For each model considered, the maximum likelihood estimates $\hat{\vec{\alpha}}$ are identified as the best fit parameter values. The 1σ and 2σ confidence level (CL) intervals for one-dimensional measurements of each POI are determined as the union of intervals for which $q(\vec{\alpha}) < 1$ and $q(\vec{\alpha}) < 4$, respectively, unless otherwise stated. In models with more than one POI, these intervals are determined treating the other POIs as NPs. The differences between the boundaries of the 1σ and 2σ CL intervals and the best fit value yield the $\pm 1\sigma$ and $\pm 2\sigma$ uncertainties on the measurement. In cases where a physical boundary restricts the interval, we report a truncated interval and determine the uncertainty from that interval. (See Fig. 6 and Table 3, for example). In these cases, the intervals are not expected to maintain coverage. In the case where the intervals are not contiguous, the interval that contains the best fit point is used to determine these uncertainties. The 2D 1σ and 2σ CL regions are determined from the set of parameter values for which $q(\vec{\alpha}) < 2.30$ and $q(\vec{\alpha}) < 6.18$, respectively, unless otherwise stated.

The likelihood functions are constructed with respect to either the observed data or an Asimov data set [92] constructed using the expected values of the POIs for the SM, in order to obtain the observed or expected results, respectively. Because of fluctuations in the observed data the observed intervals may differ from the expected ones.

Finally, the SM predictions for the production and decay rates of the Higgs boson depend on the mass of the Higgs boson, m_{H}. For all measurements in this paper, the mass is taken to be $m_{\mathrm{H}} = 125.09 \pm 0.21(\mathrm{stat}) \pm 0.11(\mathrm{syst})$ GeV, determined from the ATLAS and CMS combined measurement, from the LHC Run 1 data, using the high-resolution $\mathrm{H} \to \gamma\gamma$ and $\mathrm{H} \to \mathrm{ZZ}^{(*)} \to 4\ell$ decay channels [93].

6 Systematic uncertainties

For many of the POIs, the systematic uncertainties in their determination are expected to be as large as, or larger than, the statistical uncertainties. The theoretical uncertainties affecting the signal are among the most important contributions to the systematic uncertainties. The uncertainties in the total cross section prediction for the signal processes arising from the parton distribution functions, the renormalization and factorization scales used in the calculations and the branching fraction predictions are correlated between all input analyses. Instead, theoretical uncertainties that affect kinematic distributions and cause migrations between event categories are largely uncorrelated between the input analyses. An exception is the set of theoretical uncertainties for the ggH production mode, where the correlation scheme described in Sect. 4.2 is used to correlate both the normalization and shape uncertainties between input analyses. The theoretical uncertainties affecting the background predictions, including the parton distribution function uncertainties, are assumed to be uncorrelated with those affecting the signal predictions [88], with the exception of the uncertainties from the underlying event and parton shower model.

The majority of the systematic uncertainties arising from experimental sources are uncorrelated between the input analyses, with a few exceptions. The uncertainties in the integrated luminosity measurement [94], and in the modeling of additional collisions in the event (pileup), are correlated between all of the input input analyses. Certain analyses, namely the $\mathrm{H} \to \tau\tau$, VH(bb), and ttH(bb) analyses, are able to further constrain the jet energy scale uncertainties determined in auxiliary measurements. The jet energy scale uncertainty in these analyses is decomposed into several nuisance parameters corresponding to different sources of uncertainty (for example, different flavor composition and kinematic regions) that are correlated among these analyses but uncorrelated with the other analyses. An independent jet energy scale uncertainty is assumed to be correlated between the input analyses that are not sensitive to the different sources of uncertainty. The uncertainties in the b tagging efficiency are correlated between the ttH analyses, but are uncorrelated from the VH(bb) analysis, which is sensitive to different kinematic regions. A separate set of NPs is used to describe the uncertainty in the b tagging efficiency in the $\mathrm{H} \to \mathrm{WW}$, $\mathrm{H} \to \gamma\gamma$, and $\mathrm{H} \to \mathrm{ZZ}$ analyses. The uncertainty in the efficiency of the double-b-tagger algorithm described in Sect. 3.6 is taken to be uncorrelated from the single b tagging uncertainties. Finally, the uncertainties in the lepton efficiency and misidentification rate in the ttH-τ_{h} and ttH-e/μ event classes are correlated, since the same reconstruction and identification algorithms were used. In other input analyses, different algorithms were used and therefore the uncertainties are assumed to be uncorrelated.

The free parameters describing the shapes and normalizations of the background models, and parameters that allow for the choice of the background parametrization in each of the $\mathrm{H} \to \gamma\gamma$ analysis categories are fully determined by the data without any additional constraints, and are therefore assigned to the statistical uncertainty of a measurement. The remaining uncertainties are assigned to groups of systematic uncertainties.

7 Signal strength and cross section fits

The signal strength modifier μ, defined as the ratio between the measured Higgs boson yield and its SM expectation, has been used extensively to characterize the Higgs boson yields. However, the specific meaning of μ varies depending on the analysis. For a specific production and decay channel $i \to H \to f$, the signal strengths for the production, μ_i, and for the decay, μ^f, are defined as:

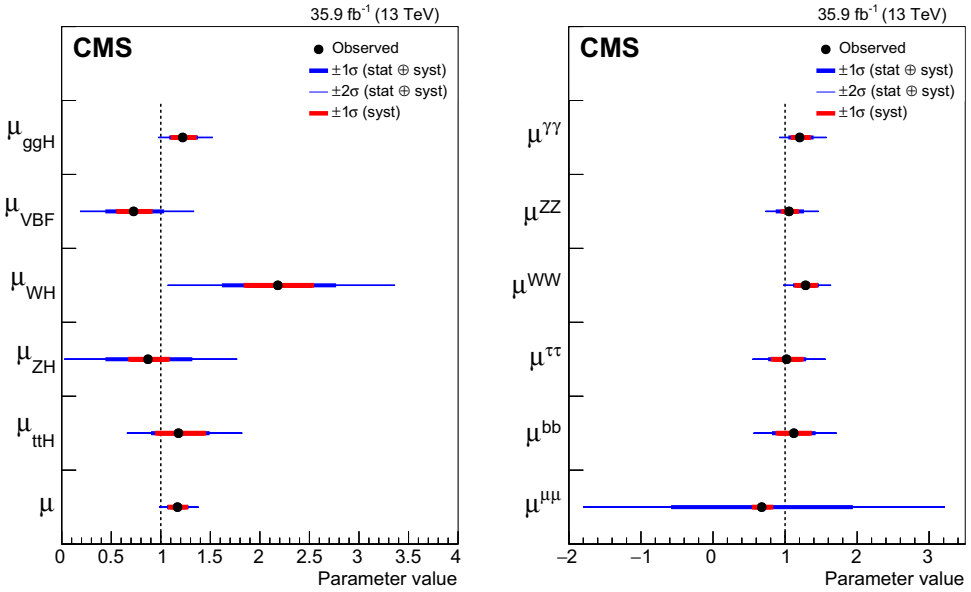

Fig. 5 Summary plot of the fit to the per-production mode (left) and per-decay mode (right) signal strength modifiers. The thick and thin horizontal bars indicate the $\pm 1\sigma$ and $\pm 2\sigma$ uncertainties, respectively. Also shown are the $\pm 1\sigma$ systematic components of the uncertainties. The last point in the per-production mode summary plot is taken from a separate fit and indicates the result of the combined overall signal strength μ

$$\mu_i = \frac{\sigma_i}{(\sigma_i)_{\mathrm{SM}}} \quad \text{and} \quad \mu^f = \frac{\mathcal{B}^f}{(\mathcal{B}^f)_{\mathrm{SM}}}, \tag{2}$$

respectively. Here σ_i (i = ggH, VBF, WH, ZH, ttH) and $\mathcal{B}^f$ (f = ZZ, WW, $\gamma\gamma$, $\tau\tau$, bb, $\mu\mu$) are, respectively, the production cross section for $i \to \mathrm{H}$ and the branching fraction for $\mathrm{H} \to f$. The subscript "SM" refers to their respective SM predictions, so by definition, the SM corresponds to $\mu_i = \mu^f = 1$. Since σ_i and $\mathcal{B}^f$ cannot be separately measured without additional assumptions, only the product of μ_i and μ^f can be extracted experimentally, leading to a signal strength μ_i^f for the combined production and decay:

$$\mu_i^f = \frac{\sigma_i \mathcal{B}^f}{(\sigma_i)_{\mathrm{SM}}(\mathcal{B}^f)_{\mathrm{SM}}} = \mu_i \mu^f. \tag{3}$$

This parametrization makes use of the narrow width approximation, and the reliability of this approximation was studied in Ref. [95] and found to be adequate for global fits.

In this section, results are presented for several signal strength parametrizations starting with a single global signal strength μ, which is the most restrictive in terms of the number of assumptions. Further parametrizations are defined by relaxing the constraint that all production and decay rates scale with a common signal strength modifier.

The combined measurement of the common signal strength modifier at $m_{\mathrm{H}} = 125.09$ GeV is,

$$\begin{aligned}\mu &= 1.17 \pm 0.10 \\ &= 1.17 \pm 0.06\,(\mathrm{stat})\,^{+0.06}_{-0.05}\,(\mathrm{sig\ theo}) \pm 0.06\,(\mathrm{other\ syst}),\end{aligned} \tag{4}$$

where the total uncertainty has been decomposed into statistical, signal theoretical systematic, and other systematic components. The largest single source of uncertainty apart from the signal theoretical systematic uncertainties is the integrated luminosity ($\Delta\mu/\mu = 2.5\%$), which is correlated between all of the input analyses. In this measurement and others, however, the other systematic uncertainty component is mostly dominated by uncertainties that only affect a single input analysis.

Relaxing the assumption of a common production mode scaling, but still assuming the relative SM branching fractions, leads to a parametrization with five production signal strength modifiers: μ_{ggH}, μ_{VBF}, μ_{WH}, μ_{ZH}, and μ_{ttH}. In this parametrization, as well as all subsequent parametrizations involving signal strengths or cross sections, the tH production is assumed to scale like ttH. Conversely, relaxing the common decay mode scaling, but assuming the relative SM production cross sections, leads to one with the modifiers: $\mu^{\gamma\gamma}$, μ^{ZZ}, μ^{WW}, $\mu^{\tau\tau}$, $\mu^{\mu\mu}$, and μ^{bb}. Results of the fits in these two parametrizations are summarized in Fig. 5. The numerical values, including the decomposition of the uncertainties into statistical and systematic components, and the corresponding expected uncertainties, are given in Table 2.

The improvement in the precision of the measurement of the ggH production rate of ∼50% (from ∼20% to ∼10%) compared to Ref. [55] and ∼33% (from ∼15% to ∼10%) compared to Ref. [56], can be attributed to the combined effects of an increased ggH production cross section, and a reduction in the associated theoretical uncertainties. The improvements in the precision are up to ∼20% for the VBF and VH production rates compared to Ref. [55]. The uncertainty in the measurement of the ttH production rate is reduced by around 50% compared to Ref. [56]. This is in

Table 2 Best fit values and $\pm 1\sigma$ uncertainties for the parametrizations with per-production mode and per-decay mode signal strength modifiers. The expected uncertainties are given in brackets

Production process	Best fit value		Uncertainty	
			stat.	syst.
ggH	1.22	$^{+0.14}_{-0.12}$	$^{+0.08}_{-0.08}$	$^{+0.12}_{-0.10}$
		$(^{+0.11}_{-0.11})$	$(^{+0.07}_{-0.07})$	$(^{+0.09}_{-0.08})$
VBF	0.73	$^{+0.30}_{-0.27}$	$^{+0.24}_{-0.23}$	$^{+0.17}_{-0.15}$
		$(^{+0.29}_{-0.27})$	$(^{+0.24}_{-0.23})$	$(^{+0.16}_{-0.15})$
WH	2.18	$^{+0.58}_{-0.55}$	$^{+0.46}_{-0.45}$	$^{+0.34}_{-0.32}$
		$(^{+0.53}_{-0.51})$	$(^{+0.43}_{-0.42})$	$(^{+0.30}_{-0.29})$
ZH	0.87	$^{+0.44}_{-0.42}$	$^{+0.39}_{-0.38}$	$^{+0.20}_{-0.18}$
		$(^{+0.43}_{-0.41})$	$(^{+0.38}_{-0.37})$	$(^{+0.19}_{-0.17})$
ttH	1.18	$^{+0.30}_{-0.27}$	$^{+0.16}_{-0.16}$	$^{+0.26}_{-0.21}$
		$(^{+0.28}_{-0.25})$	$(^{+0.16}_{-0.15})$	$(^{+0.23}_{-0.20})$
Decay mode	**Best fit value**		**Uncertainty**	
			stat.	syst.
$H \to bb$	1.12	$^{+0.29}_{-0.29}$	$^{+0.19}_{-0.18}$	$^{+0.22}_{-0.22}$
		$(^{+0.28}_{-0.27})$	$(^{+0.18}_{-0.18})$	$(^{+0.21}_{-0.20})$
$H \to \tau\tau$	1.02	$^{+0.26}_{-0.24}$	$^{+0.15}_{-0.15}$	$^{+0.21}_{-0.19}$
		$(^{+0.24}_{-0.22})$	$(^{+0.15}_{-0.14})$	$(^{+0.19}_{-0.17})$
$H \to WW$	1.28	$^{+0.17}_{-0.16}$	$^{+0.09}_{-0.09}$	$^{+0.14}_{-0.13}$
		$(^{+0.14}_{-0.13})$	$(^{+0.09}_{-0.09})$	$(^{+0.11}_{-0.10})$
$H \to ZZ$	1.06	$^{+0.19}_{-0.17}$	$^{+0.16}_{-0.15}$	$^{+0.11}_{-0.08}$
		$(^{+0.18}_{-0.16})$	$(^{+0.15}_{-0.14})$	$(^{+0.10}_{-0.08})$
$H \to \gamma\gamma$	1.20	$^{+0.18}_{-0.14}$	$^{+0.13}_{-0.11}$	$^{+0.12}_{-0.09}$
		$(^{+0.14}_{-0.12})$	$(^{+0.10}_{-0.10})$	$(^{+0.09}_{-0.07})$
$H \to \mu\mu$	0.68	$^{+1.25}_{-1.24}$	$^{+1.24}_{-1.24}$	$^{+0.13}_{-0.11}$
		$(^{+1.20}_{-1.17})$	$(^{+1.18}_{-1.17})$	$(^{+0.19}_{-0.03})$

part due to the increase in the ttH cross section between 8 and 13 TeV, but also due to the inclusion of additional exclusive event categories for this production process.

The most generic signal strength parametrization has one signal strength parameter for each production and decay mode combination, μ_i^f. Given the five production and six decay modes listed above, this implies a model with 30 parameters of interest. However not all can be experimentally constrained in this combination. There is no dedicated analysis from CMS at $\sqrt{s} = 13$ TeV targeting WH and ZH production with $H \to \tau\tau$ decay, or VBF production with $H \to bb$ decay, therefore these signal strength modifiers are fixed to the SM expectation and are not included in the maximum likelihood fit. Likewise, the WH, ZH, and ttH production rates with $H \to \mu\mu$ decay are fixed to the SM expectation. In the case of WH, ZH, and ttH production with $H \to ZZ$ decay, as well as ZH production with $H \to \gamma\gamma$

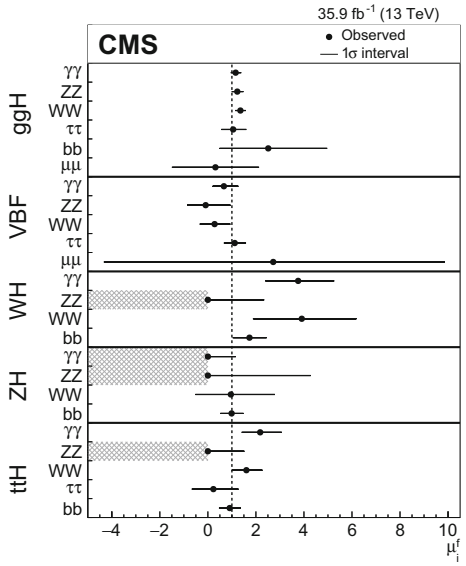

Fig. 6 Summary plot of the fit to the production–decay signal strength products $\mu_i^f = \mu_i \mu^f$. The points indicate the best fit values while the horizontal bars indicate the 1σ CL intervals. The hatched areas indicate signal strengths that are restricted to nonnegative values as described in the text

decay, the background contamination is sufficiently low so that a negative signal strength can result in an overall negative event yield. Therefore, these signal strengths are restricted to nonnegative values. Figure 6 summarizes the results in this model along with the 1σ CL intervals. The numerical values, including the uncertainty decomposition into statistical and systematic parts, and the corresponding expected uncertainties, are given in Table 3.

7.1 Ratios of cross sections and branching fractions, relative to ggH $\to$ ZZ

Results are presented for a model based on the ratios of cross sections and branching fractions. These are given relative to a well-measured reference process, chosen to be ggH $\to$ ZZ (μ_{ggH}^{ZZ}). Using ratios has the advantage that some systematic or theoretical uncertainties common to both the numerator and denominator cancel. The following ratios are used: $\mu^{\gamma\gamma}/\mu^{ZZ}$, μ^{WW}/μ^{ZZ}, $\mu^{\tau\tau}/\mu^{ZZ}$,$\mu^{\mu\mu}/\mu^{ZZ}$, μ^{bb}/μ^{ZZ}, μ_{VBF}/μ_{ggH}, μ_{WH}/μ_{ggH}, μ_{ZH}/μ_{ggH}, and μ_{ttH}/μ_{ggH}. These results are summarized in Fig. 7, and the numerical values are given in Table 4. The uncertainties in the SM predictions are included in the measurements.

7.2 Stage 0 simplified template cross sections

Measurements of production cross sections, which are complementary to the signal strength parametrization, are made for seven processes defined according to the simplified tem-

Table 3 Best fit values and $\pm 1\sigma$ uncertainties for the parameters of the model with one signal strength parameter for each production and decay mode combination. The entries in the table represent the parameter $\mu_i^f = \mu_i \mu^f$, where i is indicated by the column and f by the row. The expected uncertainties are given in brackets. Some of the signal strengths are restricted to nonnegative values, as described in the text

Decay mode	Production process																	
	ggH				VBF				WH				ZH				ttH			
	Best fit		Uncertainty		Best fit		Uncertainty		Best fit		Uncertainty		Best fit		Uncertainty		Best fit		Uncertainty	
	value		stat.	syst.	value		stat.	syst.	value		stat.	syst.	value		stat.	syst.	value		stat.	syst.
$H \to bb$	2.51	$^{+2.43}_{-2.01}$	$^{+1.96}_{-1.92}$	$^{+1.44}_{-0.59}$	—				1.73	$^{+0.70}_{-0.68}$	$^{+0.53}_{-0.51}$	$^{+0.46}_{-0.45}$	0.99	$^{+0.47}_{-0.45}$	$^{+0.41}_{-0.40}$	$^{+0.23}_{-0.20}$	0.91	$^{+0.45}_{-0.43}$	$^{+0.24}_{-0.23}$	$^{+0.38}_{-0.36}$
		$(^{+2.06}_{-1.86})$	$(^{+1.85}_{-1.83})$	$(^{+0.89}_{-0.33})$	—					$(^{+0.69}_{-0.67})$	$(^{+0.52}_{-0.51})$	$(^{+0.45}_{-0.44})$		$(^{+0.46}_{-0.44})$	$(^{+0.40}_{-0.39})$	$(^{+0.23}_{-0.20})$		$(^{+0.44}_{-0.42})$	$(^{+0.23}_{-0.23})$	$(^{+0.37}_{-0.35})$
$H \to \tau\tau$	1.05	$^{+0.53}_{-0.47}$	$^{+0.25}_{-0.25}$	$^{+0.46}_{-0.40}$	1.12	$^{+0.45}_{-0.43}$	$^{+0.37}_{-0.35}$	$^{+0.25}_{-0.25}$	—				—				0.23	$^{+1.03}_{-0.88}$	$^{+0.80}_{-0.71}$	$^{+0.65}_{-0.52}$
		$(^{+0.45}_{-0.41})$	$(^{+0.23}_{-0.23})$	$(^{+0.38}_{-0.34})$		$(^{+0.45}_{-0.43})$	$(^{+0.37}_{-0.35})$	$(^{+0.25}_{-0.24})$	—				—					$(^{+0.98}_{-0.87})$	$(^{+0.80}_{-0.73})$	$(^{+0.56}_{-0.47})$
$H \to WW$	1.35	$^{+0.21}_{-0.19}$	$^{+0.12}_{-0.12}$	$^{+0.17}_{-0.15}$	0.28	$^{+0.64}_{-0.60}$	$^{+0.58}_{-0.53}$	$^{+0.28}_{-0.28}$	3.91	$^{+2.26}_{-2.01}$	$^{+1.89}_{-1.72}$	$^{+1.24}_{-1.05}$	0.96	$^{+1.81}_{-1.46}$	$^{+1.74}_{-1.44}$	$^{+0.50}_{-0.22}$	1.60	$^{+0.65}_{-0.59}$	$^{+0.40}_{-0.39}$	$^{+0.52}_{-0.45}$
		$(^{+0.17}_{-0.16})$	$(^{+0.10}_{-0.10})$	$(^{+0.13}_{-0.12})$		$(^{+0.62}_{-0.58})$	$(^{+0.57}_{-0.53})$	$(^{+0.26}_{-0.25})$		$(^{+1.47}_{-1.19})$	$(^{+1.32}_{-1.06})$	$(^{+0.64}_{-0.54})$		$(^{+1.67}_{-1.37})$	$(^{+1.61}_{-1.35})$	$(^{+0.45}_{-0.20})$		$(^{+0.56}_{-0.53})$	$(^{+0.38}_{-0.38})$	$(^{+0.41}_{-0.37})$
$H \to ZZ$	1.22	$^{+0.23}_{-0.21}$	$^{+0.20}_{-0.19}$	$^{+0.12}_{-0.10}$	−0.09	$^{+1.02}_{-0.76}$	$^{+1.00}_{-0.72}$	$^{+0.21}_{-0.22}$	0.00	$^{+2.33}_{+0.00}$	$^{+2.31}_{-0.00}$	$^{+0.30}_{-0.00}$	0.00	$^{+4.26}_{+0.00}$	$^{+4.19}_{-0.00}$	$^{+0.80}_{-0.00}$	0.00	$^{+1.50}_{+0.00}$	$^{+1.47}_{-0.00}$	$^{+0.30}_{-0.00}$
		$(^{+0.22}_{-0.20})$	$(^{+0.20}_{-0.19})$	$(^{+0.10}_{-0.07})$		$(^{+1.27}_{-0.99})$	$(^{+1.25}_{-0.97})$	$(^{+0.23}_{-0.21})$		$(^{+4.46}_{-0.99})$	$(^{+4.42}_{-0.99})$	$(^{+0.57}_{-0.00})$		$(^{+7.57}_{-1.00})$	$(^{+7.45}_{-1.00})$	$(^{+1.33}_{-0.00})$		$(^{+2.95}_{-0.99})$	$(^{+2.89}_{-0.99})$	$(^{+0.59}_{-0.00})$
$H \to \gamma\gamma$	1.16	$^{+0.21}_{-0.18}$	$^{+0.17}_{-0.15}$	$^{+0.13}_{-0.10}$	0.67	$^{+0.59}_{-0.46}$	$^{+0.49}_{-0.42}$	$^{+0.32}_{-0.18}$	3.76	$^{+1.48}_{-1.35}$	$^{+1.45}_{-1.33}$	$^{+0.33}_{-0.24}$	0.00	$^{+1.14}_{+0.00}$	$^{+1.14}_{-0.00}$	$^{+0.09}_{-0.00}$	2.18	$^{+0.88}_{-0.75}$	$^{+0.82}_{-0.74}$	$^{+0.32}_{-0.14}$
		$(^{+0.17}_{-0.16})$	$(^{+0.14}_{-0.14})$	$(^{+0.11}_{-0.08})$		$(^{+0.59}_{-0.48})$	$(^{+0.48}_{-0.43})$	$(^{+0.34}_{-0.21})$		$(^{+1.28}_{-1.16})$	$(^{+1.27}_{-1.16})$	$(^{+0.13}_{-0.06})$		$(^{+2.51}_{-1.04})$	$(^{+2.50}_{-1.04})$	$(^{+0.25}_{-0.00})$		$(^{+0.74}_{-0.63})$	$(^{+0.72}_{-0.63})$	$(^{+0.16}_{-0.06})$
$H \to \mu\mu$	0.31	$^{+1.80}_{-1.79}$	$^{+1.79}_{-1.78}$	$^{+0.19}_{-0.19}$	2.72	$^{+7.12}_{-7.03}$	$^{+7.12}_{-7.04}$	$^{+0.26}_{-0.00}$	—				—				—			
		$(^{+1.69}_{-1.65})$	$(^{+1.67}_{-1.67})$	$(^{+0.28}_{-0.00})$		$(^{+7.02}_{-6.94})$	$(^{+7.01}_{-6.93})$	$(^{+0.38}_{-0.50})$	—				—				—			

Table 4 Best fit values and $\pm 1\sigma$ uncertainties for the parameters of the cross section and branching fraction ratio model. The expected uncertainties are given in brackets

Parameter	Best fit		Uncertainty		Parameter	Best fit		Uncertainty	
			stat.	syst.				stat.	syst.
μ^{ZZ}_{ggH}	1.07	$^{+0.20}_{-0.18}$	$^{+0.16}_{-0.15}$	$^{+0.11}_{-0.09}$	$\mathcal{B}^{bb}/\mathcal{B}^{ZZ}$	0.84	$^{+0.37}_{-0.27}$	$^{+0.27}_{-0.21}$	$^{+0.26}_{-0.17}$
		$(^{+0.19}_{-0.16})$	$(^{+0.15}_{-0.14})$	$(^{+0.11}_{-0.08})$			$(^{+0.56}_{-0.37})$	$(^{+0.38}_{-0.28})$	$(^{+0.40}_{-0.25})$
μ_{VBF}/μ_{ggH}	0.60	$^{+0.30}_{-0.24}$	$^{+0.24}_{-0.21}$	$^{+0.17}_{-0.13}$	$\mathcal{B}^{\tau\tau}/\mathcal{B}^{ZZ}$	1.07	$^{+0.37}_{-0.30}$	$^{+0.25}_{-0.21}$	$^{+0.27}_{-0.22}$
		$(^{+0.40}_{-0.32})$	$(^{+0.31}_{-0.27})$	$(^{+0.24}_{-0.17})$			$(^{+0.35}_{-0.28})$	$(^{+0.25}_{-0.20})$	$(^{+0.25}_{-0.19})$
μ_{WH}/μ_{ggH}	2.19	$^{+0.86}_{-0.69}$	$^{+0.68}_{-0.56}$	$^{+0.52}_{-0.39}$	$\mathcal{B}^{WW}/\mathcal{B}^{ZZ}$	1.23	$^{+0.27}_{-0.22}$	$^{+0.22}_{-0.18}$	$^{+0.16}_{-0.13}$
		$(^{+0.65}_{-0.52})$	$(^{+0.53}_{-0.44})$	$(^{+0.39}_{-0.29})$			$(^{+0.24}_{-0.19})$	$(^{+0.19}_{-0.16})$	$(^{+0.14}_{-0.11})$
μ_{ZH}/μ_{ggH}	0.88	$^{+0.57}_{-0.44}$	$^{+0.49}_{-0.41}$	$^{+0.30}_{-0.17}$	$\mathcal{B}^{\gamma\gamma}/\mathcal{B}^{ZZ}$	1.14	$^{+0.28}_{-0.20}$	$^{+0.23}_{-0.18}$	$^{+0.16}_{-0.09}$
		$(^{+0.68}_{-0.47})$	$(^{+0.53}_{-0.41})$	$(^{+0.43}_{-0.23})$			$(^{+0.23}_{-0.18})$	$(^{+0.20}_{-0.16})$	$(^{+0.11}_{-0.08})$
μ_{ttH}/μ_{ggH}	1.06	$^{+0.34}_{-0.27}$	$^{+0.20}_{-0.18}$	$^{+0.27}_{-0.20}$	$\mathcal{B}^{\mu\mu}/\mathcal{B}^{ZZ}$	0.63	$^{+1.24}_{-1.21}$	$^{+1.24}_{-1.20}$	$^{+0.15}_{-0.11}$
		$(^{+0.36}_{-0.30})$	$(^{+0.23}_{-0.21})$	$(^{+0.27}_{-0.21})$			$(^{+1.26}_{-1.19})$	$(^{+1.25}_{-1.19})$	$(^{+0.20}_{-0.03})$

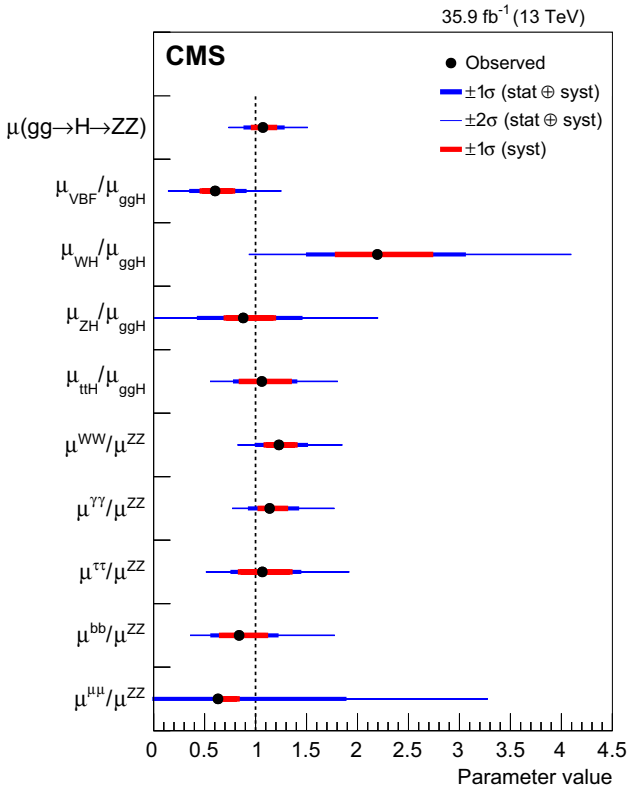

Fig. 7 Summary of the cross section and branching fraction ratio model. The thick and thin horizontal bars indicate the $\pm 1\sigma$ and $\pm 2\sigma$ uncertainties, respectively. Also shown are the $\pm 1\sigma$ systematic components of the uncertainties

plate cross sections proposed in Ref. [53]. The results given here are for the stage 0 fiducial regions defined by the rapidity of the Higgs boson $|y_H| < 2.5$. All input analyses have a negligible acceptance for $|y_H| > 2.5$. Defining the fiducial region in this way reduces the theoretical uncertainty that would otherwise apply while extrapolating to the fully inclusive phase space. Subsequent stages involve splitting the fiducial regions into a number of smaller ones, for example based on ranges of the Higgs boson p_T. The measured cross sections are defined as:

- $\sigma_{ggH+bbH}$: gluon fusion and b-associated production. While Ref. [53] proposes separate bins for these modes, they are merged here because of the current lack of sensitivity to the associated production with b quarks.
- σ_{VBF}: VBF production.
- $\sigma_{H+V(qq)}$: Associated production with a Z or W boson, either quark or gluon initiated, in which the vector boson decays hadronically.
- $\sigma_{H+Z(\ell\ell/\nu\nu)}$: Associated production with a Z boson, in which the Z boson decays leptonically. While Ref. [53] proposes separate bins for the quark- and gluon-initiated modes, they are merged here because they cannot easily be distinguished experimentally, and therefore, their measurements would be highly anticorrelated.
- $\sigma_{H+W(\ell\nu)}$: Associated production with a W boson, in which the W decays leptonically.
- σ_{ttH+tH}: Associated production with a pair of top quarks or a single top quark. While Ref. [53] proposes separate bins for these modes, they are merged here because of the lack of a dedicated analysis targeting tH production in this combination.

In addition to the cross sections, the Higgs boson branching fractions are also included as POIs via ratios with respect to $\mathcal{B}^{ZZ}$. A summary of the results in this model, normalized to the expected SM cross sections, is given in Fig. 8 and Table 5. Since cross sections are measured and not signal strength modifiers, the theoretical uncertainties in these cross sections do not enter as sources of uncertainty. In Fig. 8, the uncertainties in the SM predictions are indicated by gray bands.

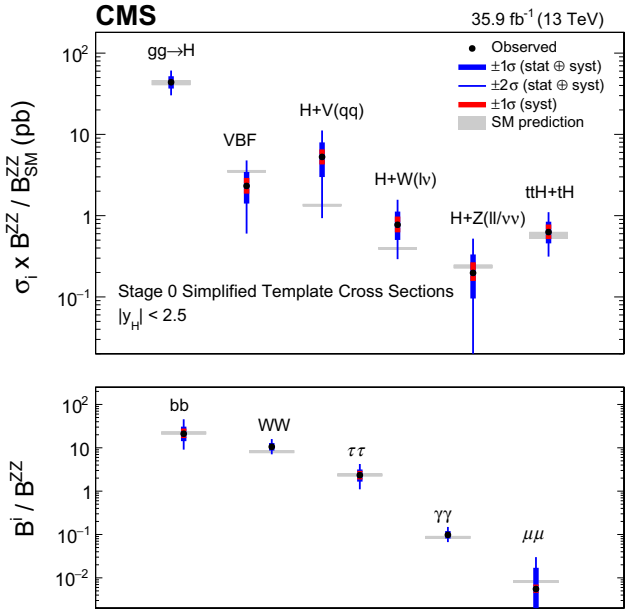

Fig. 8 Summary of the stage 0 model, ratios of cross sections and branching fractions. The points indicate the best fit values, while the error bars show the $\pm 1\sigma$ and $\pm 2\sigma$ uncertainties. The $\pm 1\sigma$ uncertainties on the measurements considering only the contributions from the systematic uncertainties are also shown. The uncertainties in the SM predictions are indicated

8 Measurements of Higgs boson couplings

In the κ-framework [96], coupling modifiers are introduced in order to test for deviations in the couplings of the Higgs boson to other particles. In order to measure the individual Higgs couplings in this framework, some assumption must be made to constrain the total Higgs boson width since it cannot be directly measured at the LHC. Unless stated otherwise, it is assumed that there are no BSM contributions to the total Higgs boson width. With this assumption, the cross section times branching fraction for a production process i and decay f can be expressed as,

$$\sigma_i \mathcal{B}^f = \frac{\sigma_i(\vec{\kappa})\Gamma^f(\vec{\kappa})}{\Gamma_{\mathrm{H}}(\vec{\kappa})}, \tag{5}$$

where $\Gamma_{\mathrm{H}}(\vec{\kappa})$ is the total width of the Higgs boson and $\Gamma^f(\vec{\kappa})$ is the partial width of the Higgs boson decay to the final state f. A set of coupling modifiers, $\vec{\kappa}$, is introduced to parameterize potential deviations in the bosonic and fermionic couplings of the Higgs boson from the SM predictions. For a given production process or decay mode j, a coupling modifier κ_j is defined such that,

$$\kappa_j^2 = \sigma_j/\sigma_j^{\mathrm{SM}} \quad \text{or} \quad \kappa_j^2 = \Gamma^j/\Gamma_{\mathrm{SM}}^j. \tag{6}$$

In the SM, all κ_j values are positive and equal to unity. In this parametrization it is assumed that the higher-order accuracy of the QCD and electroweak corrections to the SM cross sections and branching fractions is preserved when the values of κ_j deviate from unity. While this does not hold in general, for the parameter ranges considered in this paper the dominant higher-order QCD corrections largely factorize from the rescaling of the couplings, therefore the approach is considered valid. Individual coupling modifiers, corresponding to tree-level Higgs boson couplings to the different particles, are introduced, as well as effective coupling modifiers κ_{g} and κ_γ that describe ggH production and $\mathrm{H} \to \gamma\gamma$ decay. This is possible because the presence of any BSM particles in these loops is not expected to significantly change the corresponding kinematic properties of the processes. This approach is not possible for gg → ZH production, which occurs at lead-

Table 5 Best fit values and $\pm 1\sigma$ uncertainties for the parameters of the stage 0 simplified template cross section model. The values are all normalized to the SM predictions. The expected uncertainties are given in brackets

Parameter	Best fit		Uncertainty		Parameter	Best fit		Uncertainty	
			stat.	syst.				stat.	syst.
$\sigma_{\mathrm{ggH}}\mathcal{B}^{\mathrm{ZZ}}$	1.00	$^{+0.19}_{-0.16}$	$^{+0.16}_{-0.15}$	$^{+0.09}_{-0.07}$	$\mathcal{B}^{\mathrm{bb}}/\mathcal{B}^{\mathrm{ZZ}}$	0.96	$^{+0.44}_{-0.31}$	$^{+0.32}_{-0.24}$	$^{+0.30}_{-0.20}$
		$(^{+0.18}_{-0.16})$	$(^{+0.16}_{-0.15})$	$(^{+0.09}_{-0.07})$			$(^{+0.57}_{-0.38})$	$(^{+0.40}_{-0.29})$	$(^{+0.41}_{-0.25})$
$\sigma_{\mathrm{VBF}}\mathcal{B}^{\mathrm{ZZ}}$	0.66	$^{+0.32}_{-0.26}$	$^{+0.27}_{-0.22}$	$^{+0.17}_{-0.13}$	$\mathcal{B}^{\tau\tau}/\mathcal{B}^{\mathrm{ZZ}}$	0.98	$^{+0.35}_{-0.28}$	$^{+0.24}_{-0.20}$	$^{+0.25}_{-0.20}$
		$(^{+0.40}_{-0.32})$	$(^{+0.33}_{-0.27})$	$(^{+0.22}_{-0.16})$			$(^{+0.36}_{-0.29})$	$(^{+0.26}_{-0.21})$	$(^{+0.25}_{-0.19})$
$\sigma_{\mathrm{H+V(qq)}}\mathcal{B}^{\mathrm{ZZ}}$	3.93	$^{+2.00}_{-1.71}$	$^{+1.77}_{-1.53}$	$^{+0.93}_{-0.75}$	$\mathcal{B}^{\mathrm{WW}}/\mathcal{B}^{\mathrm{ZZ}}$	1.30	$^{+0.29}_{-0.24}$	$^{+0.24}_{-0.20}$	$^{+0.17}_{-0.13}$
		$(^{+1.66}_{-1.05})$	$(^{+1.49}_{-1.05})$	$(^{+0.72}_{-0.00})$			$(^{+0.24}_{-0.20})$	$(^{+0.20}_{-0.16})$	$(^{+0.14}_{-0.11})$
$\sigma_{\mathrm{H+W}(\ell\nu)}\mathcal{B}^{\mathrm{ZZ}}$	1.95	$^{+0.88}_{-0.68}$	$^{+0.72}_{-0.57}$	$^{+0.51}_{-0.38}$	$\mathcal{B}^{\gamma\gamma}/\mathcal{B}^{\mathrm{ZZ}}$	1.14	$^{+0.26}_{-0.20}$	$^{+0.23}_{-0.18}$	$^{+0.13}_{-0.09}$
		$(^{+0.69}_{-0.52})$	$(^{+0.56}_{-0.44})$	$(^{+0.40}_{-0.29})$			$(^{+0.23}_{-0.19})$	$(^{+0.21}_{-0.17})$	$(^{+0.11}_{-0.08})$
$\sigma_{\mathrm{H+Z}(\ell\ell/\nu\nu)}\mathcal{B}^{\mathrm{ZZ}}$	0.84	$^{+0.57}_{-0.43}$	$^{+0.49}_{-0.40}$	$^{+0.29}_{-0.17}$	$\mathcal{B}^{\mu\mu}/\mathcal{B}^{\mathrm{ZZ}}$	0.67	$^{+1.40}_{-1.36}$	$^{+1.39}_{-1.35}$	$^{+0.18}_{-0.13}$
		$(^{+0.71}_{-0.46})$	$(^{+0.56}_{-0.41})$	$(^{+0.44}_{-0.22})$			$(^{+1.35}_{-1.28})$	$(^{+1.34}_{-1.28})$	$(^{+0.17}_{-0.05})$
$\sigma_{\mathrm{ttH}}\mathcal{B}^{\mathrm{ZZ}}$	1.08	$^{+0.37}_{-0.30}$	$^{+0.26}_{-0.22}$	$^{+0.26}_{-0.19}$					
		$(^{+0.38}_{-0.31})$	$(^{+0.28}_{-0.23})$	$(^{+0.26}_{-0.20})$					

Table 6 Normalization scaling factors for all relevant production cross sections and decay partial widths. For the κ parameters representing loop processes, the resolved scaling in terms of the fundamental SM couplings is also given

Effective	Loops	Interference	Scaling factor	Resolved scaling factor
Production				
$\sigma(\mathrm{ggH})$	✓	g-t	κ_g^2	$1.04\kappa_\mathrm{t}^2 + 0.002\kappa_\mathrm{b}^2 - 0.038\kappa_\mathrm{t}\kappa_\mathrm{b}$
$\sigma(\mathrm{VBF})$	—	—		$0.73\kappa_\mathrm{W}^2 + 0.27\kappa_\mathrm{Z}^2$
$\sigma(\mathrm{WH})$	—	—		κ_W^2
$\sigma(\mathrm{qq/qg} \to \mathrm{ZH})$	—	—		κ_Z^2
$\sigma(\mathrm{gg} \to \mathrm{ZH})$	✓	Z-t		$2.46\kappa_\mathrm{Z}^2 + 0.47\kappa_\mathrm{t}^2 - 1.94\kappa_\mathrm{Z}\kappa_\mathrm{t}$
$\sigma(\mathrm{ttH})$	—	—		κ_t^2
$\sigma(\mathrm{gb} \to \mathrm{WtH})$	—	W-t		$2.91\kappa_\mathrm{t}^2 + 2.31\kappa_\mathrm{W}^2 - 4.22\kappa_\mathrm{t}\kappa_\mathrm{W}$
$\sigma(\mathrm{qb} \to \mathrm{tHq})$	—	W-t		$2.63\kappa_\mathrm{t}^2 + 3.58\kappa_\mathrm{W}^2 - 5.21\kappa_\mathrm{t}\kappa_\mathrm{W}$
$\sigma(\mathrm{bbH})$	—	—		κ_b^2
Partial decay width				
Γ^{ZZ}	—	—		κ_Z^2
Γ^{WW}	—	—		κ_W^2
$\Gamma^{\gamma\gamma}$	✓	W-t	κ_γ^2	$1.59\kappa_\mathrm{W}^2 + 0.07\kappa_\mathrm{t}^2 - 0.67\kappa_\mathrm{W}\kappa_\mathrm{t}$
$\Gamma^{\tau\tau}$	—	—		κ_τ^2
Γ^{bb}	—	—		κ_b^2
$\Gamma^{\mu\mu}$	—	—		κ_μ^2
Total width for $\mathcal{B}_{\mathrm{BSM}} = 0$				
Γ_H	✓	—	κ_H^2	$0.58\kappa_\mathrm{b}^2 + 0.22\kappa_\mathrm{W}^2 + 0.08\kappa_\mathrm{g}^2$ $+ 0.06\kappa_\tau^2 + 0.026\kappa_\mathrm{Z}^2 + 0.029\kappa_\mathrm{c}^2$ $+ 0.0023\kappa_\gamma^2 + 0.0015\kappa_{\mathrm{Z}\gamma}^2$ $+ 0.00025\kappa_\mathrm{s}^2 + 0.00022\kappa_\mu^2$

ing order through box and triangular loop diagrams, because a tree-level contact interaction from BSM physics would likely exhibit a kinematic structure very different from the SM, and is expected to be highly suppressed [97]. Other possible BSM effects on the $\mathrm{gg} \to \mathrm{ZH}$ process are related to modifications of the HZZ and ttH vertices, which are best taken into account, within the limitation of the framework, by resolving the loop in terms of the corresponding coupling modifiers, κ_Z and κ_t. More details on the development of this framework as well as its theoretical and phenomenological foundations and extensions can be found, for example, in Refs. [98–112].

The normalization scaling effects of each of the κ parameters are given in Table 6. Loop processes such as ggH and $\mathrm{H} \to \gamma\gamma$ can be studied through either the effective coupling modifiers, thereby providing sensitivity to potential BSM physics in the loops, or the modifiers of the SM particles themselves. Interference between different diagrams, such as those that contribute to $\mathrm{gg} \to \mathrm{ZH}$, provides some sensitivity to relative signs between Higgs boson couplings to different particles. Modifications to the kinematic distributions of the tH production are also expected when the relative sign of κ_t and κ_W is negative. These effects were studied and the distributions of the final observables were found to be insensitive with the present dataset to the relative sign of κ_t and κ_W.

8.1 Generic model within κ-framework assuming resolved loops

Under the assumption that there are no BSM particles contributing to the ggH production or $\mathrm{H} \to \gamma\gamma$ decay loops, these processes can be expressed in terms of the coupling modifiers to the SM particles as described previously. There are six free coupling parameters: κ_W, κ_Z, κ_t, κ_τ, κ_b, and κ_μ. Without loss of generality, the value of κ_t is restricted to be positive, while both negative and positive values of κ_W, κ_Z and κ_b are allowed. In this model, the rates of the ggH and $\mathrm{H} \to \gamma\gamma$ processes, which occur through loop diagrams at leading order, are resolved, meaning that they are described by the functions of κ_W, κ_Z, κ_τ, and κ_b given in Table 6. The results of the fits with this parametrization are given in Fig. 9 and Table 7.

The rate of the $\mathrm{H} \to \mathrm{ZZ}$ decay and ZH production depend only on the absolute value of κ_Z. The interference between the two diagrams shown in Fig. 3, however, allows contributions from the $\mathrm{gg} \to \mathrm{ZH}$ production mode to break the degeneracy between the signs, leading to a positive value of κ_Z being preferred. As these contributions are typically small compared to other production modes, the 1σ and 2σ intervals also include negative values of κ_Z. Although a negative value of κ_b is preferred in this model, the difference in q between

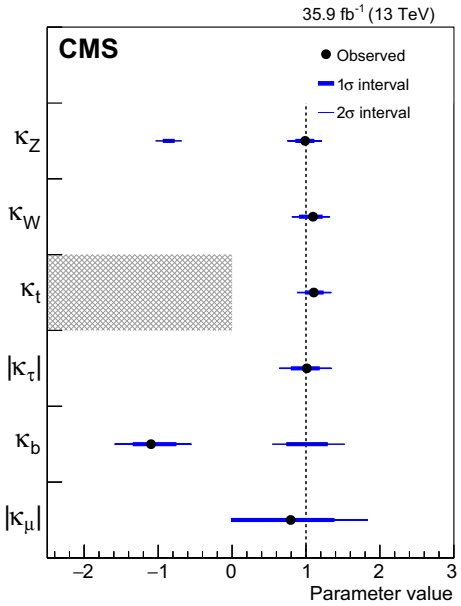

Fig. 9 Summary of the κ-framework model assuming resolved loops and $\mathcal{B}_{\text{BSM}} = 0$. The points indicate the best fit values while the thick and thin horizontal bars show the 1σ and 2σ CL intervals, respectively. In this model, the ggH and $\text{H} \to \gamma\gamma$ loops are resolved in terms of the remaining coupling modifiers. For this model, both positive and negative values of κ_{W}, κ_{Z}, and κ_{b} are considered. Negative values of κ_{W} in this model are disfavored by more than 2σ

Table 7 Best fit values and $\pm 1\sigma$ uncertainties for the parameters of the κ model in which the loop processes are resolved. The expected uncertainties are given in brackets

Parameter	Best fit value		Uncertainty	
			stat.	syst.
κ_{W}	1.10	$^{+0.12}_{-0.17}$	$^{+0.08}_{-0.16}$	$^{+0.08}_{-0.06}$
		$(^{+0.11}_{-0.10})$	$(^{+0.08}_{-0.08})$	$(^{+0.06}_{-0.06})$
κ_{Z}	0.99	$^{+0.11}_{-0.12}$	$^{+0.09}_{-0.10}$	$^{+0.06}_{-0.07}$
		$(^{+0.11}_{-0.11})$	$(^{+0.09}_{-0.09})$	$(^{+0.06}_{-0.06})$
κ_{t}	1.11	$^{+0.12}_{-0.10}$	$^{+0.07}_{-0.07}$	$^{+0.09}_{-0.08}$
		$(^{+0.11}_{-0.12})$	$(^{+0.07}_{-0.08})$	$(^{+0.09}_{-0.09})$
κ_{b}	−1.10	$^{+0.33}_{-0.23}$	$^{+0.29}_{-0.16}$	$^{+0.15}_{-0.17}$
		$(^{+0.22}_{-0.22})$	$(^{+0.15}_{-0.15})$	$(^{+0.17}_{-0.16})$
κ_{τ}	1.01	$^{+0.16}_{-0.20}$	$^{+0.11}_{-0.17}$	$^{+0.12}_{-0.11}$
		$(^{+0.17}_{-0.15})$	$(^{+0.12}_{-0.10})$	$(^{+0.12}_{-0.11})$
κ_{μ}	0.79	$^{+0.58}_{-0.79}$	$^{+0.56}_{-0.80}$	$^{+0.14}_{-0.00}$
		$(^{+0.50}_{-1.01})$	$(^{+0.50}_{-1.01})$	$(^{+0.08}_{-0.10})$

the best fit point and the minimum in the region $\kappa_{\text{b}} > 0$ is smaller than 0.1.

An additional fit is performed using a phenomenological parametrization relating the masses of the fermions and vector bosons to the corresponding κ modifiers using two parameters, denoted M and ϵ [113,114]. In such a model one can relate the coupling modifiers to M and ϵ as $\kappa_{\text{F}} = v\, m_{\text{f}}^{\epsilon}/M^{1+\epsilon}$ for fermions and $\kappa_{\text{V}} = v\, m_{\text{V}}^{2\epsilon}/M^{1+2\epsilon}$ for vector bosons. Here, $v = 246.22\,\text{GeV}$, is the SM Higgs boson vacuum expectation value [115]. The SM expectation, $\kappa_i = 1$, is recovered when $(M, \epsilon) = (v, 0)$.

The lepton and vector boson mass values are taken from Ref. [115], while the top quark mass is taken to be 172.5 GeV for consistency with theoretical calculations used in setting the SM predictions. The bottom quark mass is evaluated at the scale of the Higgs boson mass, $m_{\text{b}}(m_{\text{H}} = 125\,\text{GeV}) = 2.76\,\text{GeV}$.

The 1σ and 2σ CL regions in the (M, ϵ) fit are shown in Fig. 10 (left). The results of the fit using the six parameter κ model are plotted versus the particle masses in Fig. 10 (right), and the result of the (M, ϵ) fit is also shown for comparison. For the b quark, since the best fit point for κ_{b} is negative, the absolute value of this coupling modifier is shown. In order to show both the Yukawa and vector boson couplings in the same plot, a "reduced" vector boson coupling $\sqrt{\kappa_{\text{V}}} m_{\text{V}}/v$ is shown.

8.2 Generic model within κ-framework with effective loops

The results of the fits to the generic κ model where the ggH and $\text{H} \to \gamma\gamma$ loops are scaled using the effective coupling modifiers κ_{g} and κ_{γ} are given in Fig. 11 and Table 8. In this parametrization, additional contributions from BSM decays are allowed for by rewriting the total width of the Higgs boson, relative to its SM value, as,

$$\frac{\Gamma_{\text{H}}}{\Gamma_{\text{H}}^{\text{SM}}} = \frac{\kappa_{\text{H}}^2}{1 - (\mathcal{B}_{\text{undet}} + \mathcal{B}_{\text{inv}})}, \tag{7}$$

where κ_{H} is defined in Table 6.

Two different model assumptions are made concerning the BSM branching fraction. In the first parametrization, it is assumed that $\mathcal{B}_{\text{BSM}} = \mathcal{B}_{\text{inv}} + \mathcal{B}_{\text{undet}} = 0$, whereas in the second, $\mathcal{B}_{\text{inv}}$ and $\mathcal{B}_{\text{undet}}$ are allowed to vary as POIs, and instead the constraint $|\kappa_{\text{W}}|,\ |\kappa_{\text{Z}}| \leq 1$ is imposed. This avoids a complete degeneracy in the total width where all of the coupling modifiers can be scaled equally to account for a non-zero $\mathcal{B}_{\text{undet}}$. The parameter $\mathcal{B}_{\text{undet}}$ represents the total branching fraction to any final state that is not detected by the analyses included in this combined analysis. The likelihood scan for the $\mathcal{B}_{\text{inv}}$ parameter in this model, and the 2D likelihood scan of $\mathcal{B}_{\text{inv}}$ vs. $\mathcal{B}_{\text{undet}}$ are given in Fig. 12. The 68 and 95% CL regions for Fig. 12 (right) are determined as the regions for which $q(\mathcal{B}_{\text{undet}}, \mathcal{B}_{\text{inv}}) < 2.28$ and 5.99, respectively. The 95% CL upper limits of $\mathcal{B}_{\text{inv}} < 0.22$ and $\mathcal{B}_{\text{undet}} < 0.38$ are determined, corresponding to the value for which $q < 3.84$ [92]. The uncertainty in the measurement of κ_{t} is reduced by nearly 40% compared to Ref. [56]. This

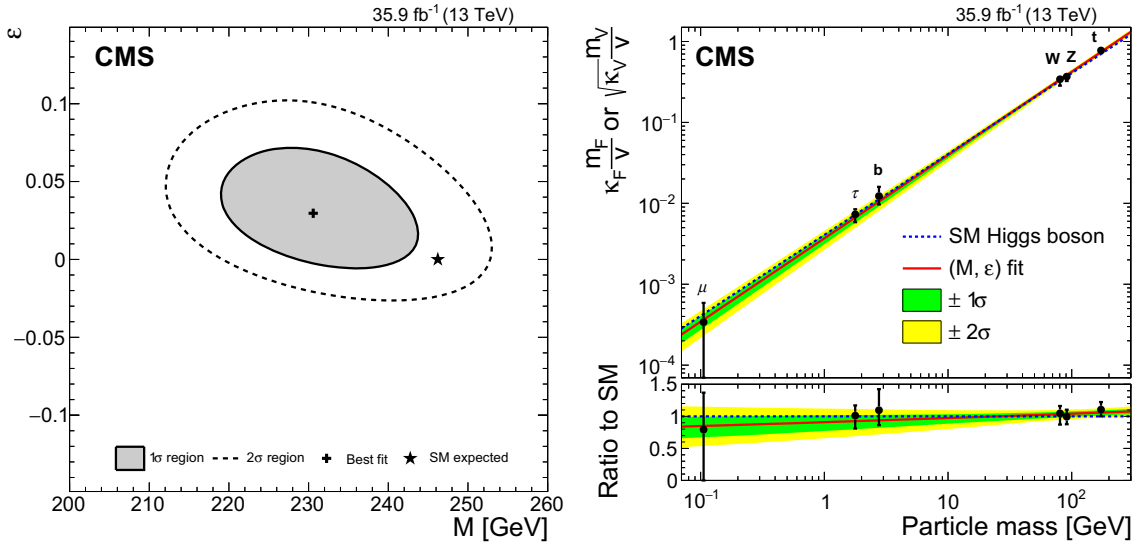

Fig. 10 Likelihood scan in the M-ϵ plane (left). The best fit point and the 1σ and 2σ CL regions are shown, along with the SM prediction. Result of the phenomenological (M, ϵ) fit overlayed with the resolved κ-framework model (right)

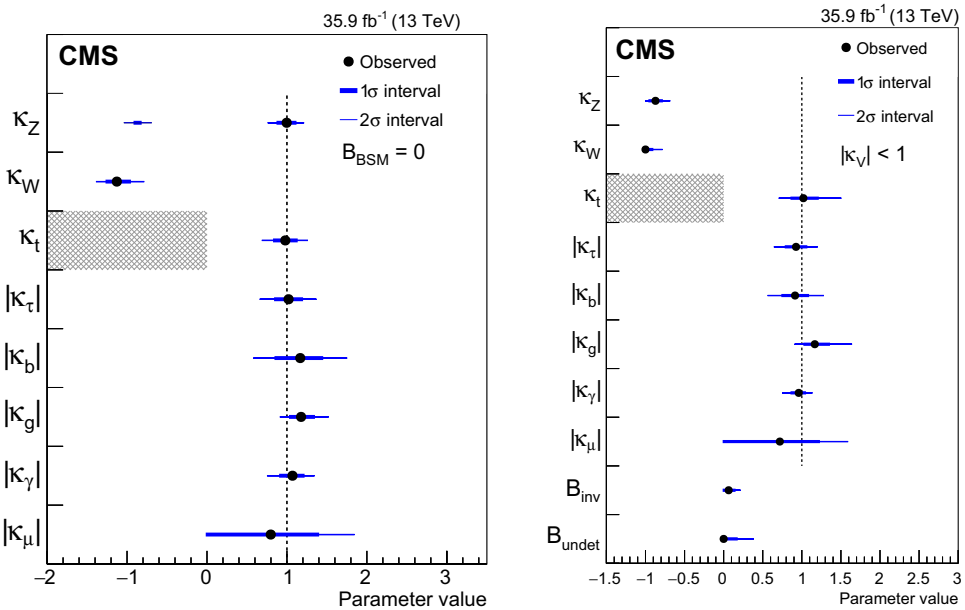

Fig. 11 Summary plots for the κ-framework model in which the ggH and $H \to \gamma\gamma$ loops are scaled with effective couplings. The points indicate the best fit values while the thick and thin horizontal bars show the 1σ and 2σ CL intervals, respectively. In the left figure the constraint $\mathcal{B}_{BSM} = 0$ is imposed, and both positive and negative values of κ_W and κ_Z are considered. In the right figure a constraint $|\kappa_W|, |\kappa_Z| \leq 1$ is imposed (same sign of κ_W and κ_Z), while $\mathcal{B}_{inv} > 0$ and $\mathcal{B}_{undet} > 0$ are free parameters

improvement is because of the improved sensitivity to the ttH production mode as described in Section 7.

In both of the generic κ models, the best fit point for κ_W is negative. The value of $q(\kappa_W)$ as a function of κ_W in the two cases is shown in Fig. 13. While different combinations of signs for κ_W and κ_Z are shown, the minimum value of q across all combinations is used to determine the best fit point and the 1σ and 2σ CL regions.

The preferred negative value of κ_W is due to the interference between some of the diagrams describing tH production, which contributes in several analyses entering the combination. In particular, the excess in the ttH tagged categories of the $H \to \gamma\gamma$ analysis can be accounted for by a negative value of κ_W as this increases the contribution of tH production. In these models, the $H \to \gamma\gamma$ decay is treated as an effective coupling so that it has no dependence on κ_W. This means that a negative value of κ_W will not result in excesses in the other categories of the $H \to \gamma\gamma$ analysis.

Using Eq. (7), this model is also reinterpreted as a constraint on the total Higgs boson width, and the corresponding likelihood scan is shown in Fig. 14. Using this parametrization, the total Higgs boson width relative to the SM expectation is determined to be $\Gamma_H/\Gamma_H^{SM} = 0.98^{+0.31}_{-0.25}$. The different behavior between the observed and expected likelihood scans for large Γ_H/Γ_H^{SM} is due to the preference in data for the $\kappa_t\kappa_W < 0$ relative sign combination.

Table 8 Best fit values and $\pm 1\sigma$ uncertainties for the parameters of the κ-framework model with effective loops. The expected uncertainties are given in brackets

$\mathcal{B}_{\text{BSM}} = 0$					$\mathcal{B}_{\text{BSM}} > 0,\ \lvert\kappa_{\text{V}}\rvert < 1$				
Parameter	Best fit		Uncertainty		Parameter	Best fit		Uncertainty	
			stat.	syst.				stat.	syst.
κ_{Z}	1.00	$^{+0.11}_{-0.11}$	$^{+0.09}_{-0.09}$	$^{+0.06}_{-0.07}$	κ_{Z}	-0.87	$^{+0.08}_{-0.08}$	$^{+0.07}_{-0.06}$	$^{+0.04}_{-0.04}$
		$(^{+0.11}_{-0.11})$	$(^{+0.09}_{-0.09})$	$(^{+0.06}_{-0.06})$			$(^{+0.00}_{-0.12})$	$(^{+0.00}_{-0.10})$	$(^{+0.00}_{-0.06})$
κ_{W}	-1.13	$^{+0.16}_{-0.13}$	$^{+0.15}_{-0.10}$	$^{+0.06}_{-0.08}$	κ_{W}	-1.00	$^{+0.09}_{-0.00}$	$^{+0.07}_{-0.00}$	$^{+0.05}_{-0.00}$
		$(^{+0.12}_{-0.12})$	$(^{+0.09}_{-0.09})$	$(^{+0.07}_{-0.07})$			$(^{+0.00}_{-0.12})$	$(^{+0.00}_{-0.09})$	$(^{+0.00}_{-0.07})$
κ_{t}	0.98	$^{+0.14}_{-0.14}$	$^{+0.08}_{-0.08}$	$^{+0.12}_{-0.11}$	κ_{t}	1.02	$^{+0.19}_{-0.15}$	$^{+0.13}_{-0.09}$	$^{+0.13}_{-0.13}$
		$(^{+0.14}_{-0.15})$	$(^{+0.08}_{-0.09})$	$(^{+0.12}_{-0.12})$			$(^{+0.18}_{-0.15})$	$(^{+0.13}_{-0.09})$	$(^{+0.13}_{-0.12})$
κ_{τ}	1.02	$^{+0.17}_{-0.17}$	$^{+0.11}_{-0.13}$	$^{+0.12}_{-0.10}$	κ_{τ}	0.93	$^{+0.13}_{-0.13}$	$^{+0.08}_{-0.09}$	$^{+0.11}_{-0.10}$
		$(^{+0.16}_{-0.15})$	$(^{+0.11}_{-0.11})$	$(^{+0.12}_{-0.11})$			$(^{+0.14}_{-0.15})$	$(^{+0.09}_{-0.10})$	$(^{+0.11}_{-0.11})$
κ_{b}	1.17	$^{+0.27}_{-0.31}$	$^{+0.18}_{-0.29}$	$^{+0.20}_{-0.10}$	κ_{b}	0.91	$^{+0.17}_{-0.16}$	$^{+0.11}_{-0.12}$	$^{+0.13}_{-0.11}$
		$(^{+0.25}_{-0.23})$	$(^{+0.18}_{-0.17})$	$(^{+0.17}_{-0.16})$			$(^{+0.19}_{-0.22})$	$(^{+0.14}_{-0.16})$	$(^{+0.13}_{-0.15})$
κ_{g}	1.18	$^{+0.16}_{-0.14}$	$^{+0.10}_{-0.09}$	$^{+0.12}_{-0.10}$	κ_{g}	1.16	$^{+0.18}_{-0.13}$	$^{+0.14}_{-0.09}$	$^{+0.12}_{-0.10}$
		$(^{+0.14}_{-0.12})$	$(^{+0.10}_{-0.09})$	$(^{+0.10}_{-0.09})$			$(^{+0.17}_{-0.12})$	$(^{+0.13}_{-0.09})$	$(^{+0.11}_{-0.09})$
κ_{γ}	1.07	$^{+0.14}_{-0.15}$	$^{+0.10}_{-0.14}$	$^{+0.09}_{-0.05}$	κ_{γ}	0.96	$^{+0.09}_{-0.09}$	$^{+0.06}_{-0.08}$	$^{+0.06}_{-0.06}$
		$(^{+0.12}_{-0.12})$	$(^{+0.10}_{-0.09})$	$(^{+0.07}_{-0.07})$			$(^{+0.09}_{-0.11})$	$(^{+0.07}_{-0.09})$	$(^{+0.05}_{-0.07})$
κ_{μ}	0.80	$^{+0.59}_{-0.80}$	$^{+0.56}_{-0.81}$	$^{+0.17}_{-0.00}$	κ_{μ}	0.72	$^{+0.50}_{-0.72}$	$^{+0.50}_{-0.71}$	$^{+0.00}_{-0.07}$
		$(^{+0.51}_{-1.01})$	$(^{+0.50}_{-1.01})$	$(^{+0.09}_{-0.09})$			$(^{+0.49}_{-1.01})$	$(^{+0.48}_{-1.00})$	$(^{+0.06}_{-0.08})$
					$\mathcal{B}_{\text{inv}}$	0.07	$^{+0.08}_{-0.07}$	$^{+0.03}_{-0.03}$	$^{+0.07}_{-0.06}$
							$(^{+0.09}_{+0.00})$	$(^{+0.04}_{-0.00})$	$(^{+0.08}_{-0.00})$
					$\mathcal{B}_{\text{undet}}$	0.00	$^{+0.17}_{+0.00}$	$^{+0.14}_{-0.00}$	$^{+0.09}_{-0.00}$
							$(^{+0.20}_{+0.00})$	$(^{+0.17}_{-0.00})$	$(^{+0.11}_{-0.00})$

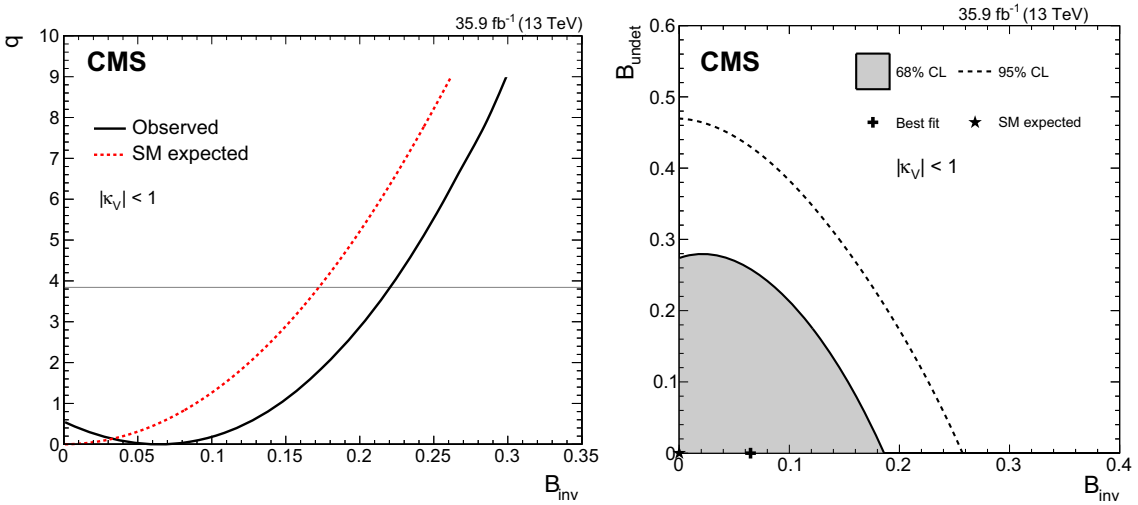

Fig. 12 Results within the generic κ-framework model with effective loops and with the constraint $|\kappa_{\text{W}}|,\ |\kappa_{\text{Z}}| \leq 1$ (same sign of κ_{W} and κ_{Z}), and with $\mathcal{B}_{\text{inv}} > 0$ and $\mathcal{B}_{\text{undet}} > 0$ as free parameters. Scan of the test statistic q as a function of $\mathcal{B}_{\text{inv}}$ (left), and 68 and 95% CL regions for $\mathcal{B}_{\text{inv}}$ vs. $\mathcal{B}_{\text{undet}}$ (right). The scan of the test statistic q as a function of $\mathcal{B}_{\text{inv}}$ expected assuming the SM is also shown in the left figure

An additional fit is performed assuming that the only BSM contributions to the Higgs couplings appear in the loop-induced ggH and H $\rightarrow \gamma\gamma$ processes. In this fit, κ_{g} and κ_{γ} are the POIs, $\mathcal{B}_{\text{inv}}$ and $\mathcal{B}_{\text{undet}}$ are floated, and the other couplings are fixed to their SM predictions. The best fit point

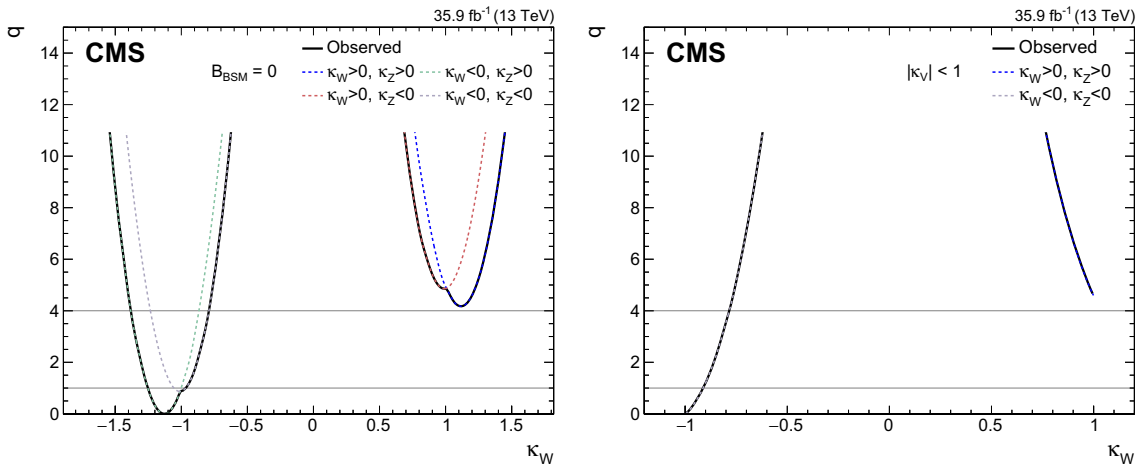

Fig. 13 Scan of the test statistic q as a function of κ_W in the generic κ model assuming $\mathcal{B}_{BSM} = 0$ (left) and allowing $\mathcal{B}_{inv}$ and $\mathcal{B}_{undet}$ to float (right). The different colored lines indicate the value of q for different combinations of signs for κ_W and κ_Z. The solid black line shows the minimum value of $q(\kappa_W)$ in each case and is used to determine the best fit point and the 1σ and 2σ CL regions. The scan in the right figure is truncated because of the constraints of $|\kappa_W| \leq 1$ and $|\kappa_Z| \leq 1$, which are imposed in this model

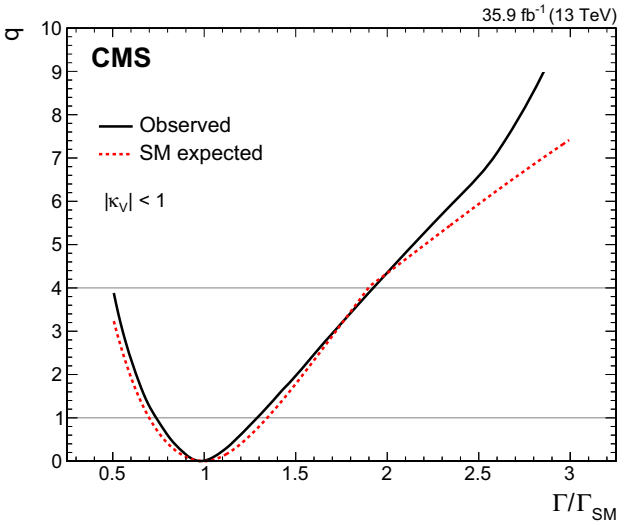

Fig. 14 The scan of the test statistic q as a function of Γ_H/Γ_H^{SM} obtained by reinterpreting the model allowing for BSM decays of the Higgs boson. The expected scan of q as a function of Γ_H/Γ_H^{SM} assuming the SM is also shown

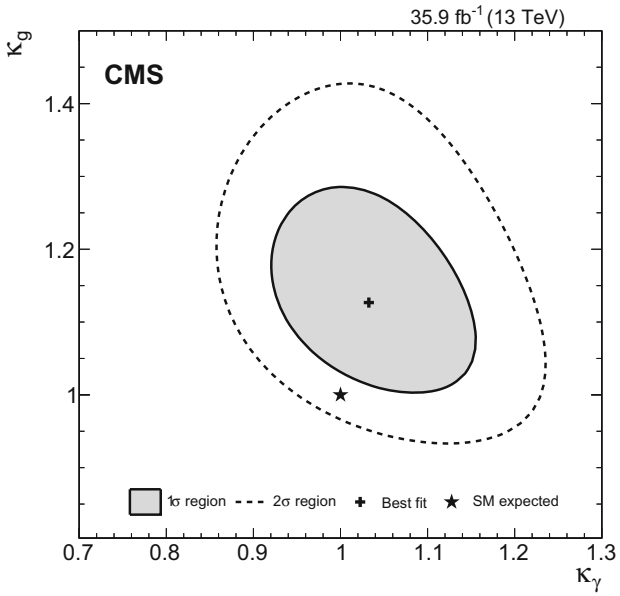

Fig. 15 The 1σ and 2σ CL regions in the κ_g vs. κ_γ parameter space for the model assuming the only BSM contributions to the Higgs boson couplings appear in the loop-induced processes or in BSM Higgs decays

and the 1σ and 2σ CL regions in the κ_g-κ_γ plane for this model are shown in Fig. 15.

8.3 Generic model with effective loops and coupling modifier ratios

An analogous parametrization to the ratios of cross sections and branching fractions described in the previous section can be derived in terms of ratios of the coupling modifiers ($\lambda_{ij} = \kappa_i/\kappa_j$). In this parametrization a reference combined coupling modifier is defined that accounts for modifications to the total event yield of a specific production times decay process, thereby avoiding the need for assumptions on the total Higgs boson width. The reference coupling modifier is taken to be $\kappa_{gZ} = \kappa_g\kappa_Z/\kappa_H$. The remaining parameters of interest are ratios of the form: λ_{Zg}, λ_{tg}, λ_{WZ}, $\lambda_{\gamma Z}$, $\lambda_{\tau Z}$, λ_{bZ}. A summary of the results in this model is given in Fig. 16, and the numerical values along with the $\pm1\sigma$ uncertainties are shown in Table 9.

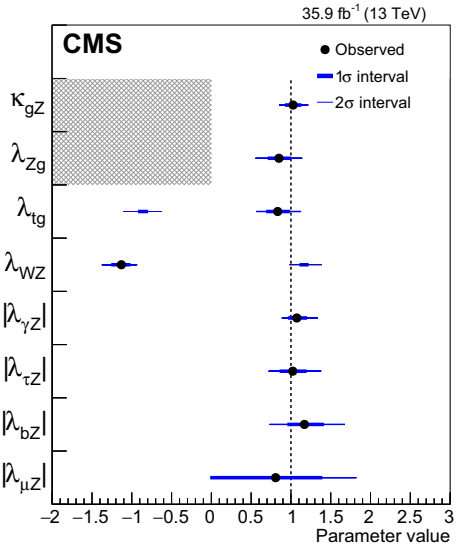

Fig. 16 Summary of the model with coupling ratios and effective couplings for the ggH and H $\rightarrow \gamma\gamma$ loops. The points indicate the best fit values while the thick and thin horizontal bars show the 1σ and 2σ CL intervals, respectively. For this model, both positive and negative values of λ_{WZ} and λ_{tg} are considered

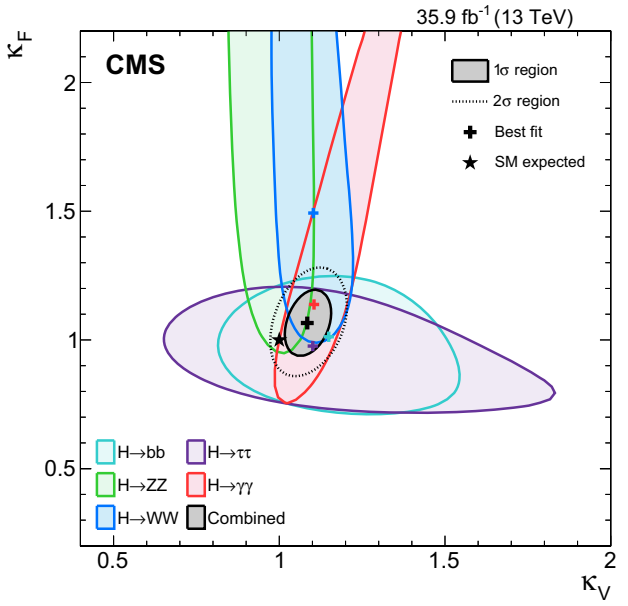

Fig. 17 The 1σ and 2σ CL regions in the κ_F vs. κ_V parameter space for the model assuming a common scaling of all the vector boson and fermion couplings

8.4 Fits of vector boson and fermion coupling modifiers

A more constrained version of the loop-resolved κ model is defined by assuming a common scaling of all vector boson and fermion couplings, respectively. Two models are defined: one in which all signal processes are scaled according to these two κ_V and κ_F parameters, and one in which separate κ_V^f and κ_F^f parameters are defined for each of the five decay processes. The best fit points and the 1σ and 2σ CL regions in the κ_V-κ_F plane for both models are shown in Fig. 17, and the results are summarized in Table 10. For large values of κ_F^{ZZ} the likelihood becomes essentially flat, resulting in the best fit point for this parameter being beyond the scale of the axis shown. The 1D 68% CL region for κ_F^{ZZ} can be expressed as $[1.22, \infty]$.

8.5 Benchmark models with resolved loops to test the symmetry of fermion couplings

Several BSM models predict the existence of an extended Higgs sector. In such scenarios, the couplings to up-and down-type fermions, or to leptons and quarks, can be separately modified. In order to probe such models, parametrizations are introduced in which the couplings of the Higgs boson to fermions are scaled either by separate common modifiers for up-type (κ_u) and down-type (κ_d) fermions or by separate common modifiers for quarks κ_q and leptons κ_l ($l = e, \mu, \tau$).

Figure 18 shows the results of the fits where the ratio of the couplings to up- and down-type fermions $\lambda_{du} = \kappa_d/\kappa_u$ is determined along with the ratio $\lambda_{Vu} = \kappa_V/\kappa_u$ and $\kappa_{uu} =$

Table 9 Best fit values and $\pm 1\sigma$ uncertainties for the parameters of the coupling modifier ratio model. The expected uncertainties are given in brackets

Parameter	Best fit		Uncertainty		Parameter	Best fit		Uncertainty	
			stat.	syst.				stat.	syst.
κ_{gZ}	1.03	$^{+0.09}_{-0.09}$	$^{+0.07}_{-0.07}$	$^{+0.05}_{-0.05}$	$\lambda_{\gamma Z}$	1.07	$^{+0.12}_{-0.10}$	$^{+0.10}_{-0.08}$	$^{+0.06}_{-0.05}$
		$(^{+0.09}_{-0.09})$	$(^{+0.07}_{-0.07})$	$(^{+0.05}_{-0.05})$			$(^{+0.11}_{-0.09})$	$(^{+0.09}_{-0.08})$	$(^{+0.05}_{-0.04})$
λ_{WZ}	-1.13	$^{+0.10}_{-0.11}$	$^{+0.08}_{-0.09}$	$^{+0.06}_{-0.06}$	λ_{bZ}	1.17	$^{+0.23}_{-0.20}$	$^{+0.16}_{-0.14}$	$^{+0.16}_{-0.14}$
		$(^{+0.11}_{-0.09})$	$(^{+0.09}_{-0.08})$	$(^{+0.06}_{-0.05})$			$(^{+0.22}_{-0.19})$	$(^{+0.16}_{-0.14})$	$(^{+0.15}_{-0.13})$
λ_{tg}	0.83	$^{+0.14}_{-0.13}$	$^{+0.08}_{-0.08}$	$^{+0.11}_{-0.10}$	$\lambda_{\tau Z}$	1.02	$^{+0.16}_{-0.15}$	$^{+0.11}_{-0.10}$	$^{+0.12}_{-0.11}$
		$(^{+0.17}_{-0.16})$	$(^{+0.11}_{-0.11})$	$(^{+0.12}_{-0.12})$			$(^{+0.16}_{-0.14})$	$(^{+0.11}_{-0.10})$	$(^{+0.11}_{-0.10})$
λ_{Zg}	0.85	$^{+0.14}_{-0.13}$	$^{+0.10}_{-0.12}$	$^{+0.09}_{-0.05}$	$\lambda_{\mu Z}$	0.81	$^{+0.57}_{-0.81}$	$^{+0.56}_{-0.82}$	$^{+0.11}_{-0.00}$
		$(^{+0.17}_{-0.16})$	$(^{+0.13}_{-0.13})$	$(^{+0.11}_{-0.09})$			$(^{+0.50}_{-1.01})$	$(^{+0.49}_{-1.01})$	$(^{+0.07}_{-0.07})$

Table 10 Best fit values and $\pm 1\sigma$ uncertainties for the parameters of the κ_V, κ_F model. The expected uncertainties are given in brackets

Parameter	Best fit		Uncertainty		Parameter	Best fit		Uncertainty	
			stat.	syst.				stat.	syst.
κ_V^{WW}	1.10	$^{+0.08}_{-0.08}$	$^{+0.06}_{-0.06}$	$^{+0.06}_{-0.06}$	κ_F^{WW}	1.49	$^{+1.55}_{-0.38}$	$^{+1.04}_{-0.33}$	$^{+1.15}_{-0.18}$
		$(^{+0.08}_{-0.08})$	$(^{+0.06}_{-0.06})$	$(^{+0.05}_{-0.05})$			$(^{+0.38}_{-0.20})$	$(^{+0.31}_{-0.17})$	$(^{+0.21}_{-0.11})$
κ_V^{ZZ}	0.96	$^{+0.09}_{-0.08}$	$^{+0.08}_{-0.07}$	$^{+0.05}_{-0.04}$	κ_F^{ZZ}	—		—	—
		$(^{+0.12}_{-0.11})$	$(^{+0.11}_{-0.10})$	$(^{+0.05}_{-0.05})$			$(^{+1.79}_{-0.31})$	$(^{+1.55}_{-0.30})$	$(^{+0.91}_{-0.06})$
κ_V^{bb}	1.15	$^{+0.23}_{-0.22}$	$^{+0.18}_{-0.18}$	$^{+0.15}_{-0.13}$	κ_F^{bb}	1.01	$^{+0.16}_{-0.18}$	$^{+0.09}_{-0.10}$	$^{+0.13}_{-0.15}$
		$(^{+0.22}_{-0.22})$	$(^{+0.17}_{-0.18})$	$(^{+0.13}_{-0.12})$			$(^{+0.16}_{-0.18})$	$(^{+0.09}_{-0.10})$	$(^{+0.13}_{-0.15})$
$\kappa_V^{\tau\tau}$	1.10	$^{+0.38}_{-0.29}$	$^{+0.26}_{-0.24}$	$^{+0.27}_{-0.18}$	$\kappa_F^{\tau\tau}$	0.98	$^{+0.15}_{-0.16}$	$^{+0.08}_{-0.09}$	$^{+0.13}_{-0.14}$
		$(^{+0.32}_{-0.29})$	$(^{+0.24}_{-0.23})$	$(^{+0.20}_{-0.17})$			$(^{+0.14}_{-0.14})$	$(^{+0.07}_{-0.08})$	$(^{+0.11}_{-0.12})$
$\kappa_V^{\gamma\gamma}$	1.10	$^{+0.14}_{-0.08}$	$^{+0.11}_{-0.07}$	$^{+0.09}_{-0.05}$	$\kappa_F^{\gamma\gamma}$	1.14	$^{+0.67}_{-0.29}$	$^{+0.53}_{-0.26}$	$^{+0.41}_{-0.14}$
		$(^{+0.10}_{-0.08})$	$(^{+0.08}_{-0.06})$	$(^{+0.05}_{-0.04})$			$(^{+0.47}_{-0.25})$	$(^{+0.41}_{-0.23})$	$(^{+0.23}_{-0.10})$

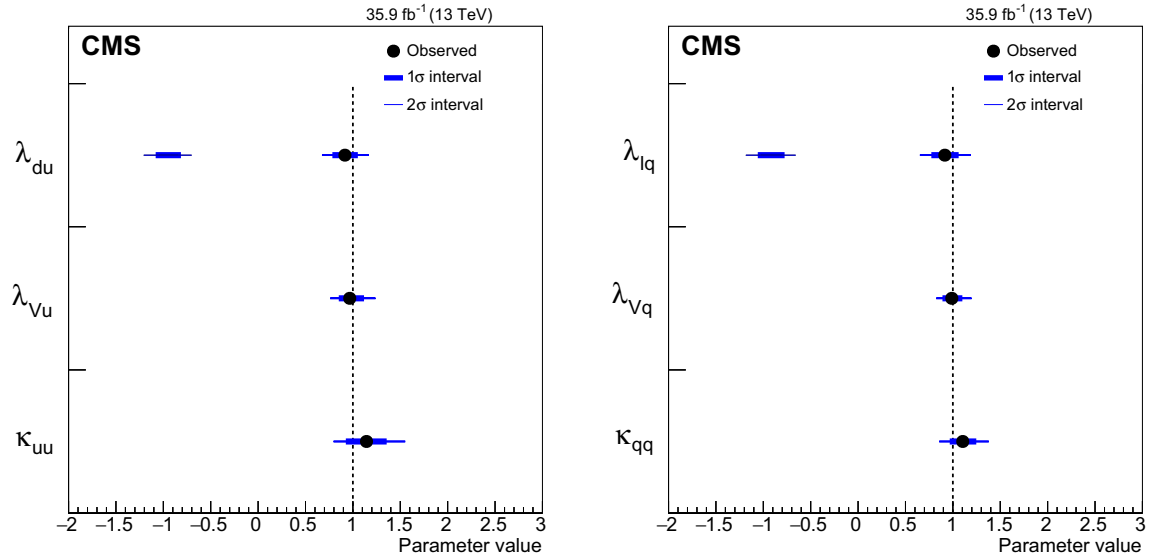

Fig. 18 Summary plots of the 3-parameter models comparing up- and down-type fermions, and floating the ratio of the vector coupling to the up-type coupling (left) and comparing lepton and quark couplings (right). The points indicate the best fit values while the thick and thin horizontal bars show the 1σ and 2σ CL intervals, respectively. Both positive and negative values of λ_{du}, λ_{Vu}, λ_{lq}, and λ_{Vq} are considered

κ_u^2/Γ_H. Also shown are the results of the fit where the ratio of the coupling to leptons and to quarks $\lambda_{lq} = \kappa_l/\kappa_q$ is determined along with the ratio $\lambda_{Vq} = \kappa_V/\kappa_q$ and $\kappa_{qq} = \kappa_q^2/\Gamma_H$. The results of these two parametrizations are summarized in Table 11.

8.6 Compatibility of measurements with the SM

Table 12 shows a summary of the compatibility of the different models considered, as described in Sects. 7 and 8, with the SM predictions. For each model, the value of q at the values of the POIs for the SM expectation (q_{SM}) is converted to a p-value with respect to the SM. This is done assuming q is distributed according to a χ^2 function with the number of degrees of freedom equal to the number of POIs. This p-value is found to be greater than 5% for all parametrizations.

9 Constraints on benchmark two Higgs doublet models

The generic models described in Sect. 8.5 can also be interpreted in the context of explicit benchmark BSM models that contain a second Higgs doublet (2HDM) [116–118]. Only models with CP conservation and a discrete $\mathbb{Z}_2$ symmetry to prevent tree-level flavor changing neutral currents are considered. Under these assumptions, four 2HDM types are possible, referred to as Types I, II, III, and IV. Each of these 2HDMs contain seven free parameters. Under the additional assumption that the Higgs boson with a mass of 125.09 GeV

Table 11 Best fit values and $\pm 1\sigma$ uncertainties for the parameters of the two benchmark models with resolved loops to test the symmetry of fermion couplings. The expected uncertainties are given in brackets

λ_{Vu}				λ_{du}				κ_{uu}			
Best fit		Uncertainty		Best fit		Uncertainty		Best fit		Uncertainty	
value		stat.	syst.	value		stat.	syst.	value		stat.	syst.
0.97	$^{+0.14}_{-0.10}$ ($^{+0.15}_{-0.11}$)	$^{+0.11}_{-0.08}$ ($^{+0.12}_{-0.09}$)	$^{+0.09}_{-0.06}$ ($^{+0.09}_{-0.07}$)	0.92	$^{+0.12}_{-0.12}$ ($^{+0.13}_{-0.13}$)	$^{+0.09}_{-0.09}$ ($^{+0.10}_{-0.10}$)	$^{+0.08}_{-0.08}$ ($^{+0.08}_{-0.08}$)	1.14	$^{+0.20}_{-0.20}$ ($^{+0.16}_{-0.19}$)	$^{+0.13}_{-0.16}$ ($^{+0.12}_{-0.16}$)	$^{+0.15}_{-0.12}$ ($^{+0.11}_{-0.11}$)
λ_{Vq}				λ_{lq}				κ_{qq}			
Best fit		Uncertainty		Best fit		Uncertainty		Best fit		Uncertainty	
value		stat.	syst.	value		stat.	syst.	value		stat.	syst.
0.99	$^{+0.10}_{-0.08}$ ($^{+0.12}_{-0.09}$)	$^{+0.07}_{-0.06}$ ($^{+0.08}_{-0.07}$)	$^{+0.07}_{-0.06}$ ($^{+0.09}_{-0.07}$)	0.92	$^{+0.13}_{-0.13}$ ($^{+0.15}_{-0.14}$)	$^{+0.09}_{-0.08}$ ($^{+0.10}_{-0.09}$)	$^{+0.10}_{-0.10}$ ($^{+0.11}_{-0.10}$)	1.10	$^{+0.13}_{-0.12}$ ($^{+0.13}_{-0.13}$)	$^{+0.08}_{-0.08}$ ($^{+0.09}_{-0.09}$)	$^{+0.10}_{-0.09}$ ($^{+0.10}_{-0.10}$)

Table 12 Compatibility of the fit results with the SM prediction under various signal parametrizations. The value of q at the values of the POIs for which the SM expectation is obtained (q_{SM}) is shown along with the corresponding p-value, with respect to the SM, assuming q is distributed according to a χ^2 function with the specified number of degrees of freedom (DOF)

Parameterization	p-value (q_{SM})	DOF	Parameters of interest
Global signal strength	6.28% (3.46)	1	μ
Production processes	9.87% (9.27)	5	μ_{ggH}, μ_{VBF}, μ_{WH}, μ_{ZH}, μ_{ttH}
Decay modes	53.8% (5.05)	6	$\mu^{\gamma\gamma}$, μ^{ZZ}, μ^{WW}, $\mu^{\tau\tau}$, μ^{bb}, $\mu^{\mu\mu}$
$\sigma_i \mathcal{B}^f$ products	61.2% (21.5)	24	$\sigma_{ggH}\mathcal{B}^{bb}$, $\sigma_{ggH}\mathcal{B}^{\tau\tau}$, $\sigma_{ggH}\mathcal{B}^{\mu\mu}$, $\sigma_{ggH}\mathcal{B}^{WW}$, $\sigma_{ggH}\mathcal{B}^{ZZ}$, $\sigma_{ggH}\mathcal{B}^{\gamma\gamma}$, $\sigma_{VBF}\mathcal{B}^{\tau\tau}$, $\sigma_{VBF}\mathcal{B}^{\mu\mu}$, $\sigma_{VBF}\mathcal{B}^{WW}$, $\sigma_{VBF}\mathcal{B}^{ZZ}$, $\sigma_{VBF}\mathcal{B}^{\gamma\gamma}$, $\sigma_{WH}\mathcal{B}^{bb}$, $\sigma_{WH}\mathcal{B}^{WW}$, $\sigma_{WH}\mathcal{B}^{ZZ}$, $\sigma_{WH}\mathcal{B}^{\gamma\gamma}$, $\sigma_{ZH}\mathcal{B}^{bb}$, $\sigma_{ZH}\mathcal{B}^{WW}$, $\sigma_{ZH}\mathcal{B}^{ZZ}$, $\sigma_{ZH}\mathcal{B}^{\gamma\gamma}$, $\sigma_{ttH}\mathcal{B}^{\tau\tau}$, $\sigma_{ttH}\mathcal{B}^{WW}$, $\sigma_{ttH}\mathcal{B}^{ZZ}$, $\sigma_{ttH}\mathcal{B}^{\gamma\gamma}$, $\sigma_{ttH}\mathcal{B}^{bb}$
Ratios of σ and $\mathcal{B}$ relative to $gg \to H \to ZZ$	32.3% (11.5)	10	μ^{ZZ}_{ggH}, μ_{VBF}/μ_{ggH}, μ_{WH}/μ_{ggH}, μ_{ZH}/μ_{ggH}, μ_{ttH}/μ_{ggH}, μ^{WW}/μ^{ZZ}, $\mu^{\gamma\gamma}/\mu^{ZZ}$, $\mu^{\tau\tau}/\mu^{ZZ}$, μ^{bb}/μ^{ZZ}, $\mu^{bb}/\mu^{\mu\mu}$
Simplified template cross sections with branching fractions relative to $\mathcal{B}^{ZZ}$	21.2% (14.4)	11	$\sigma_{ggH}\mathcal{B}^{ZZ}$, $\sigma_{VBF}\mathcal{B}^{ZZ}$, $\sigma_{H+V(qq)}\mathcal{B}^{ZZ}$, $\sigma_{H+W(\ell\nu)}\mathcal{B}^{ZZ}$, $\sigma_{H+Z(\ell\ell/\nu\nu)}\mathcal{B}^{ZZ}$, $\sigma_{ttH}\mathcal{B}^{ZZ}$, $\mathcal{B}^{bb}/\mathcal{B}^{ZZ}$, $\mathcal{B}^{\tau\tau}/\mathcal{B}^{ZZ}$, $\mathcal{B}^{\mu\mu}/\mathcal{B}^{ZZ}$, $\mathcal{B}^{WW}/\mathcal{B}^{ZZ}$, $\mathcal{B}^{\gamma\gamma}/\mathcal{B}^{ZZ}$
Couplings, SM loops	45.6% (5.71)	6	κ_Z, κ_W, κ_t, κ_τ, κ_b, κ_μ
Couplings vs. mass	16.8% (3.57)	2	M, ϵ
Couplings, BSM loops	18.5% (11.3)	8	κ_Z, κ_W, κ_t, κ_τ, κ_b, κ_μ, κ_γ, κ_g
Couplings, BSM loops and decays including $H \to$ invisible analyses	32.4% (11.5)	10	κ_Z, κ_W, κ_t, κ_τ, κ_b, κ_μ, κ_γ, κ_g, $\mathcal{B}_{inv}$, $\mathcal{B}_{undet}$
Ratios of coupling modifiers	18.1% (11.4)	8	κ_{gZ}, λ_{WZ}, $\lambda_{\gamma Z}$, λ_{tg}, λ_{bZ}, $\lambda_{\tau Z}$, $\lambda_{\mu Z}$, λ_{Zg}
Fermion and vector couplings	16.9% (3.55)	2	κ_F, κ_V
Fermion and vector couplings, per decay mode	76.7% (8.2)	12	κ^{bb}_F, $\kappa^{\tau\tau}_F$, $\kappa^{\mu\mu}_F$, κ^{WW}_F, κ^{ZZ}_F, $\kappa^{\gamma\gamma}_F$, κ^{bb}_V, $\kappa^{\tau\tau}_V$, $\kappa^{\mu\mu}_V$, κ^{WW}_V, κ^{ZZ}_V, $\kappa^{\gamma\gamma}_V$
Up vs. down-type couplings	25.5% (4.06)	3	λ_{Vu}, λ_{du}, κ_{uu}
Lepton vs. quark couplings	27.2% (3.91)	3	λ_{lq}, λ_{Vq}, κ_{qq}

is the lightest CP-even, neutral Higgs boson in the extended Higgs sector, the predicted rates for its production and decay are sensitive at leading order to only two 2HDM parameters: the angles α and β that diagonalize the mass-squared matrices of the scalars and pseudoscalars. These two parameters are conventionally substituted by $\cos(\beta-\alpha)$ and $\tan\beta$, without loss of generality. In all of the 2HDMs, the coupling of the Higgs boson to vector bosons is modified by a factor $\sin(\beta-\alpha)$. The 2HDM types differ in how the fermions couple to the Higgs doublets. In the Type I model, all fermions couple to just one of the Higgs doublets. In Type II, the up-type fermions couple to one of the Higgs doublets, while the down-type fermions and the right-handed leptons couple to the second. In Type III 2HDM, also referred to as "lepton-specific", the quarks couple to one of the Higgs doublets and the right-handed leptons couple to the other. In the Type

Table 13 Modifications to the couplings of the Higgs bosons to up-type (κ_u) and down-type (κ_d) fermions, and vector bosons (κ_V), with respect to the SM expectation, in 2HDM and for the hMSSM. The coupling modifications for the hMSSM are completed by the expressions for s_u and s_d, as given by Eqs. (8) and (9)

	2HDM				**hMSSM**
	Type I	Type II	Type III	Type IV	
κ_V	$\sin(\beta-\alpha)$	$\sin(\beta-\alpha)$	$\sin(\beta-\alpha)$	$\sin(\beta-\alpha)$	$\frac{s_d+s_u\tan\beta}{\sqrt{1+\tan^2\beta}}$
κ_u	$\cos(\alpha)/\sin(\beta)$	$\cos(\alpha)/\sin(\beta)$	$\cos(\alpha)/\sin(\beta)$	$\cos(\alpha)/\sin(\beta)$	$s_u\frac{\sqrt{1+\tan^2\beta}}{\tan\beta}$
κ_d	$\cos(\alpha)/\sin(\beta)$	$-\sin(\alpha)/\cos(\beta)$	$\cos(\alpha)/\sin(\beta)$	$-\sin(\alpha)/\cos(\beta)$	$s_d\sqrt{1+\tan^2\beta}$
κ_l	$\cos(\alpha)/\sin(\beta)$	$-\sin(\alpha)/\cos(\beta)$	$-\sin(\alpha)/\cos(\beta)$	$\cos(\alpha)/\sin(\beta)$	$s_d\sqrt{1+\tan^2\beta}$

IV 2HDM, also referred to as "flipped", the up-type fermions and right-handed leptons couple to one of the Higgs doublets, while the down-type quarks couple to the other. Table 13 shows the relation between the coupling modifiers to vector bosons, quarks and leptons and the 2HDM model parameters.

The minimal supersymmetric standard model (MSSM) [119–122] is a specific example of a 2HDM of Type II that includes additional particle content compared to the SM. The additional strong constraints given by the nontrivial fermion-boson symmetry fix all mass relations between the Higgs bosons and the angle α, at tree-level, leaving only two free parameters to fully constrain the MSSM Higgs sector, usually chosen to be m_A and $\tan\beta$. The hMSSM scenario [123,124], in particular, is an effective MSSM model, trading the precise knowledge of m_H against unknown higher-order corrections such that $m_H = 125.09\,\text{GeV}$ across the m_A, $\tan\beta$ parameter space. Another requirement of the scenario is that H be identified as the lightest of the two neutral scalar Higgs bosons. Furthermore, one also obtains relatively simple relations between m_A, $\tan\beta$, and the Higgs boson coupling modifiers [125], which are shown in Table 13 and completed by Eqs. (8) and (9). Although many other MSSM benchmark models have also been defined [126], the lack of analytic expressions for the Higgs boson couplings renders these models technically more challenging to consider and they are therefore beyond the scope of this paper.

$$s_u = \frac{1}{\sqrt{1+\frac{(m_A^2+m_Z^2)^2\tan^2\beta}{(m_Z^2+m_A^2\tan^2\beta-m_H^2(1+\tan^2\beta))^2}}} \tag{8}$$

$$s_d = s_u\frac{(m_A^2+m_Z^2)\tan\beta}{m_Z^2+m_A^2\tan^2\beta-m_H^2(1+\tan^2\beta)} \tag{9}$$

To set constraints on the 2HDM model parameters, 3-dimensional likelihood scans of the parametrizations described in Sect. 8.5 (with necessary modifications to the lepton coupling modifiers to describe the Type IV 2HDM) are performed. A test-statistic is then defined, for example in the Types I, II and hMSSM scenarios,

$$q(\lambda_{du},\lambda_{Vu},\kappa_{uu}) = -2\ln\left(\frac{L(\lambda_{du},\lambda_{Vu},\kappa_{uu})}{L(\hat{\lambda}_{du},\hat{\lambda}_{Vu},\hat{\kappa}_{uu})}\right), \tag{10}$$

where $\hat{\lambda}_{du}$, $\hat{\lambda}_{Vu}$, $\hat{\kappa}_{uu}$ are the values of the POIs that maximize the likelihood. An interpolation scheme is used to determine the value of q as a function of $\cos(\beta-\alpha)$ and $\tan\beta$, or m_A and $\tan\beta$, for the Types I and II, or hMSSM scenarios, respectively, using the relations in Table 13.

A second quantity $q\prime$ is defined as,

$$q\prime = -2\ln\left(\frac{L(\hat{\lambda}_{du},\hat{\lambda}_{Vu},\hat{\kappa}_{uu})}{L_{max}}\right), \tag{11}$$

where L_{max} is the maximum likelihood value attained in the planes of $\cos(\beta-\alpha)$–$\tan\beta$, or m_A–$\tan\beta$. The allowed regions are determined as the points in each plane for which the difference between q and $q\prime$ (Δq) is less than 5.99. This value corresponds to the 95% confidence region assuming Δq is distributed as a χ^2 function with 2 degrees of freedom. A similar procedure is performed using the model with the parameters λ_{lq}, λ_{Vq} and κ_{qq}, to determine the allowed region for the Type III scenario.

Figure 19 shows the results of the fits for the different 2HDM benchmark scenarios. The lobe features that can be seen in the Types II, III, and IV constraints for $\cos(\beta-\alpha) > 0$ are due to negative values of κ_d, κ_τ, and κ_b, which are not excluded with the current sensitivity. In all of these 2HDM models, the Higgs boson couplings are the same as those predicted in the SM for $\cos(\beta-\alpha) = 0$.

The results for the hMSSM scenario are also shown in Fig. 19. The constraints observed are more stringent than those expected under the SM. This is due to the best fit value of λ_{du} being smaller than 1, while in the hMSSM for $\tan\beta > 1$, λ_{du} is strictly greater than 1 and asymptotically approaches unity only at large m_A. Therefore the observed data disfavors small values of m_A, leading to the stronger constraint.

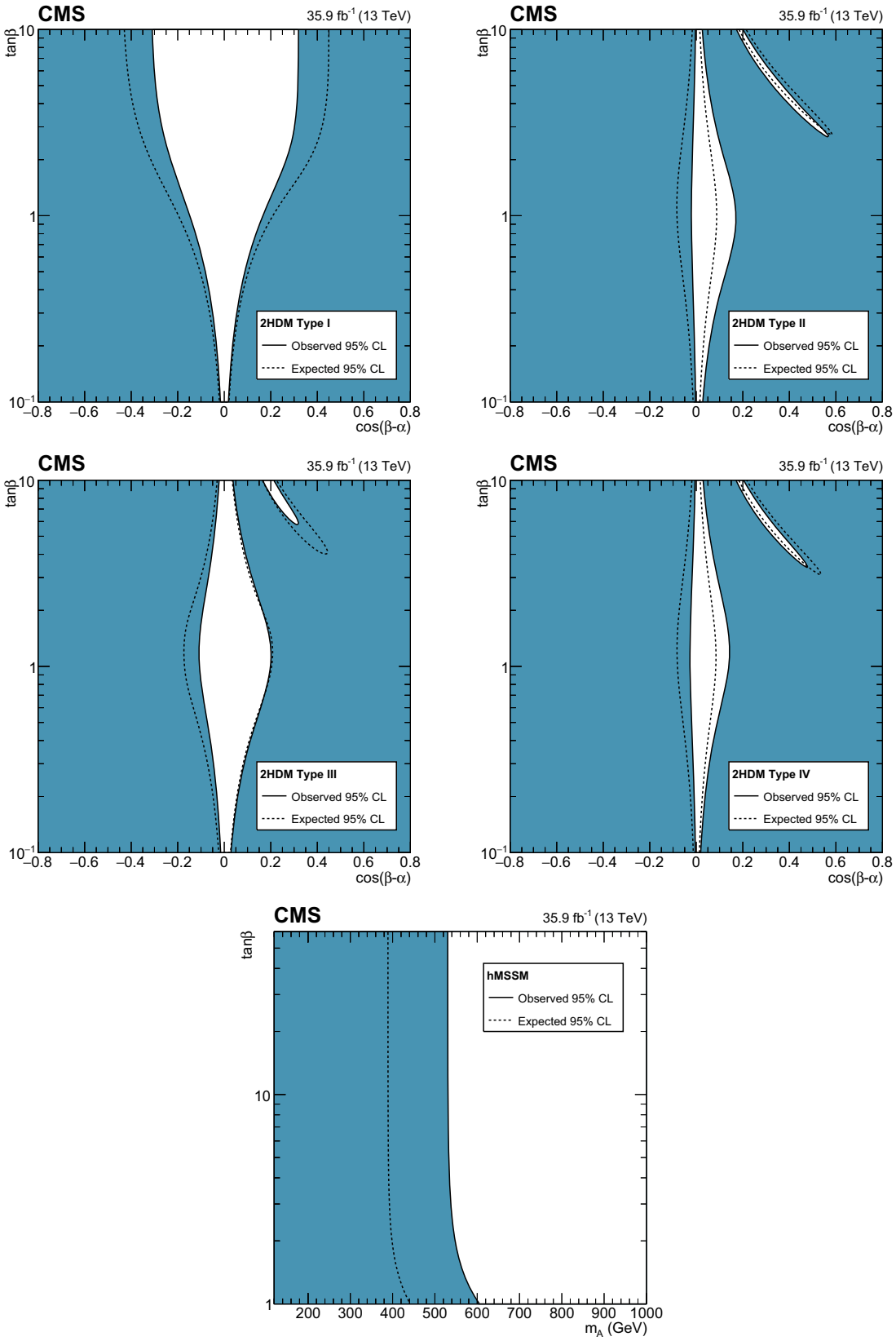

Fig. 19 Constraints in the $\cos(\beta-\alpha)$ vs. $\tan\beta$ plane for the Types I, II, III, and IV 2HDM, and constraints in the m_{A} vs. $\tan\beta$ plane for the hMSSM. The white regions, bounded by the solid black lines, in each plane represent the regions of the parameter space that are allowed at the 95% CL, given the data observed. The dashed lines indicate the boundaries of the allowed regions expected for the SM Higgs boson

The constraints in the 2HDM and hMSSM scenarios are complementary to those obtained from direct searches for additional Higgs bosons [127–131].

10 Summary

A set of combined measurements of Higgs boson production and decay rates has been presented, along with the consequential constraints placed on its couplings to standard model (SM) particles, and on the parameter spaces of several beyond the standard model (BSM) scenarios. The combination is based on analyses targeting the gluon fusion and vector boson fusion production modes, and associated production with a vector boson or a pair of top quarks. The analyses included in the combination target Higgs boson production in the $H \to ZZ$, WW, $\gamma\gamma$, $\tau\tau$, bb, and $\mu\mu$ decay channels, using 13 TeV proton–proton collision data collected in 2016 and corresponding to an integrated luminosity of $35.9\,\text{fb}^{-1}$. Additionally, searches for invisible Higgs boson decays are included to increase the sensitivity to potential interactions with BSM particles.

Measurements of the Higgs boson production cross section times branching fractions are presented, along with a generic parametrization in terms of ratios of production cross sections and branching fractions, which makes no assumptions about the Higgs boson total width. The combined signal yield relative to the SM prediction has been measured as 1.17 ± 0.10 at $m_{\text{H}} = 125.09\,\text{GeV}$. An improvement in the measured precision of the gluon fusion production rate of around ∼50% is achieved compared to previous ATLAS and CMS measurements. Additionally, a set of fiducial Higgs boson cross sections, in the context of the simplified template cross section framework, is presented for the first time from a combination of six decay channels. Furthermore, interpretations are provided in the context of a leading-order coupling modifier framework, including variants for which effective couplings to the photon and gluon are introduced. All of the results presented are compatible with the SM prediction. The invisible (undetected) branching fraction of the Higgs boson is constrained to be less than 22 (38%) at 95% Confidence Level. The results are additionally interpreted in two BSM models, the minimal supersymmetric model and the generic two Higgs doublet model. The constraints placed on the parameter spaces of these models are complementary to those that can be obtained from direct searches for additional Higgs bosons.

Acknowledgements We congratulate our colleagues in the CERN accelerator departments for the excellent performance of the LHC and thank the technical and administrative staffs at CERN and at other CMS institutes for their contributions to the success of the CMS effort. In addition, we gratefully acknowledge the computing centres and personnel of the Worldwide LHC Computing Grid for delivering so effectively the computing infrastructure essential to our analyses. Finally, we acknowledge the enduring support for the construction and operation of the LHC and the CMS detector provided by the following funding agencies: the Austrian Federal Ministry of Science, Research and Economy and the Austrian Science Fund; the Belgian Fonds de la Recherche Scientifique, and Fonds voor Wetenschappelijk Onderzoek; the Brazilian Funding Agencies (CNPq, CAPES, FAPERJ, and FAPESP); the Bulgarian Ministry of Education and Science; CERN; the Chinese Academy of Sciences, Ministry of Science and Technology, and National Natural Science Foundation of China; the Colombian Funding Agency (COLCIENCIAS); the Croatian Ministry of Science, Education and Sport, and the Croatian Science Foundation; the Research Promotion Foundation, Cyprus; the Secretariat for Higher Education, Science, Technology and Innovation, Ecuador; the Ministry of Education and Research, Estonian Research Council via IUT23-4 and IUT23-6 and European Regional Development Fund, Estonia; the Academy of Finland, Finnish Ministry of Education and Culture, and Helsinki Institute of Physics; the Institut National de Physique Nucléaire et de Physique des Particules / CNRS, and Commissariat à l'Énergie Atomique et aux Énergies Alternatives / CEA, France; the Bundesministerium für Bildung und Forschung, Deutsche Forschungsgemeinschaft, and Helmholtz-Gemeinschaft Deutscher Forschungszentren, Germany; the General Secretariat for Research and Technology, Greece; the National Research, Development and Innovation Fund, Hungary; the Department of Atomic Energy and the Department of Science and Technology, India; the Institute for Studies in Theoretical Physics and Mathematics, Iran; the Science Foundation, Ireland; the Istituto Nazionale di Fisica Nucleare, Italy; the Ministry of Science, ICT and Future Planning, and National Research Foundation (NRF), Republic of Korea; the Lithuanian Academy of Sciences; the Ministry of Education, and University of Malaya (Malaysia); the Mexican Funding Agencies (BUAP, CINVESTAV, CONACYT, LNS, SEP, and UASLP-FAI); the Ministry of Business, Innovation and Employment, New Zealand; the Pakistan Atomic Energy Commission; the Ministry of Science and Higher Education and the National Science Centre, Poland; the Fundação para a Ciência e a Tecnologia, Portugal; JINR, Dubna; the Ministry of Education and Science of the Russian Federation, the Federal Agency of Atomic Energy of the Russian Federation, Russian Academy of Sciences, the Russian Foundation for Basic Research and the Russian Competitiveness Program of NRNU "MEPhI"; the Ministry of Education, Science and Technological Development of Serbia; the Secretaría de Estado de Investigación, Desarrollo e Innovación, Programa Consolider-Ingenio 2010, Plan Estatal de Investigación Científica y Técnica y de Innovación 2013–2016, Plan de Ciencia, Tecnología e Innovación 2013–2017 del Principado de Asturias and Fondo Europeo de Desarrollo Regional, Spain; the Swiss Funding Agencies (ETH Board, ETH Zurich, PSI, SNF, UniZH, Canton Zurich, and SER); the Ministry of Science and Technology, Taipei; the Thailand Center of Excellence in Physics, the Institute for the Promotion of Teaching Science and Technology of Thailand, Special Task Force for Activating Research and the National Science and Technology Development Agency of Thailand; the Scientific and Technical Research Council of Turkey, and Turkish Atomic Energy Authority; the National Academy of Sciences of Ukraine, and State Fund for Fundamental Researches, Ukraine; the Science and Technology Facilities Council, UK; the US Department of Energy, and the US National Science Foundation. Individuals have received support from the Marie-Curie programme and the European Research Council and Horizon 2020 Grant, Contract No. 675440 (European Union); the Leventis Foundation; the A. P. Sloan Foundation; the Alexander von Humboldt Foundation; the Belgian Federal Science Policy Office; the Fonds pour la Formation à la Recherche dans l'Industrie et dans l'Agriculture (FRIA-Belgium); the Agentschap voor Innovatie door Wetenschap en Technologie (IWT-Belgium); the F.R.S.-FNRS and FWO (Belgium) under the "Excellence of Science - EOS" - be.h project n. 30820817; the Ministry of Education, Youth and Sports (MEYS) of the Czech Republic; the Lendület ("Momen-

tum") Programme and the János Bolyai Research Scholarship of the Hungarian Academy of Sciences, the New National Excellence Program ÚNKP, the NKFIA Research Grants 123842, 123959, 124845, 124850 and 125105 (Hungary); the Council of Scientific and Industrial Research, India; the HOMING PLUS programme of the Foundation for Polish Science, cofinanced from European Union, Regional Development Fund, the Mobility Plus programme of the Ministry of Science and Higher Education, the National Science Center (Poland), contracts Harmonia 2014/14/M/ST2/00428, Opus 2014/13/B/ST2/02543, 2014/15/B/ST2/03998, and 2015/19/B/ST2/02861, Sonata-bis 2012/07/E/ST2/01406; the National Priorities Research Program by Qatar National Research Fund; the Programa de Excelencia María de Maeztu and the Programa Severo Ochoa del Principado de Asturias; the Thalis and Aristeia programmes cofinanced by EU-ESF and the Greek NSRF; the Rachadapisek Sompot Fund for Postdoctoral Fellowship, Chulalongkorn University and the Chulalongkorn Academic into Its second Century Project Advancement Project (Thailand); the Welch Foundation, contract C-1845; and the Weston Havens Foundation (USA).

Data Availability Statement This manuscript has no associated data or the data will not be deposited. [Authors' comment: Release and preservation of data used by the CMS Collaboration as the basis for publications is guided by the CMS policy as written in its document "CMS data preservation, re-use and open access policy" (https://cmsdocdb.cern.ch/cgi-bin/PublicDocDB/RetrieveFile?docid=6032&filename=CMSDataPolicyV1.2.pdf&version=2).]

Funded by SCOAP[3].

References

1. S.L. Glashow, Partial-symmetries of weak interactions. Nucl. Phys. **22**, 579 (1961). https://doi.org/10.1016/0029-5582(61)90469-2
2. S. Weinberg, A model of leptons. Phys. Rev. Lett. **19**, 1264 (1967). https://doi.org/10.1103/PhysRevLett.19.1264
3. A. Salam, "Weak and electromagnetic interactions", in Elementary particle physics: relativistic groups and analyticity. N. Svartholm, ed. Almqvist & Wiskell. Proceedings of the 8th Nobel symposium, p. 367 (1968)
4. G 't Hooft, M .J .G. Veltman, Regularization and renormalization of gauge fields. Nucl. Phys. B **44**, 189 (1972). https://doi.org/10.1016/0550-3213(72)90279-9
5. F. Englert, R. Brout, Broken symmetry and the mass of gauge vector mesons. Phys. Rev. Lett. **13**, 321 (1964). https://doi.org/10.1103/PhysRevLett.13.321
6. P.W. Higgs, Broken symmetries, massless particles and gauge fields. Phys. Lett. **12**, 132 (1964). https://doi.org/10.1016/0031-9163(64)91136-9
7. P.W. Higgs, Broken symmetries and the masses of gauge bosons. Phys. Rev. Lett. **13**, 508 (1964). https://doi.org/10.1103/PhysRevLett.13.508
8. G.S. Guralnik, C.R. Hagen, T.W.B. Kibble, Global conservation laws and massless particles. Phys. Rev. Lett. **13**, 585 (1964). https://doi.org/10.1103/PhysRevLett.13.585
9. P.W. Higgs, Spontaneous symmetry breakdown without massless bosons. Phys. Rev. **145**, 1156 (1966). https://doi.org/10.1103/PhysRev.145.1156
10. T.W.B. Kibble, Symmetry breaking in non-Abelian gauge theories. Phys. Rev. **155**, 1554 (1967). https://doi.org/10.1103/PhysRev.155.1554
11. Y. Nambu, G. Jona-Lasinio, Dynamical model of elementary particles based on an analogy with superconductivity. I. Phys. Rev. **122**, 345 (1961). https://doi.org/10.1103/PhysRev.122.345
12. ATLAS Collaboration, "Observation of a new particle in the search for the standard model Higgs boson with the ATLAS detector at the LHC", Phys. Lett. B **716**, 1 (2012). https://doi.org/10.1016/j.physletb.2012.08.020. arXiv:1207.7214
13. CMS Collaboration, Observation of a new boson at a mass of 125 GeV with the CMS experiment at the LHC. Phys. Lett. B **716**, 30 (2012). https://doi.org/10.1016/j.physletb.2012.08.021. arXiv:1207.7235
14. CMS Collaboration, Observation of a new boson with mass near 125 GeV in pp collisions at $\sqrt{s} = 7$ and 8 TeV. JHEP **06**, 81 (2013). https://doi.org/10.1007/JHEP06(2013)081. arXiv:1303.4571
15. K.G. Wilson, Renormalization group and strong interactions. Phys. Rev. D **3**, 1818 (1971). https://doi.org/10.1103/PhysRevD.3.1818
16. E. Gildener, Gauge-symmetry hierarchies. Phys. Rev. D **14**, 1667 (1976). https://doi.org/10.1103/PhysRevD.14.1667
17. S. Weinberg, Gauge hierarchies. Phys. Lett. B **82**, 387 (1979). https://doi.org/10.1016/0370-2693(79)90248-X
18. G 't Hooft, Naturalness, chiral symmetry, and spontaneous chiral symmetry breaking. NATO Sci. Ser. B **59**, 135 (1980). https://doi.org/10.1007/978-1-4684-7571-5_9
19. L. Susskind, Dynamics of spontaneous symmetry breaking in the Weinberg-Salam theory. Phys. Rev. D **20**, 2619 (1979). https://doi.org/10.1103/PhysRevD.20.2619
20. S. Dimopoulos, H. Georgi, Softly broken supersymmetry and SU(5). Nucl. Phys. B **193**, 150 (1981). https://doi.org/10.1016/0550-3213(81)90522-8
21. E. Witten, Dynamical breaking of supersymmetry. Nucl. Phys. B **188**, 513 (1981). https://doi.org/10.1016/0550-3213(81)90006-7
22. N. Arkani-Hamed, S. Dimopoulos, G. Dvali, The hierarchy problem and new dimensions at a millimeter. Phys. Lett. B **429**, 263 (1998). https://doi.org/10.1016/S0370-2693(98)00466-3. arXiv:hep-ph/9803315
23. L. Randall, R. Sundrum, Large mass hierarchy from a small extra dimension. Phys. Rev. Lett. **83**, 3370 (1999). https://doi.org/10.1103/PhysRevLett.83.3370. arXiv:hep-ph/9905221
24. N. Arkani-Hamed, A.G. Cohen, H. Georgi, Electroweak symmetry breaking from dimensional deconstruction. Phys. Lett. B **513**, 232 (2001). https://doi.org/10.1016/S0370-2693(01)00741-9. arXiv:hep-ph/0105239
25. G. Bélanger et al., The MSSM invisible Higgs in the light of dark matter and g-2. Phys. Lett. B **519**, 93 (2001). https://doi.org/10.1016/S0370-2693(01)00976-5. arXiv:hep-ph/0106275
26. G.F. Giudice, R. Rattazzi, J.D. Wells, Graviscalars from higher-dimensional metrics and curvature-Higgs mixing. Nucl. Phys. B **595**, 250 (2001). https://doi.org/10.1016/S0550-3213(00)00686-6. arXiv:hep-ph/0002178
27. D. Dominici, J.F. Gunion, Invisible Higgs decays from Higgs-graviscalar mixing. Phys. Rev. D **80**, 115006 (2009). https://doi.org/10.1103/PhysRevD.80.115006. arXiv:0902.1512
28. C. Bonilla, J.C. Romão, J.W.F. Valle, Neutrino mass and invisible Higgs decays at the LHC. Phys. Rev. D **91**, 113015 (2015). https://doi.org/10.1103/PhysRevD.91.113015. arXiv:1502.01649
29. C. Anastasiou et al., Higgs boson gluon–fusion production in QCD at three loops. Phys. Rev. Lett. **114**, 212001 (2015). https://doi.org/10.1103/PhysRevLett.114.212001. arXiv:1503.06056
30. C. Anastasiou et al., High precision determination of the gluon–fusion Higgs boson cross-section at the LHC. JHEP **05**, 58 (2016). https://doi.org/10.1007/JHEP05(2016)058. arXiv:1602.00695

31. M. Ciccolini, A. Denner, S. Dittmaier, Strong and electroweak corrections to the production of a Higgs boson+2 jets via weak interactions at the Large Hadron Collider. Phys. Rev. Lett. **99**, 161803 (2007). https://doi.org/10.1103/PhysRevLett.99.161803. arXiv:0707.0381
32. M. Ciccolini, A. Denner, S. Dittmaier, Electroweak and QCD corrections to Higgs production via vector-boson fusion at the LHC. Phys. Rev. D **77**, 013002 (2008). https://doi.org/10.1103/PhysRevD.77.013002. arXiv:0710.4749
33. P. Bolzoni, F. Maltoni, S.-O. Moch, M. Zaro, Higgs production via vector-boson fusion at NNLO in QCD. Phys. Rev. Lett. **105**, 011801 (2010). https://doi.org/10.1103/PhysRevLett.105.011801. arXiv:1003.4451
34. P. Bolzoni, F. Maltoni, S.-O. Moch, M. Zaro, Vector boson fusion at next-to-next-to-leading order in QCD: standard model Higgs boson and beyond. Phys. Rev. D **85**, 035002 (2012). https://doi.org/10.1103/PhysRevD.85.035002. arXiv:1109.3717
35. O. Brein, A. Djouadi, R. Harlander, NNLO QCD corrections to the Higgs-strahlung processes at hadron colliders. Phys. Lett. B **579**, 149 (2004). https://doi.org/10.1016/j.physletb.2003.10.112. arXiv:hep-ph/0307206
36. M.L. Ciccolini, S. Dittmaier, M. Krämer, Electroweak radiative corrections to associated WH and ZH production at hadron colliders. Phys. Rev. D **68**, 073003 (2003). https://doi.org/10.1103/PhysRevD.68.073003. arXiv:hep-ph/0306234
37. W. Beenakker et al., Higgs radiation off top quarks at the Tevatron and the LHC. Phys. Rev. Lett. **87**, 201805 (2001). https://doi.org/10.1103/PhysRevLett.87.201805. arXiv:hep-ph/0107081
38. W. Beenakker et al., NLO QCD corrections to $t\bar{t}$ H production in hadron collisions. Nucl. Phys. B **653**, 151 (2003). https://doi.org/10.1016/S0550-3213(03)00044-0. arXiv:hep-ph/0211352
39. S. Dawson, L.H. Orr, L. Reina, D. Wackeroth, Associated top quark Higgs boson production at the LHC. Phys. Rev. D **67**, 071503 (2003). https://doi.org/10.1103/PhysRevD.67.071503. arXiv:hep-ph/0211438
40. S. Dawson et al., Associated Higgs production with top quarks at the Large Hadron Collider: NLO QCD corrections. Phys. Rev. D **68**, 034022 (2003). https://doi.org/10.1103/PhysRevD.68.034022. arXiv:hep-ph/0305087
41. Z. Yu et al., QCD NLO and EW NLO corrections to $t\bar{t}H$ production with top quark decays at hadron collider. Phys. Lett. B **738**, 1 (2014). https://doi.org/10.1016/j.physletb.2014.09.022. arXiv:1407.1110
42. S.S. Frixione et al., Weak corrections to Higgs hadroproduction in association with a top-quark pair. JHEP **09**, 65 (2014). https://doi.org/10.1007/JHEP09(2014)065. arXiv:1407.0823
43. F. Demartin, F. Maltoni, K. Mawatari, M. Zaro, Higgs production in association with a single top quark at the LHC. Eur. Phys. J. C **75**, 267 (2015). https://doi.org/10.1140/epjc/s10052-015-3475-9. arXiv:1504.0611
44. S. Frixione et al., Electroweak and QCD corrections to top-pair hadroproduction in association with heavy bosons. JHEP **06**, 184 (2015). https://doi.org/10.1007/JHEP06(2015)184. arXiv:1504.03446
45. F. Demartin et al., tWH associated production at the LHC. Eur. Phys. J. C **77**, 34 (2017). https://doi.org/10.1140/epjc/s10052-017-4601-7. arXiv:1607.05862
46. A. Denner et al., Standard model Higgs-boson branching ratios with uncertainties. Eur. Phys. J. C **71**, 1753 (2011). https://doi.org/10.1140/epjc/s10052-011-1753-8. arXiv:1107.5909
47. A. Djouadi, J. Kalinowski, M. Spira, HDECAY: a program for Higgs boson decays in the standard model and its supersymmetric extension. Comput. Phys. Commun. **108**, 56 (1998). https://doi.org/10.1016/S0010-4655(97)00123-9. arXiv:hep-ph/9704448
48. A. Djouadi, J. Kalinowski, M. Muhlleitner, M. Spira, "An update of the program HDECAY", in The Les Houches 2009 workshop on TeV colliders: the tools and Monte Carlo working group summary report. (2010). arXiv:1003.1643
49. A. Bredenstein, A. Denner, S. Dittmaier, M.M. Weber, Precise predictions for the Higgs-boson decay H → WW/ZZ → 4 leptons. Phys. Rev. D **74**, 013004 (2006). https://doi.org/10.1103/PhysRevD.74.013004. arXiv:hep-ph/0604011
50. A. Bredenstein, A. Denner, S. Dittmaier, M.M. Weber, Radiative corrections to the semileptonic and hadronic Higgs-boson decays H →WW/ZZ→ 4 fermions. JHEP **02**, 80 (2007). https://doi.org/10.1088/1126-6708/2007/02/080. arXiv:hep-ph/0611234
51. S. Boselli et al., Higgs boson decay into four leptons at NLOPS electroweak accuracy. JHEP **06**, 23 (2015). https://doi.org/10.1007/JHEP06(2015)023. arXiv:1503.07394
52. S. Actis, G. Passarino, C. Sturm, S. Uccirati, NNLO computational techniques: the cases $H \to \gamma\gamma$ and $H \to gg$. Nucl. Phys. B **811**, 182 (2009). https://doi.org/10.1016/j.nuclphysb.2008.11.024. arXiv:0809.3667
53. LHC Higgs Cross Section Working Group, Handbook of LHC Higgs cross sections: 4. Deciphering the nature of the Higgs sector (2016). arXiv:1610.07922
54. ATLAS Collaboration, Measurements of the Higgs boson production and decay rates and coupling strengths using pp collision data at $\sqrt{s} = 7$ and 8 TeV in the ATLAS experiment. Eur. Phys. J. C **76**, 6 (2016). https://doi.org/10.1140/epjc/s10052-015-3769-y. arXiv:1507.04548
55. CMS Collaboration, Precise determination of the mass of the Higgs boson and tests of compatibility of its couplings with the standard model predictions using proton collisions at 7 and 8 TeV. Eur. Phys. J. C **75**, 212 (2015). https://doi.org/10.1140/epjc/s10052-015-3351-7. arXiv:1412.8662
56. ATLAS and CMS Collaborations, Measurements of the Higgs boson production and decay rates and constraints on its couplings from a combined ATLAS and CMS analysis of the LHC pp collision data at $\sqrt{s} = 7$ and 8 TeV. JHEP **08**, 45 (2016). https://doi.org/10.1007/JHEP08(2016)045. arXiv:1606.02266
57. CMS Collaboration, The CMS experiment at the CERN LHC. JINST **3**, S08004 (2008). https://doi.org/10.1088/1748-0221/3/08/S08004
58. CMS Collaboration, Measurements of Higgs boson properties in the diphoton decay channel in proton–proton collisions at $\sqrt{s} =$ 13 TeV. (2018). arXiv:1804.02716. *Submitted to JHEP*
59. CMS Collaboration, Measurements of properties of the Higgs boson decaying into the four-lepton final state in pp collisions at $\sqrt{s} = 13$ TeV. JHEP **11**, 47 (2017). https://doi.org/10.1007/JHEP11(2017)047. arXiv:1706.09936
60. CMS Collaboration, Measurements of properties of the Higgs boson decaying to a W boson pair in pp collisions at $\sqrt{s} = 13$ TeV (2018). arXiv:1806.05246. Submitted to Phys. Lett. B
61. CMS Collaboration, Observation of the Higgs boson decay to a pair of τ leptons with the CMS detector. Phys. Lett. B **779**, 283 (2018). https://doi.org/10.1016/j.physletb.2018.02.004. arXiv:1708.00373
62. CMS Collaboration, Evidence for the Higgs boson decay to a bottom quark–antiquark pair. Phys. Lett. B **780**, 501 (2018). https://doi.org/10.1016/j.physletb.2018.02.050. arXiv:1709.07497
63. CMS Collaboration, Inclusive search for a highly boosted Higgs boson decaying to a bottom quark–antiquark pair. Phys. Rev. Lett. **120**, 071802 (2018). https://doi.org/10.1103/PhysRevLett.120.071802. arXiv:1709.05543
64. M. Cacciari, G.P. Salam, G. Soyez, The anti-k_T jet clustering algorithm. JHEP **04**, 63 (2008). https://doi.org/10.1088/1126-6708/2008/04/063. arXiv:0802.1189
65. M. Cacciari, G.P. Salam, G. Soyez, FastJet user manual. Eur. Phys. J. C **72**, 1896 (2012). https://doi.org/10.1140/epjc/s10052-012-1896-2. arXiv:1111.6097

66. M. Dasgupta, A. Fregoso, S. Marzani, G.P. Salam, Towards an understanding of jet substructure. JHEP **09**, 29 (2013). https://doi.org/10.1007/JHEP09(2013)029. arXiv:1307.0007
67. A.J. Larkoski, S. Marzani, G. Soyez, J. Thaler, Soft drop. JHEP **05**, 146 (2014). https://doi.org/10.1007/JHEP05(2014)146. arXiv:1402.2657
68. CMS Collaboration, Observation of $t\bar{t}H$ production. Phys. Rev. Lett. **120**, 231801 (2018). https://doi.org/10.1103/PhysRevLett.120.231801. arXiv:1804.02610
69. CMS Collaboration, Evidence for associated production of a Higgs boson with a top quark pair in final states with electrons, muons, and hadronically decaying τ leptons at $\sqrt{s} = 13$ TeV. JHEP **08**, 066 (2018). https://doi.org/10.1007/JHEP08(2018)066. arXiv:1803.05485
70. CMS Collaboration, Search for $t\bar{t}$H production in the H$b\bar{b}$ decay channel with leptonic $t\bar{t}$ decays in proton–proton collisions at $sqrts = 13$ TeV. (2018). arXiv:1804.03682. Submitted to JHEP
71. CMS Collaboration, Search for t$\bar{t}$H production in the all-jet final state in proton-proton collisions at $\sqrt{s} = 13$ TeV (2018). arXiv:1803.06986. Submitted to JHEP
72. J. Schmidhuber, Deep learning in neural networks: an overview. Neural Netw. **61**, 85 (2015). https://doi.org/10.1016/j.neunet.2014.09.003
73. CMS Collaboration, Search for the Higgs boson decaying to two muons in proton–proton collisions at $\sqrt{s} = 13$ TeV (2018). arXiv:1807.06325. Submitted to Phys. Rev. Lett
74. R.E. Shrock, M. Suzuki, Invisible decays of Higgs bosons. Phys. Lett. B **110**, 250 (1982). https://doi.org/10.1016/0370-2693(82)91247-3
75. CMS Collaboration, Search for invisible decays of a Higgs boson produced through vector boson fusion in proton–proton collisions at $\sqrt{s} = 13$ TeV (2018). arXiv:1809.05937. Submitted to Phys. Lett. B
76. CMS Collaboration, Search for new physics in events with a leptonically decaying Z boson and a large transverse momentum imbalance in proton–proton collisions at $\sqrt{s} = 13$ TeV. Eur. Phys. J. C **78**, 291 (2017). https://doi.org/10.1140/epjc/s10052-018-5740-1. arXiv:1711.00431
77. CMS Collaboration, Search for new physics in final states with an energetic jet or a hadronically decaying W or Z boson and transverse momentum imbalance at $\sqrt{s} = 13$ TeV. Phys. Rev. D **97**, 092005 (2018). https://doi.org/10.1103/PhysRevD.97.092005. arXiv:1712.02345
78. E. Bagnaschi, G. Degrassi, P. Slavich, A. Vicini, Higgs production via gluon fusion in the POWHEG approach in the SM and in the MSSM. JHEP **02**, 88 (2012). https://doi.org/10.1007/JHEP02(2012)088. arXiv:1111.2854
79. P. Nason, A new method for combining NLO QCD with shower Monte Carlo algorithms. JHEP **11**, 040 (2004). https://doi.org/10.1088/1126-6708/2004/11/040. arXiv:hep-ph/0409146
80. S. Frixione, P. Nason, C. Oleari, Matching NLO QCD computations with parton shower simulations: the *powheg* method. JHEP **11**, 070 (2007). https://doi.org/10.1088/1126-6708/2007/11/070. arXiv:0709.2092
81. S. Alioli, P. Nason, C. Oleari, E. Re, A general framework for implementing NLO calculations in shower Monte Carlo programs: the POWHEG BOX. JHEP **06**, 043 (2010). https://doi.org/10.1007/JHEP06(2010)043. arXiv:1002.2581
82. J. Alwall et al., The automated computation of tree-level and next-to-leading order differential cross sections, and their matching to parton shower simulations. JHEP **07**, 079 (2014). https://doi.org/10.1007/JHEP07(2014)079. arXiv:1405.0301
83. R. Frederix, S. Frixione, Merging meets matching in MC@NLO. JHEP **12**, 61 (2012). https://doi.org/10.1007/JHEP12(2012)061. arXiv:1209.6215
84. K. Hamilton, P. Nason, E. Re, G. Zanderighi, NNLOPS simulation of Higgs boson production. JHEP **10**, 222 (2013). https://doi.org/10.1007/JHEP10(2013)222. arXiv:1309.0017
85. K. Hamilton, P. Nason, G. Zanderighi, Finite quark-mass effects in the NNLOPS POWHEG + MiNLO Higgs generator (2015). arXiv:1501.04637
86. R. Barlow, C. Beeston, Fitting using finite Monte Carlo samples. Comput. Phys. Commun. **77**, 219 (1993). https://doi.org/10.1016/0010-4655(93)90005-W
87. J.S. Conway, Incorporating nuisance parameters in likelihoods for multisource spectra (2011). arXiv:1103.0354
88. The ATLAS Collaboration, The CMS Collaboration, The LHC Higgs Combination Group, Procedure for the LHC Higgs boson search combination in Summer 2011. Technical Report CMS-NOTE-2011-005, ATL-PHYS-PUB-2011-11 (2011)
89. CMS Collaboration, Combined results of searches for the standard model Higgs boson in pp collisions at $\sqrt{s} = 7$ TeV. Phys. Lett. B **710**, 26 (2012). https://doi.org/10.1016/j.physletb.2012.02.064. arXiv:1202.1488
90. W. Verkerke, D.P. Kirkby, The RooFit toolkit for data modeling. In 13$^{\text{th}}$ International Conference for Computing in High Energy and Nuclear Physics (CHEP03). 2003. arXiv:physics/0306116. CHEP-2003-MOLT007
91. L. Monetaet al., The RooStats project. In: 13th International Workshop on Advanced Computing and Analysis Techniques in Physics Research (ACAT2010). SISSA (2010). arXiv:1009.1003. PoS(ACAT2010)057
92. G. Cowan, K. Cranmer, E. Gross, O. Vitells, Asymptotic formulae for likelihood-based tests of new physics. Eur. Phys. J. C **71**, 1554 (2011). https://doi.org/10.1140/epjc/s10052-011-1554-0. arXiv:1007.1727. [Erratum: 10.1140/epjc/s10052-013-2501-z]
93. ATLAS and CMS Collaborations, Combined Measurement of the Higgs Boson Mass in pp Collisions at $\sqrt{s} = 7$ and 8 TeV with the ATLAS and CMS Experiments. Phys. Rev. Lett. **114**, 191803 (2015). https://doi.org/10.1103/PhysRevLett.114.191803. arXiv:1503.07589
94. CMS Collaboration, CMS luminosity measurements for the 2016 data taking period. CMS Physics Analysis Summary CMS-PAS-LUM-17-001 (2017)
95. E. Boos, V. Bunichev, M. Dubinin, Y. Kurihara, Higgs boson signal at complete tree level in the SM extension by dimension-six operators. Phys. Rev. D **89**, 035001 (2014). https://doi.org/10.1103/PhysRevD.89.035001. arXiv:1309.5410
96. LHC Higgs Cross Section Working Group, Handbook of LHC Higgs Cross Sections: 3. Higgs Properties. (2013). arXiv:1307.1347
97. C. Englert, M. McCullough, M. Spannowsky, Gluon-initiated associated production boosts Higgs physics. Phys. Rev. D **89**, 013013 (2014). https://doi.org/10.1103/PhysRevD.89.013013. arXiv:1310.4828
98. K. Hagiwara, R. Szalapski, D. Zeppenfeld, Anomalous Higgs boson production and decay. Phys. Lett. B **318**, 155 (1993). https://doi.org/10.1016/0370-2693(93)91799-S. arXiv:hep-ph/9308347
99. C. Arzt, M.B. Einhorn, J. Wudka, Patterns of deviation from the standard model. Nucl. Phys. B **433**, 41 (1995). https://doi.org/10.1016/0550-3213(94)00336-D. arXiv:hep-ph/9405214
100. D. Zeppenfeld, R. Kinnunen, A. Nikitenko, E. Richter-Was, Measuring Higgs boson couplings at the CERN LHC. Phys. Rev. D **62**, 013009 (2000). https://doi.org/10.1103/PhysRevD.62.013009. arXiv:hep-ph/0002036
101. V. Barger et al., Effects of genuine dimension-six Higgs operators. Phys. Rev. D **67**, 115001 (2003). https://doi.org/10.1103/PhysRevD.67.115001. arXiv:hep-ph/0301097
102. M. Duhrssen et al., Extracting Higgs boson couplings from CERN LHC data. Phys. Rev. D **70**, 113009 (2004). https://doi.org/10.1103/PhysRevD.70.113009. arXiv:hep-ph/0406323

103. A. Manohar, M. Wise, Modifications to the properties of the Higgs boson. Phys. Lett. B **636**, 107 (2006). https://doi.org/10.1016/j.physletb.2006.03.030. arXiv:hep-ph/0601212
104. I. Low, R. Rattazzi, A. Vichi, Theoretical constraints on the Higgs effective couplings. JHEP **04**, 126 (2010). https://doi.org/10.1007/JHEP04(2010)126. arXiv:0907.5413
105. J. Ellis, T. You, Global analysis of experimental constraints on a possible Higgs-like particle with mass 125 GeV. JHEP **06**, 140 (2012). https://doi.org/10.1007/JHEP06(2012)140. arXiv:1204.0464
106. T. Corbett, O.J.P. Eboli, J. Gonzalez-Fraile, M.C. Gonzalez-Garcia, Constraining anomalous Higgs boson interactions. Phys. Rev. D **86**, 075013 (2012). https://doi.org/10.1103/PhysRevD.86.075013. arXiv:1207.1344
107. G. Passarino, NLO inspired effective Lagrangians for Higgs physics. Nucl. Phys. B **868**, 416 (2013). https://doi.org/10.1016/j.nuclphysb.2012.11.018. arXiv:1209.5538
108. M. Klute et al., Measuring Higgs couplings from LHC data. Phys. Rev. Lett. **109**, 101801 (2012). https://doi.org/10.1103/PhysRevLett.109.101801. arXiv:1205.2699
109. R. Contino et al., Effective Lagrangian for a light Higgs-like scalar. JHEP **07**, 35 (2013). https://doi.org/10.1007/JHEP07(2013)035. arXiv:1303.3876
110. W.-F. Chang, W.-P. Pan, F. Xu, Effective gauge-Higgs operators analysis of new physics associated with the Higgs boson. Phys. Rev. D **88**, 033004 (2013). https://doi.org/10.1103/PhysRevD.88.033004. arXiv:1303.7035
111. P.P. Giardino et al., The universal Higgs fit. JHEP **05**, 46 (2014). https://doi.org/10.1007/JHEP05(2014)046. arXiv:1303.3570
112. M. Ghezzi, R. Gomez-Ambrosio, G. Passarino, S. Uccirati, NLO Higgs effective field theory and κ-framework. JHEP **07**, 175 (2015). https://doi.org/10.1007/JHEP07(2015)175. arXiv:1505.03706
113. J. Ellis, T. You, Global analysis of the Higgs candidate with mass $\sim$ 125 GeV. JHEP **09**, 123 (2012). https://doi.org/10.1007/JHEP09(2012)123. arXiv:1207.1693
114. J. Ellis, T. You, Updated global analysis of Higgs couplings. JHEP **06**, 103 (2013). https://doi.org/10.1007/JHEP06(2013)103. arXiv:1303.3879
115. Particle Data Group, Review of particle physics. Chin. Phys. C **40**, 100001 (2016). https://doi.org/10.1088/1674-1137/40/10/100001
116. G.C. Branco et al., Theory and phenomenology of two-Higgs-doublet models. Phys. Rept. **516**, 1 (2012). https://doi.org/10.1016/j.physrep.2012.02.002. arXiv:1106.0034
117. J.F. Gunion, H.E. Haber, CP-conserving two-Higgs-doublet model: the approach to the decoupling limit. Phys. Rev. D **67**, 075019 (2003). https://doi.org/10.1103/PhysRevD.67.075019. arXiv:hep-ph/0207010
118. L. Maiani, A.D. Polosa, V. Riquer, Bounds to the Higgs sector masses in minimal supersymmetry from LHC data. Phys. Lett. B **724**, 274 (2013). https://doi.org/10.1016/j.physletb.2013.06.026. arXiv:1305.2172
119. A. Djouadi, The Anatomy of electroweak symmetry breaking Tome II. The Higgs bosons in the minimal supersymmetric model. Phys. Rept. **459**, 1 (2008). https://doi.org/10.1016/j.physrep.2007.10.005. arXiv:hep-ph/0503173
120. J.F. Gunion, H.E. Haber, Higgs bosons in supersymmetric models (I). Nucl. Phys. B **272**, 1 (1986). https://doi.org/10.1016/0550-3213(86)90340-8
121. H.E. Haber, G.L. Kane, The search for supersymmetry: probing physics beyond the standard model. Phys. Rept. **117**, 75 (1985). https://doi.org/10.1016/0370-1573(85)90051-1
122. H.P. Nilles, Supersymmetry, supergravity and particle physics. Phys. Rept. **110**, 1 (1984). https://doi.org/10.1016/0370-1573(84)90008-5
123. A. Djouadi et al., The post-Higgs MSSM scenario: habemus MSSM? Eur. Phys. J. C **73**, 2650 (2013). https://doi.org/10.1140/epjc/s10052-013-2650-0. arXiv:1307.5205
124. A. Djouadi et al., Fully covering the MSSM Higgs sector at the LHC. JHEP **06**, 168 (2015). https://doi.org/10.1007/JHEP06(2015)168. arXiv:1502.05653
125. ATLAS Collaboration, Constraints on new phenomena via Higgs boson couplings and invisible decays with the ATLAS detector. JHEP **11**, 206 (2015). https://doi.org/10.1007/JHEP11(2015)206. arXiv:1509.00672
126. M. Carena et al., MSSM Higgs boson searches at the LHC: benchmark scenarios after the discovery of a Higgs-like particle. Eur. Phys. J. C **73**, 2552 (2013). https://doi.org/10.1140/epjc/s10052-013-2552-1. arXiv:1302.7033
127. ATLAS Collaboration, Search for heavy resonances decaying into WW in the $e\nu\mu\nu$ final state in pp collisions at $\sqrt{s} = 13$ TeV with the ATLAS detector. Eur. Phys. J. C **78**, 24 (2018). https://doi.org/10.1140/epjc/s10052-017-5491-4. arXiv:1710.01123
128. ATLAS Collaboration, Search for additional heavy neutral Higgs and gauge bosons in the ditau final state produced in 36 fb^{-1} of pp collisions at $\sqrt{s}$ = 13 TeV with the ATLAS detector. JHEP **01**, 55 (2018). https://doi.org/10.1007/JHEP01(2018)055. arXiv:1709.07242
129. ATLAS Collaboration, Search for charged Higgs bosons produced in association with a top quark and decaying via $H^{\pm} \to \tau\nu$ using pp collision data recorded at $\sqrt{s} = 13$ TeV by the ATLAS detector. Phys. Lett. B **759**, 555 (2016). https://doi.org/10.1016/j.physletb.2016.06.017. arXiv:1603.09203
130. CMS Collaboration, Search for neutral MSSM Higgs bosons decaying to a pair of tau leptons in pp collisions. JHEP **10**, 160 (2014). https://doi.org/10.1007/JHEP10(2014)160. arXiv:1408.3316
131. CMS Collaboration, Search for a standard-model-like Higgs boson with a mass in the range 145 to 1000 GeV at the LHC. Eur. Phys. J. C **73**, 2469 (2013). https://doi.org/10.1140/epjc/s10052-013-2469-8. arXiv:1304.0213

CMS Collaboration

Yerevan Physics Institute, Yerevan, Armenia
A. M. Sirunyan, A. Tumasyan

Institut für Hochenergiephysik, Wien, Austria
W. Adam, F. Ambrogi, E. Asilar, T. Bergauer, J. Brandstetter, M. Dragicevic, J. Erö, A. Escalante Del Valle, M. Flechl, R. Frühwirth[1], V. M. Ghete, J. Hrubec, M. Jeitler[1], N. Krammer, I. Krätschmer, D. Liko, T. Madlener, I. Mikulec, N. Rad, H. Rohringer, J. Schieck[1], R. Schöfbeck, M. Spanring, D. Spitzbart, A. Taurok, W. Waltenberger, J. Wittmann, C.-E. Wulz[1], M. Zarucki

Institute for Nuclear Problems, Minsk, Belarus
V. Chekhovsky, V. Mossolov, J. Suarez Gonzalez

Universiteit Antwerpen, Antwerpen, Belgium
E. A. De Wolf, D. Di Croce, X. Janssen, J. Lauwers, M. Pieters, H. Van Haevermaet, P. Van Mechelen, N. Van Remortel

Vrije Universiteit Brussel, Brussels, Belgium
S. Abu Zeid, F. Blekman, J. D'Hondt, I. De Bruyn, J. De Clercq, K. Deroover, G. Flouris, D. Lontkovskyi, S. Lowette, I. Marchesini, S. Moortgat, L. Moreels, Q. Python, K. Skovpen, S. Tavernier, W. Van Doninck, P. Van Mulders, I. Van Parijs

Université Libre de Bruxelles, Brussels, Belgium
D. Beghin, B. Bilin, H. Brun, B. Clerbaux, G. De Lentdecker, H. Delannoy, B. Dorney, G. Fasanella, L. Favart, R. Goldouzian, A. Grebenyuk, A. K. Kalsi, T. Lenzi, J. Luetic, N. Postiau, E. Starling, L. Thomas, C. Vander Velde, P. Vanlaer, D. Vannerom, Q. Wang

Ghent University, Ghent, Belgium
T. Cornelis, D. Dobur, A. Fagot, M. Gul, I. Khvastunov[2], D. Poyraz, C. Roskas, D. Trocino, M. Tytgat, W. Verbeke, B. Vermassen, M. Vit, N. Zaganidis

Université Catholique de Louvain, Louvain-la-Neuve, Belgium
H. Bakhshiansohi, O. Bondu, S. Brochet, G. Bruno, C. Caputo, P. David, C. Delaere, M. Delcourt, B. Francois, A. Giammanco, G. Krintiras, V. Lemaitre, A. Magitteri, A. Mertens, M. Musich, K. Piotrzkowski, A. Saggio, M. Vidal Marono, S. Wertz, J. Zobec

Centro Brasileiro de Pesquisas Fisicas, Rio de Janeiro, Brazil
F. L. Alves, G. A. Alves, M. Correa Martins Junior, G. Correia Silva, C. Hensel, A. Moraes, M. E. Pol, P. Rebello Teles

Universidade do Estado do Rio de Janeiro, Rio de Janeiro, Brazil
E. Belchior Batista Das Chagas, W. Carvalho, J. Chinellato[3], E. Coelho, E. M. Da Costa, G. G. Da Silveira[4], D. De Jesus Damiao, C. De Oliveira Martins, S. Fonseca De Souza, H. Malbouisson, D. Matos Figueiredo, M. Melo De Almeida, C. Mora Herrera, L. Mundim, H. Nogima, W. L. Prado Da Silva, L. J. Sanchez Rosas, A. Santoro, A. Sznajder, M. Thiel, E. J. Tonelli Manganote[3], F. Torres Da Silva De Araujo, A. Vilela Pereira

Universidade Estadual Paulista [a], Universidade Federal do ABC [b], São Paulo, Brazil
S. Ahuja[a], C. A. Bernardes[a], L. Calligaris[a], T. R. Fernandez Perez Tomei[a], E. M. Gregores[b], P. G. Mercadante[b], S. F. Novaes[a], SandraS. Padula[a]

Institute for Nuclear Research and Nuclear Energy, Bulgarian Academy of Sciences, Sofia, Bulgaria
A. Aleksandrov, R. Hadjiiska, P. Iaydjiev, A. Marinov, M. Misheva, M. Rodozov, M. Shopova, G. Sultanov

University of Sofia, Sofia, Bulgaria
A. Dimitrov, L. Litov, B. Pavlov, P. Petkov

Beihang University, Beijing, China
W. Fang[5], X. Gao[5], L. Yuan

Institute of High Energy Physics, Beijing, China
M. Ahmad, J. G. Bian, G. M. Chen, H. S. Chen, M. Chen, Y. Chen, C. H. Jiang, D. Leggat, H. Liao, Z. Liu, F. Romeo, S. M. Shaheen[6], A. Spiezia, J. Tao, C. Wang, Z. Wang, E. Yazgan, H. Zhang, S. Zhang, J. Zhao

State Key Laboratory of Nuclear Physics and Technology, Peking University, Beijing, China
Y. Ban, G. Chen, A. Levin, J. Li, L. Li, Q. Li, Y. Mao, S. J. Qian, D. Wang, Z. Xu

Tsinghua University, Beijing, China
Y. Wang

Universidad de Los Andes, Bogotá, Colombia
C. Avila, A. Cabrera, C. A. Carrillo Montoya, L. F. Chaparro Sierra, C. Florez, C. F. González Hernández, M. A. Segura Delgado

University of Split, Faculty of Electrical Engineering, Mechanical Engineering and Naval Architecture, Split, Croatia
B. Courbon, N. Godinovic, D. Lelas, I. Puljak, T. Sculac

University of Split, Faculty of Science, Split, Croatia
Z. Antunovic, M. Kovac

Institute Rudjer Boskovic, Zagreb, Croatia
V. Brigljevic, D. Ferencek, K. Kadija, B. Mesic, A. Starodumov[7], T. Susa

University of Cyprus, Nicosia, Cyprus
M. W. Ather, A. Attikis, M. Kolosova, G. Mavromanolakis, J. Mousa, C. Nicolaou, F. Ptochos, P. A. Razis, H. Rykaczewski

Charles University, Prague, Czech Republic
M. Finger[8], M. Finger Jr.[8]

Escuela Politecnica Nacional, Quito, Ecuador
E. Ayala

Universidad San Francisco de Quito, Quito, Ecuador
E. Carrera Jarrin

Academy of Scientific Research and Technology of the Arab Republic of Egypt, Egyptian Network of High Energy Physics, Cairo, Egypt
H. Abdalla[9], A. A. Abdelalim[10,11], E. Salama[12,13]

National Institute of Chemical Physics and Biophysics, Tallinn, Estonia
S. Bhowmik, A. Carvalho Antunes De Oliveira, R. K. Dewanjee, K. Ehataht, M. Kadastik, M. Raidal, C. Veelken

Department of Physics, University of Helsinki, Helsinki, Finland
P. Eerola, H. Kirschenmann, J. Pekkanen, M. Voutilainen

Helsinki Institute of Physics, Helsinki, Finland
J. Havukainen, J. K. Heikkilä, T. Järvinen, V. Karimäki, R. Kinnunen, T. Lampén, K. Lassila-Perini, S. Laurila, S. Lehti, T. Lindén, P. Luukka, T. Mäenpää, H. Siikonen, E. Tuominen, J. Tuominiemi

Lappeenranta University of Technology, Lappeenranta, Finland
T. Tuuva

IRFU, CEA, Université Paris-Saclay, Gif-sur-Yvette, France
M. Besancon, F. Couderc, M. Dejardin, D. Denegri, J. L. Faure, F. Ferri, S. Ganjour, A. Givernaud, P. Gras, G. Hamel de Monchenault, P. Jarry, C. Leloup, E. Locci, J. Malcles, G. Negro, J. Rander, A. Rosowsky, M. Ö. Sahin, M. Titov

Laboratoire Leprince-Ringuet, Ecole polytechnique, CNRS/IN2P3, Université Paris-Saclay, Palaiseau, France
A. Abdulsalam[14], C. Amendola, I. Antropov, F. Beaudette, P. Busson, C. Charlot, R. Granier de Cassagnac, I. Kucher, A. Lobanov, J. Martin Blanco, M. Nguyen, C. Ochando, G. Ortona, P. Paganini, P. Pigard, R. Salerno, J. B. Sauvan, Y. Sirois, A. G. Stahl Leiton, A. Zabi, A. Zghiche

Université de Strasbourg, CNRS, IPHC UMR 7178, Strasbourg, France
J.-L. Agram[15], J. Andrea, D. Bloch, J.-M. Brom, E. C. Chabert, V. Cherepanov, C. Collard, E. Conte[15], J.-C. Fontaine[15], D. Gelé, U. Goerlach, M. Jansová, A.-C. Le Bihan, N. Tonon, P. Van Hove

Centre de Calcul de l'Institut National de Physique Nucleaire et de Physique des Particules, CNRS/IN2P3, Villeurbanne, France
S. Gadrat

Université de Lyon, Université Claude Bernard Lyon 1, CNRS-IN2P3, Institut de Physique Nucléaire de Lyon, Villeurbanne, France
S. Beauceron, C. Bernet, G. Boudoul, N. Chanon, R. Chierici, D. Contardo, P. Depasse, H. El Mamouni, J. Fay, L. Finco, S. Gascon, M. Gouzevitch, G. Grenier, B. Ille, F. Lagarde, I. B. Laktineh, H. Lattaud, M. Lethuillier, L. Mirabito, A. L. Pequegnot, S. Perries, A. Popov[16], V. Sordini, G. Touquet, M. Vander Donckt, S. Viret

Georgian Technical University, Tbilisi, Georgia
A. Khvedelidze[8]

Tbilisi State University, Tbilisi, Georgia
Z. Tsamalaidze[8]

RWTH Aachen University, I. Physikalisches Institut, Aachen, Germany
C. Autermann, L. Feld, M. K. Kiesel, K. Klein, M. Lipinski, M. Preuten, M. P. Rauch, C. Schomakers, J. Schulz, M. Teroerde, B. Wittmer, V. Zhukov[16]

RWTH Aachen University, III. Physikalisches Institut A, Aachen, Germany
A. Albert, D. Duchardt, M. Endres, M. Erdmann, S. Ghosh, A. Güth, T. Hebbeker, C. Heidemann, K. Hoepfner, H. Keller, L. Mastrolorenzo, M. Merschmeyer, A. Meyer, P. Millet, S. Mukherjee, T. Pook, M. Radziej, H. Reithler, M. Rieger, A. Schmidt, D. Teyssier

RWTH Aachen University, III. Physikalisches Institut B, Aachen, Germany
G. Flügge, O. Hlushchenko, T. Kress, A. Künsken, T. Müller, A. Nehrkorn, A. Nowack, C. Pistone, O. Pooth, D. Roy, H. Sert, A. Stahl[17]

Deutsches Elektronen-Synchrotron, Hamburg, Germany
M. Aldaya Martin, T. Arndt, C. Asawatangtrakuldee, I. Babounikau, K. Beernaert, O. Behnke, U. Behrens, A. Bermúdez Martínez, D. Bertsche, A. A. Bin Anuar, K. Borras[18], V. Botta, A. Campbell, P. Connor, C. Contreras-Campana, F. Costanza, V. Danilov, A. De Wit, M. M. Defranchis, C. Diez Pardos, D. Domínguez Damiani, G. Eckerlin, T. Eichhorn, A. Elwood, E. Eren, E. Gallo[19], A. Geiser, J. M. Grados Luyando, A. Grohsjean, P. Gunnellini, M. Guthoff, M. Haranko, A. Harb, J. Hauk, H. Jung, M. Kasemann, J. Keaveney, C. Kleinwort, J. Knolle, D. Krücker, W. Lange, A. Lelek, T. Lenz, K. Lipka, W. Lohmann[20], R. Mankel, I.-A. Melzer-Pellmann, A. B. Meyer, M. Meyer, M. Missiroli, G. Mittag, J. Mnich, V. Myronenko, S. K. Pflitsch, D. Pitzl, A. Raspereza, M. Savitskyi, P. Saxena, P. Schütze, C. Schwanenberger, R. Shevchenko, A. Singh, H. Tholen, O. Turkot, A. Vagnerini, G. P. Van Onsem, R. Walsh, Y. Wen, K. Wichmann, C. Wissing, O. Zenaiev

University of Hamburg, Hamburg, Germany
R. Aggleton, S. Bein, L. Benato, A. Benecke, V. Blobel, M. Centis Vignali, T. Dreyer, E. Garutti, D. Gonzalez, J. Haller, A. Hinzmann, A. Karavdina, G. Kasieczka, R. Klanner, R. Kogler, N. Kovalchuk, S. Kurz, V. Kutzner, J. Lange, D. Marconi, J. Multhaup, M. Niedziela, D. Nowatschin, A. Perieanu, A. Reimers, O. Rieger, C. Scharf, P. Schleper, S. Schumann, J. Schwandt, J. Sonneveld, H. Stadie, G. Steinbrück, F. M. Stober, M. Stöver, A. Vanhoefer, B. Vormwald, I. Zoi

Karlsruher Institut fuer Technologie, Karlsruhe, Germany
M. Akbiyik, C. Barth, M. Baselga, S. Baur, E. Butz, R. Caspart, T. Chwalek, F. Colombo, W. De Boer, A. Dierlamm, K. El Morabit, N. Faltermann, B. Freund, M. Giffels, M. A. Harrendorf, F. Hartmann[17], S. M. Heindl, U. Husemann, F. Kassel[17], I. Katkov[16], S. Kudella, H. Mildner, S. Mitra, M. U. Mozer, Th. Müller, M. Plagge, G. Quast, K. Rabbertz, M. Schröder, I. Shvetsov, G. Sieber, H. J. Simonis, R. Ulrich, S. Wayand, M. Weber, T. Weiler, S. Williamson, C. Wöhrmann, R. Wolf

Institute of Nuclear and Particle Physics (INPP), NCSR Demokritos, Aghia Paraskevi, Greece
G. Anagnostou, G. Daskalakis, T. Geralis, A. Kyriakis, D. Loukas, G. Paspalaki, I. Topsis-Giotis

National and Kapodistrian University of Athens, Athens, Greece
G. Karathanasis, S. Kesisoglou, P. Kontaxakis, A. Panagiotou, I. Papavergou, N. Saoulidou, E. Tziaferi, K. Vellidis

National Technical University of Athens, Athens, Greece
K. Kousouris, I. Papakrivopoulos, G. Tsipolitis

University of Ioánnina, Ioannina, Greece
I. Evangelou, C. Foudas, P. Gianneios, P. Katsoulis, P. Kokkas, S. Mallios, N. Manthos, I. Papadopoulos, E. Paradas, J. Strologas, F. A. Triantis, D. Tsitsonis

MTA-ELTE Lendület CMS Particle and Nuclear Physics Group, Eötvös Loránd University, Budapest, Hungary
M. Bartók[21], M. Csanad, N. Filipovic, P. Major, M. I. Nagy, G. Pasztor, O. Surányi, G. I. Veres

Wigner Research Centre for Physics, Budapest, Hungary
G. Bencze, C. Hajdu, D. Horvath[22], Á. Hunyadi, F. Sikler, T. Á. Vámi, V. Veszpremi, G. Vesztergombi[†]

Institute of Nuclear Research ATOMKI, Debrecen, Hungary
N. Beni, S. Czellar, J. Karancsi[23], A. Makovec, J. Molnar, Z. Szillasi

Institute of Physics, University of Debrecen, Debrecen, Hungary
P. Raics, Z. L. Trocsanyi, B. Ujvari

Indian Institute of Science (IISc), Bangalore, India
S. Choudhury, J. R. Komaragiri, P. C. Tiwari

National Institute of Science Education and Research, HBNI, Bhubaneswar, India
S. Bahinipati[24], C. Kar, P. Mal, K. Mandal, A. Nayak[25], D. K. Sahoo[24], S. K. Swain

Panjab University, Chandigarh, India
S. Bansal, S. B. Beri, V. Bhatnagar, S. Chauhan, R. Chawla, N. Dhingra, R. Gupta, A. Kaur, M. Kaur, S. Kaur, R. Kumar, P. Kumari, M. Lohan, A. Mehta, K. Sandeep, S. Sharma, J. B. Singh, A. K. Virdi, G. Walia

University of Delhi, Delhi, India
A. Bhardwaj, B. C. Choudhary, R. B. Garg, M. Gola, S. Keshri, Ashok Kumar, S. Malhotra, M. Naimuddin, P. Priyanka, K. Ranjan, Aashaq Shah, R. Sharma

Saha Institute of Nuclear Physics, HBNI, Kolkata, India
R. Bhardwaj[26], M. Bharti, R. Bhattacharya, S. Bhattacharya, U. Bhawandeep[26], D. Bhowmik, S. Dey, S. Dutt[26], S. Dutta, S. Ghosh, K. Mondal, S. Nandan, A. Purohit, P. K. Rout, A. Roy, S. Roy Chowdhury, G. Saha, S. Sarkar, M. Sharan, B. Singh, S. Thakur[26]

Indian Institute of Technology Madras, Chennai, India
P. K. Behera

Bhabha Atomic Research Centre, Mumbai, India
R. Chudasama, D. Dutta, V. Jha, V. Kumar, P. K. Netrakanti, L. M. Pant, P. Shukla

Tata Institute of Fundamental Research-A, Mumbai, India
T. Aziz, M. A. Bhat, S. Dugad, G. B. Mohanty, N. Sur, B. Sutar, RavindraKumar Verma

Tata Institute of Fundamental Research-B, Mumbai, India
S. Banerjee, S. Bhattacharya, S. Chatterjee, P. Das, M. Guchait, Sa. Jain, S. Karmakar, S. Kumar, M. Maity[27], G. Majumder, K. Mazumdar, N. Sahoo, T. Sarkar[27]

Indian Institute of Science Education and Research (IISER), Pune, India
S. Chauhan, S. Dube, V. Hegde, A. Kapoor, K. Kothekar, S. Pandey, A. Rane, S. Sharma

Institute for Research in Fundamental Sciences (IPM), Tehran, Iran
S. Chenarani[28], E. Eskandari Tadavani, S. M. Etesami[28], M. Khakzad, M. Mohammadi Najafabadi, M. Naseri, F. Rezaei Hosseinabadi, B. Safarzadeh[29], M. Zeinali

University College Dublin, Dublin, Ireland
M. Felcini, M. Grunewald

INFN Sezione di Bari[a], Università di Bari[b], Politecnico di Bari[c], Bari, Italy
M. Abbrescia[a,b], C. Calabria[a,b], A. Colaleo[a], D. Creanza[a,c], L. Cristella[a,b], N. De Filippis[a,c], M. De Palma[a,b], A. Di Florio[a,b], F. Errico[a,b], L. Fiore[a], A. Gelmi[a,b], G. Iaselli[a,c], M. Ince[a,b], S. Lezki[a,b], G. Maggi[a,c], M. Maggi[a], G. Miniello[a,b], S. My[a,b], S. Nuzzo[a,b], A. Pompili[a,b], G. Pugliese[a,c], R. Radogna[a], A. Ranieri[a], G. Selvaggi[a,b], A. Sharma[a], L. Silvestris[a], R. Venditti[a], P. Verwilligen[a], G. Zito[a]

INFN Sezione di Bologna[a], Università di Bologna[b], Bologna, Italy
G. Abbiendi[a], C. Battilana[a,b], D. Bonacorsi[a,b], L. Borgonovi[a,b], S. Braibant-Giacomelli[a,b], R. Campanini[a,b], P. Capiluppi[a,b], A. Castro[a,b], F. R. Cavallo[a], S. S. Chhibra[a,b], C. Ciocca[a], G. Codispoti[a,b], M. Cuffiani[a,b], G. M. Dallavalle[a], F. Fabbri[a], A. Fanfani[a,b], P. Giacomelli[a], C. Grandi[a], L. Guiducci[a,b], F. Iemmi[a,b], S. Marcellini[a], G. Masetti[a], A. Montanari[a], F. L. Navarria[a,b], A. Perrotta[a], F. Primavera[a,b,17], A. M. Rossi[a,b], T. Rovelli[a,b], G. P. Siroli[a,b], N. Tosi[a]

INFN Sezione di Catania[a], Università di Catania[b], Catania, Italy
S. Albergo[a,b], A. Di Mattia[a], R. Potenza[a,b], A. Tricomi[a,b], C. Tuve[a,b]

INFN Sezione di Firenze[a], Università di Firenze[b], Firenze, Italy
G. Barbagli[a], K. Chatterjee[a,b], V. Ciulli[a,b], C. Civinini[a], R. D'Alessandro[a,b], E. Focardi[a,b], G. Latino, P. Lenzi[a,b], M. Meschini[a], S. Paoletti[a], L. Russo[a,30], G. Sguazzoni[a], D. Strom[a], L. Viliani[a]

INFN Laboratori Nazionali di Frascati, Frascati, Italy
L. Benussi, S. Bianco, F. Fabbri, D. Piccolo

INFN Sezione di Genova[a], Università di Genova[b], Genoa, Italy
F. Ferro[a], F. Ravera[a,b], E. Robutti[a], S. Tosi[a,b]

INFN Sezione di Milano-Bicocca[a], Università di Milano-Bicocca[b], Milan, Italy
A. Benaglia[a], A. Beschi[b], L. Brianza[a,b], F. Brivio[a,b], V. Ciriolo[a,b,17], S. Di Guida[a,d,17], M. E. Dinardo[a,b], S. Fiorendi[a,b], S. Gennai[a], A. Ghezzi[a,b], P. Govoni[a,b], M. Malberti[a,b], S. Malvezzi[a], A. Massironi[a,b], D. Menasce[a], L. Moroni[a], M. Paganoni[a,b], D. Pedrini[a], S. Ragazzi[a,b], T. Tabarelli de Fatis[a,b], D. Zuolo

INFN Sezione di Napoli[a], Università di Napoli 'Federico II' [b], Napoli, Italy, Università della Basilicata[c], Potenza, Italy, Università G. Marconi[d], Rome, Italy
S. Buontempo[a], N. Cavallo[a,c], A. Di Crescenzo[a,b], F. Fabozzi[a,c], F. Fienga[a], G. Galati[a], A. O. M. Iorio[a,b], W. A. Khan[a], L. Lista[a], S. Meola[a,d,17], P. Paolucci[a,17], C. Sciacca[a,b], E. Voevodina[a,b]

INFN Sezione di Padova[a], Università di Padova[b], Padova, Italy, Università di Trento[c], Trento, Italy
P. Azzi[a], N. Bacchetta[a], D. Bisello[a,b], A. Boletti[a,b], A. Bragagnolo, R. Carlin[a,b], P. Checchia[a], M. Dall'Osso[a,b], P. De Castro Manzano[a], T. Dorigo[a], U. Gasparini[a,b], A. Gozzelino[a], S. Y. Hoh, S. Lacaprara[a], P. Lujan, M. Margoni[a,b], A. T. Meneguzzo[a,b], M. Passaseo[a], J. Pazzini[a,b], N. Pozzobon[a,b], P. Ronchese[a,b], R. Rossin[a,b], F. Simonetto[a,b], A. Tiko, E. Torassa[a], M. Zanetti[a,b], P. Zotto[a,b], G. Zumerle[a,b]

INFN Sezione di Pavia[a], Università di Pavia[b], Pavia, Italy
A. Braghieri[a], A. Magnani[a], P. Montagna[a,b], S. P. Ratti[a,b], V. Re[a], M. Ressegotti[a,b], C. Riccardi[a,b], P. Salvini[a], I. Vai[a,b], P. Vitulo[a,b]

INFN Sezione di Perugia[a], Università di Perugia[b], Perugia, Italy
M. Biasini[a,b], G. M. Bilei[a], C. Cecchi[a,b], D. Ciangottini[a,b], L. Fanò[a,b], P. Lariccia[a,b], R. Leonardi[a,b], E. Manoni[a], G. Mantovani[a,b], V. Mariani[a,b], M. Menichelli[a], A. Rossi[a,b], A. Santocchia[a,b], D. Spiga[a]

INFN Sezione di Pisa[a], Università di Pisa[b], Scuola Normale Superiore di Pisa[c], Pisa, Italy
K. Androsov[a], P. Azzurri[a], G. Bagliesi[a], L. Bianchini[a], T. Boccali[a], L. Borrello, R. Castaldi[a], M. A. Ciocci[a,b], R. Dell'Orso[a], G. Fedi[a], F. Fiori[a,c], L. Giannini[a,c], A. Giassi[a], M. T. Grippo[a], F. Ligabue[a,c], E. Manca[a,c], G. Mandorli[a,c], A. Messineo[a,b], F. Palla[a], A. Rizzi[a,b], P. Spagnolo[a], R. Tenchini[a], G. Tonelli[a,b], A. Venturi[a], P. G. Verdini[a]

INFN Sezione di Roma[a], Sapienza Università di Roma[b], Rome, Italy
L. Barone[a,b], F. Cavallari[a], M. Cipriani[a,b], D. Del Re[a,b], E. Di Marco[a,b], M. Diemoz[a], S. Gelli[a,b], E. Longo[a,b], B. Marzocchi[a,b], P. Meridiani[a], G. Organtini[a,b], F. Pandolfi[a], R. Paramatti[a,b], F. Preiato[a,b], S. Rahatlou[a,b], C. Rovelli[a], F. Santanastasio[a,b]

INFN Sezione di Torino[a], Università di Torino[b], Torino, Italy, Università del Piemonte Orientale[c], Novara, Italy
N. Amapane[a,b], R. Arcidiacono[a,c], S. Argiro[a,b], M. Arneodo[a,c], N. Bartosik[a], R. Bellan[a,b], C. Biino[a], N. Cartiglia[a], F. Cenna[a,b], S. Cometti[a], M. Costa[a,b], R. Covarelli[a,b], N. Demaria[a], B. Kiani[a,b], C. Mariotti[a], S. Maselli[a], E. Migliore[a,b], V. Monaco[a,b], E. Monteil[a,b], M. Monteno[a], M. M. Obertino[a,b], L. Pacher[a,b], N. Pastrone[a], M. Pelliccioni[a], G. L. Pinna Angioni[a,b], A. Romero[a,b], M. Ruspa[a,c], R. Sacchi[a,b], K. Shchelina[a,b], V. Sola[a], A. Solano[a,b], D. Soldi[a,b], A. Staiano[a]

INFN Sezione di Trieste[a], Università di Trieste[b], Trieste, Italy
S. Belforte[a], V. Candelise[a,b], M. Casarsa[a], F. Cossutti[a], A. Da Rold[a,b], G. Della Ricca[a,b], F. Vazzoler[a,b], A. Zanetti[a]

Kyungpook National University, Daegu, Korea
D. H. Kim, G. N. Kim, M. S. Kim, J. Lee, S. Lee, S. W. Lee, C. S. Moon, Y. D. Oh, S. Sekmen, D. C. Son, Y. C. Yang

Chonnam National University, Institute for Universe and Elementary Particles, Kwangju, Korea
H. Kim, D. H. Moon, G. Oh

Hanyang University, Seoul, Korea
J. Goh[31], T. J. Kim

Korea University, Seoul, Korea
S. Cho, S. Choi, Y. Go, D. Gyun, S. Ha, B. Hong, Y. Jo, K. Lee, K. S. Lee, S. Lee, J. Lim, S. K. Park, Y. Roh

Sejong University, Seoul, Korea
H. S. Kim

Seoul National University, Seoul, Korea
J. Almond, J. Kim, J. S. Kim, H. Lee, K. Lee, K. Nam, S. B. Oh, B. C. Radburn-Smith, S. h. Seo, U. K. Yang, H. D. Yoo, G. B. Yu

University of Seoul, Seoul, Korea
D. Jeon, H. Kim, J. H. Kim, J. S. H. Lee, I. C. Park

Sungkyunkwan University, Suwon, Korea
Y. Choi, C. Hwang, J. Lee, I. Yu

Vilnius University, Vilnius, Lithuania
V. Dudenas, A. Juodagalvis, J. Vaitkus

National Centre for Particle Physics, Universiti Malaya, Kuala Lumpur, Malaysia
I. Ahmed, Z. A. Ibrahim, M. A. B. Md Ali[32], F. Mohamad Idris[33], W. A. T. Wan Abdullah, M. N. Yusli, Z. Zolkapli

Universidad de Sonora (UNISON), Hermosillo, Mexico
J. F. Benitez, A. Castaneda Hernandez, J. A. Murillo Quijada

Centro de Investigacion y de Estudios Avanzados del IPN, Mexico City, Mexico
H. Castilla-Valdez, E. De La Cruz-Burelo, M. C. Duran-Osuna, I. Heredia-De La Cruz[34], R. Lopez-Fernandez, J. Mejia Guisao, R. I. Rabadan-Trejo, M. Ramirez-Garcia, G. Ramirez-Sanchez, R Reyes-Almanza, A. Sanchez-Hernandez

Universidad Iberoamericana, Mexico City, Mexico
S. Carrillo Moreno, C. Oropeza Barrera, F. Vazquez Valencia

Benemerita Universidad Autonoma de Puebla, Puebla, Mexico
J. Eysermans, I. Pedraza, H. A. Salazar Ibarguen, C. Uribe Estrada

Universidad Autónoma de San Luis Potosí, San Luis Potosí, Mexico
A. Morelos Pineda

University of Auckland, Auckland, New Zealand
D. Krofcheck

University of Canterbury, Christchurch, New Zealand
S. Bheesette, P. H. Butler

National Centre for Physics, Quaid-I-Azam University, Islamabad, Pakistan
A. Ahmad, M. Ahmad, M. I. Asghar, Q. Hassan, H. R. Hoorani, A. Saddique, M. A. Shah, M. Shoaib, M. Waqas

National Centre for Nuclear Research, Swierk, Poland
H. Bialkowska, M. Bluj, B. Boimska, T. Frueboes, M. Górski, M. Kazana, K. Nawrocki, M. Szleper, P. Traczyk, P. Zalewski

Institute of Experimental Physics, Faculty of Physics, University of Warsaw, Warsaw, Poland
K. Bunkowski, A. Byszuk[35], K. Doroba, A. Kalinowski, M. Konecki, J. Krolikowski, M. Misiura, M. Olszewski, A. Pyskir, M. Walczak

Laboratório de Instrumentação e Física Experimental de Partículas, Lisbon, Portugal
M. Araujo, P. Bargassa, C. Beirão Da Cruz E Silva, A. Di Francesco, P. Faccioli, B. Galinhas, M. Gallinaro, J. Hollar, N. Leonardo, M. V. Nemallapudi, J. Seixas, G. Strong, O. Toldaiev, D. Vadruccio, J. Varela

Joint Institute for Nuclear Research, Dubna, Russia
S. Afanasiev, P. Bunin, M. Gavrilenko, I. Golutvin, I. Gorbunov, A. Kamenev, V. Karjavine, A. Lanev, A. Malakhov, V. Matveev[36,37], P. Moisenz, V. Palichik, V. Perelygin, S. Shmatov, S. Shulha, N. Skatchkov, V. Smirnov, N. Voytishin, A. Zarubin

Petersburg Nuclear Physics Institute, Gatchina (St. Petersburg), Russia
V. Golovtsov, Y. Ivanov, V. Kim[38], E. Kuznetsova[39], P. Levchenko, V. Murzin, V. Oreshkin, I. Smirnov, D. Sosnov, V. Sulimov, L. Uvarov, S. Vavilov, A. Vorobyev

Institute for Nuclear Research, Moscow, Russia
Yu. Andreev, A. Dermenev, S. Gninenko, N. Golubev, A. Karneyeu, M. Kirsanov, N. Krasnikov, A. Pashenkov, D. Tlisov, A. Toropin

Institute for Theoretical and Experimental Physics, Moscow, Russia
V. Epshteyn, V. Gavrilov, N. Lychkovskaya, V. Popov, I. Pozdnyakov, G. Safronov, A. Spiridonov, A. Stepennov, V. Stolin, M. Toms, E. Vlasov, A. Zhokin

Moscow Institute of Physics and Technology, Moscow, Russia
T. Aushev

National Research Nuclear University 'Moscow Engineering Physics Institute' (MEPhI), Moscow, Russia
R. Chistov[40], M. Danilov[40], P. Parygin, D. Philippov, S. Polikarpov[40], E. Tarkovskii

P.N. Lebedev Physical Institute, Moscow, Russia
V. Andreev, M. Azarkin[37], I. Dremin[37], M. Kirakosyan[37], S. V. Rusakov, A. Terkulov

Skobeltsyn Institute of Nuclear Physics, Lomonosov Moscow State University, Moscow, Russia
A. Baskakov, A. Belyaev, E. Boos, V. Bunichev, M. Dubinin[41], L. Dudko, A. Ershov, A. Gribushin, V. Klyukhin, O. Kodolova, I. Lokhtin, I. Miagkov, S. Obraztsov, S. Petrushanko, V. Savrin

Novosibirsk State University (NSU), Novosibirsk, Russia
A. Barnyakov[42], V. Blinov[42], T. Dimova[42], L. Kardapoltsev[42], Y. Skovpen[42]

Institute for High Energy Physics of National Research Centre 'Kurchatov Institute', Protvino, Russia
I. Azhgirey, I. Bayshev, S. Bitioukov, D. Elumakhov, A. Godizov, V. Kachanov, A. Kalinin, D. Konstantinov, P. Mandrik, V. Petrov, R. Ryutin, S. Slabospitskii, A. Sobol, S. Troshin, N. Tyurin, A. Uzunian, A. Volkov

National Research Tomsk Polytechnic University, Tomsk, Russia
A. Babaev, S. Baidali, V. Okhotnikov

University of Belgrade, Faculty of Physics and Vinca Institute of Nuclear Sciences, Belgrade, Serbia
P. Adzic[43], P. Cirkovic, D. Devetak, M. Dordevic, J. Milosevic

Centro de Investigaciones Energéticas Medioambientales y Tecnológicas (CIEMAT), Madrid, Spain
J. Alcaraz Maestre, A. Álvarez Fernández, I. Bachiller, M. Barrio Luna, J. A. Brochero Cifuentes, M. Cerrada, N. Colino, B. De La Cruz, A. Delgado Peris, C. Fernandez Bedoya, J. P. Fernández Ramos, J. Flix, M. C. Fouz, O. Gonzalez Lopez, S. Goy Lopez, J. M. Hernandez, M. I. Josa, D. Moran, A. Pérez-Calero Yzquierdo, J. Puerta Pelayo, I. Redondo, L. Romero, M. S. Soares, A. Triossi

Universidad Autónoma de Madrid, Madrid, Spain
C. Albajar, J. F. de Trocóniz

Universidad de Oviedo, Oviedo, Spain
J. Cuevas, C. Erice, J. Fernandez Menendez, S. Folgueras, I. Gonzalez Caballero, J. R. González Fernández, E. Palencia Cortezon, V. Rodríguez Bouza, S. Sanchez Cruz, P. Vischia, J. M. Vizan Garcia

Instituto de Física de Cantabria (IFCA), CSIC-Universidad de Cantabria, Santander, Spain
I. J. Cabrillo, A. Calderon, B. Chazin Quero, J. Duarte Campderros, M. Fernandez, P. J. Fernández Manteca, A. García Alonso, J. Garcia-Ferrero, G. Gomez, A. Lopez Virto, J. Marco, C. Martinez Rivero, P. Martinez Ruiz del Arbol, F. Matorras, J. Piedra Gomez, C. Prieels, T. Rodrigo, A. Ruiz-Jimeno, L. Scodellaro, N. Trevisani, I. Vila, R. Vilar Cortabitarte

Department of Physics, University of Ruhuna, Matara, Sri Lanka
N. Wickramage

CERN, European Organization for Nuclear Research, Geneva, Switzerland
D. Abbaneo, B. Akgun, E. Auffray, G. Auzinger, P. Baillon, A. H. Ball, D. Barney, J. Bendavid, M. Bianco, A. Bocci, C. Botta, E. Brondolin, T. Camporesi, M. Cepeda, G. Cerminara, E. Chapon, Y. Chen, G. Cucciati, D. d'Enterria, A. Dabrowski, N. Daci, V. Daponte, A. David, A. De Roeck, N. Deelen, M. Dobson, M. Dünser, N. Dupont, A. Elliott-Peisert, P. Everaerts, F. Fallavollita[44], D. Fasanella, G. Franzoni, J. Fulcher, W. Funk, D. Gigi, A. Gilbert, K. Gill, F. Glege, M. Guilbaud, D. Gulhan, J. Hegeman, C. Heidegger, V. Innocente, A. Jafari, P. Janot, O. Karacheban[20], J. Kieseler, A. Kornmayer, M. Krammer[1], C. Lange, P. Lecoq, C. Lourenço, L. Malgeri, M. Mannelli, F. Meijers, J. A. Merlin, S. Mersi, E. Meschi, P. Milenovic[45], F. Moortgat, M. Mulders, J. Ngadiuba, S. Nourbakhsh, S. Orfanelli, L. Orsini, F. Pantaleo[17], L. Pape, E. Perez, M. Peruzzi, A. Petrilli, G. Petrucciani, A. Pfeiffer, M. Pierini, F. M. Pitters, D. Rabady, A. Racz, T. Reis, G. Rolandi[46], M. Rovere, H. Sakulin, C. Schäfer, C. Schwick, M. Seidel, M. Selvaggi, A. Sharma, P. Silva, P. Sphicas[47], A. Stakia, J. Steggemann, M. Tosi, D. Treille, A. Tsirou, V. Veckalns[48], M. Verzetti, W. D. Zeuner

Paul Scherrer Institut, Villigen, Switzerland
L. Caminada[49], K. Deiters, W. Erdmann, R. Horisberger, Q. Ingram, H. C. Kaestli, D. Kotlinski, U. Langenegger, T. Rohe, S. A. Wiederkehr

ETH Zurich - Institute for Particle Physics and Astrophysics (IPA), Zurich, Switzerland
M. Backhaus, L. Bäni, P. Berger, N. Chernyavskaya, G. Dissertori, M. Dittmar, M. Donegà, C. Dorfer, C. Grab, D. Hits, J. Hoss, T. Klijnsma, W. Lustermann, R. A. Manzoni, M. Marionneau, M. T. Meinhard, F. Micheli, P. Musella, F. Nessi-Tedaldi, J. Pata, F. Pauss, G. Perrin, L. Perrozzi, S. Pigazzini, M. Quittnat, D. Ruini, D. A. Sanz Becerra, M. Schönenberger, L. Shchutska, V. R. Tavolaro, K. Theofilatos, M. L. Vesterbacka Olsson, R. Wallny, D. H. Zhu

Universität Zürich, Zurich, Switzerland
T. K. Aarrestad, C. Amsler[50], D. Brzhechko, M. F. Canelli, A. De Cosa, R. Del Burgo, S. Donato, C. Galloni, T. Hreus, B. Kilminster, S. Leontsinis, I. Neutelings, D. Pinna, G. Rauco, P. Robmann, D. Salerno, K. Schweiger, C. Seitz, Y. Takahashi, A. Zucchetta

National Central University, Chung-Li, Taiwan
Y. H. Chang, K. y. Cheng, T. H. Doan, Sh. Jain, R. Khurana, C. M. Kuo, W. Lin, A. Pozdnyakov, S. S. Yu

National Taiwan University (NTU), Taipei, Taiwan
P. Chang, Y. Chao, K. F. Chen, P. H. Chen, W.-S. Hou, Arun Kumar, Y. F. Liu, R.-S. Lu, E. Paganis, A. Psallidas, A. Steen

Chulalongkorn University, Faculty of Science, Department of Physics, Bangkok, Thailand
B. Asavapibhop, N. Srimanobhas, N. Suwonjandee

Çukurova University, Physics Department, Science and Art Faculty, Adana, Turkey
A. Bat, F. Boran, S. Cerci[51], S. Damarseckin, Z. S. Demiroglu, F. Dolek, C. Dozen, I. Dumanoglu, E. Eskut, S. Girgis, G. Gokbulut, Y. Guler, E. Gurpinar, I. Hos[52], C. Isik, E. E. Kangal[53], O. Kara, A. Kayis Topaksu, U. Kiminsu, M. Oglakci, G. Onengut, K. Ozdemir[54], S. Ozturk[55], A. Polatoz, U. G. Tok, S. Turkcapar, I. S. Zorbakir, C. Zorbilmez

Middle East Technical University, Physics Department, Ankara, Turkey
B. Isildak[56], G. Karapinar[57], M. Yalvac, M. Zeyrek

Bogazici University, Istanbul, Turkey
I. O. Atakisi, E. Gülmez, M. Kaya[58], O. Kaya[59], S. Ozkorucuklu[60], S. Tekten, E. A. Yetkin[61]

Istanbul Technical University, Istanbul, Turkey
M. N. Agaras, S. Atay, A. Cakir, K. Cankocak, Y. Komurcu, S. Sen[62]

Institute for Scintillation Materials of National Academy of Science of Ukraine, Kharkov, Ukraine
B. Grynyov

National Scientific Center, Kharkov Institute of Physics and Technology, Kharkov, Ukraine
L. Levchuk

University of Bristol, Bristol, UK
F. Ball, L. Beck, J. J. Brooke, D. Burns, E. Clement, D. Cussans, O. Davignon, H. Flacher, J. Goldstein, G. P. Heath, H. F. Heath, L. Kreczko, D. M. Newbold[63], S. Paramesvaran, B. Penning, T. Sakuma, D. Smith, V. J. Smith, J. Taylor, A. Titterton

Rutherford Appleton Laboratory, Didcot, UK
K. W. Bell, A. Belyaev[64], C. Brew, R. M. Brown, D. Cieri, D. J. A. Cockerill, J. A. Coughlan, K. Harder, S. Harper, J. Linacre, E. Olaiya, D. Petyt, C. H. Shepherd-Themistocleous, A. Thea, I. R. Tomalin, T. Williams, W. J. Womersley

Imperial College, London, UK
R. Bainbridge, P. Bloch, J. Borg, S. Breeze, O. Buchmuller, A. Bundock, S. Casasso, D. Colling, L. Corpe, P. Dauncey, G. Davies, M. Della Negra, R. Di Maria, Y. Haddad, G. Hall, G. Iles, T. James, M. Komm, C. Laner, L. Lyons, A.-M. Magnan, S. Malik, A. Martelli, J. Nash[65], A. Nikitenko[7], V. Palladino, M. Pesaresi, A. Richards, A. Rose, E. Scott, C. Seez, A. Shtipliyski, G. Singh, M. Stoye, T. Strebler, S. Summers, A. Tapper, K. Uchida, T. Virdee[17], N. Wardle, D. Winterbottom, J. Wright, S. C. Zenz

Brunel University, Uxbridge, UK
J. E. Cole, P. R. Hobson, A. Khan, P. Kyberd, C. K. Mackay, A. Morton, I. D. Reid, L. Teodorescu, S. Zahid

Baylor University, Waco, USA
K. Call, J. Dittmann, K. Hatakeyama, H. Liu, C. Madrid, B. Mcmaster, N. Pastika, C. Smith

Catholic University of America, Washington, DC, USA
R. Bartek, A. Dominguez

The University of Alabama, Tuscaloosa, USA
A. Buccilli, S. I. Cooper, C. Henderson, P. Rumerio, C. West

Boston University, Boston, USA
D. Arcaro, T. Bose, D. Gastler, D. Rankin, C. Richardson, J. Rohlf, L. Sulak, D. Zou

Brown University, Providence, USA
G. Benelli, X. Coubez, D. Cutts, M. Hadley, J. Hakala, U. Heintz, J. M. Hogan[66], K. H. M. Kwok, E. Laird, G. Landsberg, J. Lee, Z. Mao, M. Narain, S. Sagir[67], R. Syarif, E. Usai, D. Yu

University of California, Davis, Davis, USA
R. Band, C. Brainerd, R. Breedon, D. Burns, M. Calderon De La Barca Sanchez, M. Chertok, J. Conway, R. Conway, P. T. Cox, R. Erbacher, C. Flores, G. Funk, W. Ko, O. Kukral, R. Lander, M. Mulhearn, D. Pellett, J. Pilot, S. Shalhout, M. Shi, D. Stolp, D. Taylor, K. Tos, M. Tripathi, Z. Wang, F. Zhang

University of California, Los Angeles, USA
M. Bachtis, C. Bravo, R. Cousins, A. Dasgupta, A. Florent, J. Hauser, M. Ignatenko, N. Mccoll, S. Regnard, D. Saltzberg, C. Schnaible, V. Valuev

University of California, Riverside, Riverside, USA
E. Bouvier, K. Burt, R. Clare, J. W. Gary, S. M. A. Ghiasi Shirazi, G. Hanson, G. Karapostoli, E. Kennedy, F. Lacroix, O. R. Long, M. Olmedo Negrete, M. I. Paneva, W. Si, L. Wang, H. Wei, S. Wimpenny, B. R. Yates

University of California, San Diego, La Jolla, USA
J. G. Branson, S. Cittolin, M. Derdzinski, R. Gerosa, D. Gilbert, B. Hashemi, A. Holzner, D. Klein, G. Kole, V. Krutelyov, J. Letts, M. Masciovecchio, D. Olivito, S. Padhi, M. Pieri, M. Sani, V. Sharma, S. Simon, M. Tadel, A. Vartak, S. Wasserbaech[68], J. Wood, F. Würthwein, A. Yagil, G. Zevi Della Porta

University of California, Santa Barbara - Department of Physics, Santa Barbara, USA
N. Amin, R. Bhandari, J. Bradmiller-Feld, C. Campagnari, M. Citron, A. Dishaw, V. Dutta, M. Franco Sevilla, L. Gouskos, R. Heller, J. Incandela, A. Ovcharova, H. Qu, J. Richman, D. Stuart, I. Suarez, S. Wang, J. Yoo

California Institute of Technology, Pasadena, USA
D. Anderson, A. Bornheim, J. M. Lawhorn, H. B. Newman, T. Q. Nguyen, M. Spiropulu, J. R. Vlimant, R. Wilkinson, S. Xie, Z. Zhang, R. Y. Zhu

Carnegie Mellon University, Pittsburgh, USA
M. B. Andrews, T. Ferguson, T. Mudholkar, M. Paulini, M. Sun, I. Vorobiev, M. Weinberg

University of Colorado Boulder, Boulder, USA
J. P. Cumalat, W. T. Ford, F. Jensen, A. Johnson, M. Krohn, E. MacDonald, T. Mulholland, R. Patel, K. Stenson, K. A. Ulmer, S. R. Wagner

Cornell University, Ithaca, USA
J. Alexander, J. Chaves, Y. Cheng, J. Chu, A. Datta, K. Mcdermott, N. Mirman, J. R. Patterson, D. Quach, A. Rinkevicius, A. Ryd, L. Skinnari, L. Soffi, S. M. Tan, Z. Tao, J. Thom, J. Tucker, P. Wittich, M. Zientek

Fermi National Accelerator Laboratory, Batavia, USA
S. Abdullin, M. Albrow, M. Alyari, G. Apollinari, A. Apresyan, A. Apyan, S. Banerjee, L. A. T. Bauerdick, A. Beretvas, J. Berryhill, P. C. Bhat, G. Bolla[†], K. Burkett, J. N. Butler, A. Canepa, G. B. Cerati, H. W. K. Cheung, F. Chlebana, M. Cremonesi, J. Duarte, V. D. Elvira, J. Freeman, Z. Gecse, E. Gottschalk, L. Gray, D. Green, S. Grünendahl, O. Gutsche, J. Hanlon, R. M. Harris, S. Hasegawa, J. Hirschauer, Z. Hu, B. Jayatilaka, S. Jindariani, M. Johnson, U. Joshi, B. Klima, M. J. Kortelainen, B. Kreis, S. Lammel, D. Lincoln, R. Lipton, M. Liu, T. Liu, J. Lykken, K. Maeshima, J. M. Marraffino, D. Mason, P. McBride, P. Merkel, S. Mrenna, S. Nahn, V. O'Dell, K. Pedro, C. Pena, O. Prokofyev, G. Rakness, L. Ristori, A. Savoy-Navarro[69], B. Schneider, E. Sexton-Kennedy, A. Soha, W. J. Spalding, L. Spiegel, S. Stoynev, J. Strait, N. Strobbe, L. Taylor, S. Tkaczyk, N. V. Tran, L. Uplegger, E. W. Vaandering, C. Vernieri, M. Verzocchi, R. Vidal, M. Wang, H. A. Weber, A. Whitbeck

University of Florida, Gainesville, USA
D. Acosta, P. Avery, P. Bortignon, D. Bourilkov, A. Brinkerhoff, L. Cadamuro, A. Carnes, M. Carver, D. Curry, R. D. Field, S. V. Gleyzer, B. M. Joshi, J. Konigsberg, A. Korytov, P. Ma, K. Matchev, H. Mei, G. Mitselmakher, K. Shi, D. Sperka, J. Wang, S. Wang

Florida International University, Miami, USA
Y. R. Joshi, S. Linn

Florida State University, Tallahassee, USA
A. Ackert, T. Adams, A. Askew, S. Hagopian, V. Hagopian, K. F. Johnson, T. Kolberg, G. Martinez, T. Perry, H. Prosper, A. Saha, C. Schiber, V. Sharma, R. Yohay

Florida Institute of Technology, Melbourne, USA
M. M. Baarmand, V. Bhopatkar, S. Colafranceschi, M. Hohlmann, D. Noonan, M. Rahmani, T. Roy, F. Yumiceva

University of Illinois at Chicago (UIC), Chicago, USA
M. R. Adams, L. Apanasevich, D. Berry, R. R. Betts, R. Cavanaugh, X. Chen, S. Dittmer, O. Evdokimov, C. E. Gerber, D. A. Hangal, D. J. Hofman, K. Jung, J. Kamin, C. Mills, I. D. Sandoval Gonzalez, M. B. Tonjes, N. Varelas, H. Wang, X. Wang, Z. Wu, J. Zhang

The University of Iowa, Iowa City, USA
M. Alhusseini, B. Bilki[70], W. Clarida, K. Dilsiz[71], S. Durgut, R. P. Gandrajula, M. Haytmyradov, V. Khristenko, J.-P. Merlo, A. Mestvirishvili, A. Moeller, J. Nachtman, H. Ogul[72], Y. Onel, F. Ozok[73], A. Penzo, C. Snyder, E. Tiras, J. Wetzel

Johns Hopkins University, Baltimore, USA
B. Blumenfeld, A. Cocoros, N. Eminizer, D. Fehling, L. Feng, A. V. Gritsan, W. T. Hung, P. Maksimovic, J. Roskes, U. Sarica, M. Swartz, M. Xiao, C. You

The University of Kansas, Lawrence, USA
A. Al-bataineh, P. Baringer, A. Bean, S. Boren, J. Bowen, A. Bylinkin, J. Castle, S. Khalil, A. Kropivnitskaya, D. Majumder, W. Mcbrayer, M. Murray, C. Rogan, S. Sanders, E. Schmitz, J. D. Tapia Takaki, Q. Wang

Kansas State University, Manhattan, USA
S. Duric, A. Ivanov, K. Kaadze, D. Kim, Y. Maravin, D. R. Mendis, T. Mitchell, A. Modak, A. Mohammadi, L. K. Saini, N. Skhirtladze

Lawrence Livermore National Laboratory, Livermore, USA
F. Rebassoo, D. Wright

University of Maryland, College Park, USA
A. Baden, O. Baron, A. Belloni, S. C. Eno, Y. Feng, C. Ferraioli, N. J. Hadley, S. Jabeen, G. Y. Jeng, R. G. Kellogg, J. Kunkle, A. C. Mignerey, F. Ricci-Tam, Y. H. Shin, A. Skuja, S. C. Tonwar, K. Wong

Massachusetts Institute of Technology, Cambridge, USA
D. Abercrombie, B. Allen, V. Azzolini, A. Baty, G. Bauer, R. Bi, S. Brandt, W. Busza, I. A. Cali, M. D'Alfonso, Z. Demiragli, G. Gomez Ceballos, M. Goncharov, P. Harris, D. Hsu, M. Hu, Y. Iiyama, G. M. Innocenti, M. Klute, D. Kovalskyi, Y.-J. Lee, P. D. Luckey, B. Maier, A. C. Marini, C. Mcginn, C. Mironov, S. Narayanan, X. Niu, C. Paus, C. Roland, G. Roland, G. S. F. Stephans, K. Sumorok, K. Tatar, D. Velicanu, J. Wang, T. W. Wang, B. Wyslouch, S. Zhaozhong

University of Minnesota, Minneapolis, USA
A. C. Benvenuti, R. M. Chatterjee, A. Evans, P. Hansen, S. Kalafut, Y. Kubota, Z. Lesko, J. Mans, N. Ruckstuhl, R. Rusack, J. Turkewitz, M. A. Wadud

University of Mississippi, Oxford, USA
J. G. Acosta, S. Oliveros

University of Nebraska-Lincoln, Lincoln, USA
E. Avdeeva, K. Bloom, D. R. Claes, C. Fangmeier, F. Golf, R. Gonzalez Suarez, R. Kamalieddin, I. Kravchenko, J. Monroy, J. E. Siado, G. R. Snow, B. Stieger

State University of New York at Buffalo, Buffalo, USA
A. Godshalk, C. Harrington, I. Iashvili, A. Kharchilava, C. Mclean, D. Nguyen, A. Parker, S. Rappoccio, B. Roozbahani

Northeastern University, Boston, USA
G. Alverson, E. Barberis, C. Freer, A. Hortiangtham, D. M. Morse, T. Orimoto, R. Teixeira De Lima, T. Wamorkar, B. Wang, A. Wisecarver, D. Wood

Northwestern University, Evanston, USA
S. Bhattacharya, O. Charaf, K. A. Hahn, N. Mucia, N. Odell, M. H. Schmitt, K. Sung, M. Trovato, M. Velasco

University of Notre Dame, Notre Dame, USA
R. Bucci, N. Dev, M. Hildreth, K. Hurtado Anampa, C. Jessop, D. J. Karmgard, N. Kellams, K. Lannon, W. Li, N. Loukas, N. Marinelli, F. Meng, C. Mueller, Y. Musienko[36], M. Planer, A. Reinsvold, R. Ruchti, P. Siddireddy, G. Smith, S. Taroni, M. Wayne, A. Wightman, M. Wolf, A. Woodard

The Ohio State University, Columbus, USA
J. Alimena, L. Antonelli, B. Bylsma, L. S. Durkin, S. Flowers, B. Francis, A. Hart, C. Hill, W. Ji, T. Y. Ling, W. Luo, B. L. Winer, H. W. Wulsin

Princeton University, Princeton, USA
S. Cooperstein, P. Elmer, J. Hardenbrook, S. Higginbotham, A. Kalogeropoulos, D. Lange, M. T. Lucchini, J. Luo, D. Marlow, K. Mei, I. Ojalvo, J. Olsen, C. Palmer, P. Piroué, J. Salfeld-Nebgen, D. Stickland, C. Tully

University of Puerto Rico, Mayaguez, USA
S. Malik, S. Norberg

Purdue University, West Lafayette, USA
A. Barker, V. E. Barnes, S. Das, L. Gutay, M. Jones, A. W. Jung, A. Khatiwada, B. Mahakud, D. H. Miller, N. Neumeister, C. C. Peng, S. Piperov, H. Qiu, J. F. Schulte, J. Sun, F. Wang, R. Xiao, W. Xie

Purdue University Northwest, Hammond, USA
T. Cheng, J. Dolen, N. Parashar

Rice University, Houston, USA
Z. Chen, K. M. Ecklund, S. Freed, F. J. M. Geurts, M. Kilpatrick, W. Li, B. P. Padley, J. Roberts, J. Rorie, W. Shi, Z. Tu, J. Zabel, A. Zhang

University of Rochester, Rochester, USA
A. Bodek, P. de Barbaro, R. Demina, Y. t. Duh, J. L. Dulemba, C. Fallon, T. Ferbel, M. Galanti, A. Garcia-Bellido, J. Han, O. Hindrichs, A. Khukhunaishvili, K. H. Lo, P. Tan, R. Taus

Rutgers, The State University of New Jersey, Piscataway, USA
A. Agapitos, J. P. Chou, Y. Gershtein, T. A. Gómez Espinosa, E. Halkiadakis, M. Heindl, E. Hughes, S. Kaplan, R. Kunnawalkam Elayavalli, S. Kyriacou, A. Lath, R. Montalvo, K. Nash, M. Osherson, H. Saka, S. Salur, S. Schnetzer, D. Sheffield, S. Somalwar, R. Stone, S. Thomas, P. Thomassen, M. Walker

University of Tennessee, Knoxville, USA
A. G. Delannoy, J. Heideman, G. Riley, S. Spanier

Texas A&M University, College Station, USA
O. Bouhali[74], A. Celik, M. Dalchenko, M. De Mattia, A. Delgado, S. Dildick, R. Eusebi, J. Gilmore, T. Huang, T. Kamon[75], S. Luo, R. Mueller, A. Perloff, L. Perniè, D. Rathjens, A. Safonov

Texas Tech University, Lubbock, USA
N. Akchurin, J. Damgov, F. De Guio, P. R. Dudero, S. Kunori, K. Lamichhane, S. W. Lee, T. Mengke, S. Muthumuni, T. Peltola, S. Undleeb, I. Volobouev, Z. Wang

Vanderbilt University, Nashville, USA
S. Greene, A. Gurrola, R. Janjam, W. Johns, C. Maguire, A. Melo, H. Ni, K. Padeken, J. D. Ruiz Alvarez, P. Sheldon, S. Tuo, J. Velkovska, M. Verweij, Q. Xu

University of Virginia, Charlottesville, USA
M. W. Arenton, P. Barria, B. Cox, R. Hirosky, M. Joyce, A. Ledovskoy, H. Li, C. Neu, T. Sinthuprasith, Y. Wang, E. Wolfe, F. Xia

Wayne State University, Detroit, USA
R. Harr, P. E. Karchin, N. Poudyal, J. Sturdy, P. Thapa, S. Zaleski

University of Wisconsin - Madison, Madison, WI, USA
M. Brodski, J. Buchanan, C. Caillol, D. Carlsmith, S. Dasu, L. Dodd, B. Gomber, M. Grothe, M. Herndon, A. Hervé, U. Hussain, P. Klabbers, A. Lanaro, K. Long, R. Loveless, T. Ruggles, A. Savin, N. Smith, W. H. Smith, N. Woods

† **Deceased**

1: Also at Vienna University of Technology, Vienna, Austria
2: Also at IRFU, CEA, Université Paris-Saclay, Gif-sur-Yvette, France
3: Also at Universidade Estadual de Campinas, Campinas, Brazil
4: Also at Federal University of Rio Grande do Sul, Porto Alegre, Brazil
5: Also at Université Libre de Bruxelles, Bruxelles, Belgium
6: Also at University of Chinese Academy of Sciences, Beijing, China
7: Also at Institute for Theoretical and Experimental Physics, Moscow, Russia
8: Also at Joint Institute for Nuclear Research, Dubna, Russia
9: Also at Cairo University, Cairo, Egypt
10: Also at Helwan University, Cairo, Egypt
11: Now at Zewail City of Science and Technology, Zewail, Egypt
12: Also at British University in Egypt, Cairo, Egypt
13: Now at Ain Shams University, Cairo, Egypt
14: Also at Department of Physics, King Abdulaziz University, Jeddah, Saudi Arabia
15: Also at Université de Haute Alsace, Mulhouse, France
16: Also at Skobeltsyn Institute of Nuclear Physics, Lomonosov Moscow State University, Moscow, Russia
17: Also at CERN, European Organization for Nuclear Research, Geneva, Switzerland
18: Also at RWTH Aachen University, III. Physikalisches Institut A, Aachen, Germany
19: Also at University of Hamburg, Hamburg, Germany
20: Also at Brandenburg University of Technology, Cottbus, Germany
21: Also at MTA-ELTE Lendület CMS Particle and Nuclear Physics Group, Eötvös Loránd University, Budapest, Hungary
22: Also at Institute of Nuclear Research ATOMKI, Debrecen, Hungary
23: Also at Institute of Physics, University of Debrecen, Debrecen, Hungary
24: Also at Indian Institute of Technology Bhubaneswar, Bhubaneswar, India
25: Also at Institute of Physics, Bhubaneswar, India
26: Also at Shoolini University, Solan, India
27: Also at University of Visva-Bharati, Santiniketan, India
28: Also at Isfahan University of Technology, Isfahan, Iran
29: Also at Plasma Physics Research Center, Science and Research Branch, Islamic Azad University, Tehran, Iran
30: Also at Università degli Studi di Siena, Siena, Italy
31: Also at Kyunghee University, Seoul, Korea
32: Also at International Islamic University of Malaysia, Kuala Lumpur, Malaysia
33: Also at Malaysian Nuclear Agency, MOSTI, Kajang, Malaysia
34: Also at Consejo Nacional de Ciencia y Tecnología, Mexico city, Mexico
35: Also at Warsaw University of Technology, Institute of Electronic Systems, Warsaw, Poland
36: Also at Institute for Nuclear Research, Moscow, Russia
37: Now at National Research Nuclear University 'Moscow Engineering Physics Institute' (MEPhI), Moscow, Russia
38: Also at St. Petersburg State Polytechnical University, St. Petersburg, Russia
39: Also at University of Florida, Gainesville, USA
40: Also at P.N. Lebedev Physical Institute, Moscow, Russia
41: Also at California Institute of Technology, Pasadena, USA
42: Also at Budker Institute of Nuclear Physics, Novosibirsk, Russia
43: Also at Faculty of Physics, University of Belgrade, Belgrade, Serbia
44: Also at INFN Sezione di Pavia [a], Università di Pavia [b], Pavia, Italy
45: Also at University of Belgrade, Faculty of Physics and Vinca Institute of Nuclear Sciences, Belgrade, Serbia
46: Also at Scuola Normale e Sezione dell'INFN, Pisa, Italy
47: Also at National and Kapodistrian University of Athens, Athens, Greece
48: Also at Riga Technical University, Riga, Latvia

49: Also at Universität Zürich, Zurich, Switzerland
50: Also at Stefan Meyer Institute for Subatomic Physics (SMI), Vienna, Austria
51: Also at Adiyaman University, Adiyaman, Turkey
52: Also at Istanbul Aydin University, Istanbul, Turkey
53: Also at Mersin University, Mersin, Turkey
54: Also at Piri Reis University, Istanbul, Turkey
55: Also at Gaziosmanpasa University, Tokat, Turkey
56: Also at Ozyegin University, Istanbul, Turkey
57: Also at Izmir Institute of Technology, Izmir, Turkey
58: Also at Marmara University, Istanbul, Turkey
59: Also at Kafkas University, Kars, Turkey
60: Also at Istanbul University, Faculty of Science, Istanbul, Turkey
61: Also at Istanbul Bilgi University, Istanbul, Turkey
62: Also at Hacettepe University, Ankara, Turkey
63: Also at Rutherford Appleton Laboratory, Didcot, UK
64: Also at School of Physics and Astronomy, University of Southampton, Southampton, UK
65: Also at Monash University, Faculty of Science, Clayton, Australia
66: Also at Bethel University, St. Paul, USA
67: Also at Karamanoğlu Mehmetbey University, Karaman, Turkey
68: Also at Utah Valley University, Orem, USA
69: Also at Purdue University, West Lafayette, USA
70: Also at Beykent University, Istanbul, Turkey
71: Also at Bingol University, Bingol, Turkey
72: Also at Sinop University, Sinop, Turkey
73: Also at Mimar Sinan University, Istanbul, Istanbul, Turkey
74: Also at Texas A&M University at Qatar, Doha, Qatar
75: Also at Kyungpook National University, Daegu, Korea